Journal of Visualized Experiments

# Simplified protocol for meso-scale particle image velocimetry studies of neurovascular flows in vitro

--Manuscript Draft--

| | |
|---|---|
| **Article Type:** | Methods Article - JoVE Produced Video |
| **Manuscript Number:** | JoVE58902R1 |
| **Full Title:** | Simplified protocol for meso-scale particle image velocimetry studies of neurovascular flows in vitro |
| **Keywords:** | Particle Image Velocimetry; PDMS Tissue Phantom; 3D printing; Fluid Mechanics; Signal Processing; Neurovascular |
| **Corresponding Author:** | Ryan Peck<br>University of California Riverside<br>Riverside, California UNITED STATES |
| **Corresponding Author's Institution:** | University of California Riverside |
| **Corresponding Author E-Mail:** | rpeck003@ucr.edu |
| **Order of Authors:** | Ryan Peck |
| | Edver Bahena |
| | Reza Jahan |
| | Guillermo Aguilar |
| | Hideaki Tsutsui |
| | Marko Princevac |
| | Monica M. Wilhelmus |
| | Masaru P. Rao |
| **Additional Information:** | |
| **Question** | **Response** |
| Please indicate whether this article will be Standard Access or Open Access. | Standard Access (US$2,400) |
| Please indicate the **city, state/province, and country** where this article will be **filmed**. Please do not use abbreviations. | Riverside, CA, USA |

**TITLE:**

# Meso-Scale Particle Image Velocimetry Studies of Neurovascular Flows *In Vitro*

**AUTHORS AND AFFILIATIONS:**

Ryan A. Peck[1] *, Edver Bahena[1] *, Reza Jahan[2], Guillermo Aguilar[1,3,4], Hideaki Tsutsui[1,4], Marko Princevac[1], Monica M. Wilhelmus[1], Masaru P. Rao[1,3,4]

[1]Department of Mechanical Engineering, University of California, Riverside, CA, United States of America

[2]Division of Interventional Neuroradiology, University of California, Los Angeles, California, United States of America

[3]Materials Science and Engineering Program, University of California, Riverside, CA, United States of America

[4]Department of Bioengineering, University of California, Riverside, CA, United States of America

* These authors contributed equally.

**Corresponding Author:**

Masaru P. Rao (mprao@engr.ucr.edu)

**E-mail Addresses of the Co-authors:**

Ryan A. Peck (rpeck003@ucr.edu)
Edver Bahena (ebahe002@ucr.edu)
Reza Jahan (rjahan@mednet.ucla.edu)
Guillermo Aguilar (gaguilar@engr.ucr.edu)
Hideaki Tsutsui (htsutsui@engr.ucr.edu)
Marko Princevac (marko@engr.ucr.edu)
Monica M. Wilhelmus (monicamo@engr.ucr.edu)

**KEYWORDS:**

Particle image velocimetry, PDMS tissue phantom, 3-D printing, fluid mechanics, signal processing, neurovascular

**SUMMARY:**

Here we present simplified methods for fabricating transparent neurovascular phantoms and characterizing the flow therein. We highlight several important parameters and demonstrate their relationship to field accuracy.

**ABSTRACT:**

Particle image velocimetry (PIV) is used in a wide variety of fields, due to the opportunity it provides for precisely visualizing and quantifying flows across a large spatiotemporal range. However, its implementation typically requires the use of expensive and specialized instrumentation, which limits its broader utility. Moreover, within the field of bioengineering, *in vitro* flow visualization studies are also often further limited by the high cost of commercially

sourced tissue phantoms that recapitulate desired anatomical structures, particularly for those that span the mesoscale regime (*i.e.*, submillimeter to millimeter length scales). Herein, we present a simplified experimental protocol developed to address these limitations, the key elements of which include 1) a relatively low-cost method for fabricating mesoscale tissue phantoms using 3-D printing and silicone casting, and 2) an open-source image analysis and processing framework that reduces the demand upon the instrumentation for measuring mesoscale flows (*i.e.*, velocities up to tens of millimeters/second). Collectively, this lowers the barrier to entry for nonexperts, by leveraging resources already at the disposal of many bioengineering researchers. We demonstrate the applicability of this protocol within the context of neurovascular flow characterization; however, it is expected to be relevant to a broader range of mesoscale applications in bioengineering and beyond.

**INTRODUCTION:**

PIV is widely used in experimental fluid mechanics for flow visualization and quantitative investigations of fluid motion that vary in length scale from atmospheric to microcirculatory flows[1-3]. While the specifics of its implementation can vary as widely as its applications, one aspect common to nearly all PIV studies is the use of video imaging of tracer particles seeded within the working fluid, followed by a pair-wise analysis of consecutive image frames to extract desired flow characteristics. Typically, this is accomplished by first subdividing each image frame into smaller regions termed interrogation windows. As a consequence of the random positions of the dispersed particles, each interrogation window contains a unique distribution of pixel intensities. If the window size and data acquisition rate are chosen appropriately, cross-correlation of the intensity signal in each window can be used to estimate the average displacement within that region. Finally, given that the magnification and frame rate are known experimental parameters, an instantaneous velocity vector field can be readily computed.

A major advantage of PIV over single-point measurement techniques is its ability to map vector fields across a two- or three-dimensional domain. Hemodynamic applications, in particular, have benefited from this capability, since it allows a thorough investigation of local flows, which are known to play a significant role in vascular disease or remodeling (*e.g.*, atherosclerosis, angiogenesis)[4-6]. This has also been true for the evaluation of neurovascular flows, and the interactions thereof with endovascular devices (*e.g.*, flow diverters, stents, intrasaccular coils), since the relevant length-scales in such applications can often span one or more orders of magnitude (*e.g.*, from micrometer to millimeter), and device geometry and placement can significantly impact the local fluid mechanics[7].

Most groups conducting PIV-based hemodynamic studies have relied on experimental set-ups that closely mimic some of the earliest investigations of stent influence on vascular flow[7,8]. Typically, these include a) pulsed lasers and high-speed cameras, to capture high-velocity flows; b) synchronizers, to prevent aliasing between the pulse frequency of the laser and the camera acquisition frame rate; c) cylindrical optics, to form a light sheet and, thus, minimize the background fluorescence from tracer particles above and below the interrogation plane; d) in the case of commercial turn-key systems, proprietary software packages, to perform the cross-correlation analyses. However, while some applications require the performance and/or

versatility collectively afforded by these components, many others do not. Moreover, the high cost of commercially sourced tissue phantoms that recapitulate desired vascular structures can also prove limiting for many *in vitro* studies, particularly for phantoms with features that bridge the mesoscale regime (> 500 USD/phantom). Herein, we report the development of a simplified protocol for implementing PIV for the *in vitro* visualization of neurovascular flows, which typically lie both spatially and temporally within the mesoscale regime (*i.e.*, length scales ranging from submillimeter to millimeter, and velocities up to tens of millimeters/second). The protocol seeks to leverage resources already at the disposal of many bioengineering researchers, thus lowering the barrier to entry for nonexperts.

The first element of this protocol involves the use of an investment casting technique to enable the in-house fabrication of transparent, polydimethylsiloxane (PDMS)-based tissue phantoms from 3-D-printed sacrificial molds. By leveraging the increasing availability of 3-D printers in recent years, particularly those in shared/multi-user facilities (*e.g.*, institutional facilities or public makerspaces), this methodology cuts costs significantly (*e.g.*, < 100 USD/phantom in the case presented here), while enabling a rapid turnaround for the fabrication of a wide variety of designs and geometries. In the current protocol, a fused deposition modeling system is used with acrylonitrile butadiene styrene (ABS) as the building material, and the printed part serves as a sacrificial mold for the subsequent phantom casting. Our experience has shown that ABS is well-suited for such use since it is soluble in common solvents (*e.g.*, acetone), and it has sufficient strength and rigidity to maintain mold integrity after the removal of the support material (*e.g.*, to prevent the deformation or fracture of diminutive mold features). In the current protocol, mold integrity is further ensured using solid printed models, although this comes at the expense of increased dissolution time. The use of hollow models may also be possible in some cases, to enhance solvent access, and thus, reduce dissolution time. However, careful consideration should be given to the effect this may have on mold integrity. Finally, while the phantoms fabricated herein are based upon idealized representations of neurovascular structures generated using a common computer-aided design (CAD) software package, the protocol is expected to be amenable to the fabrication of more complex, patient-specific geometries as well (*e.g.*, *via* the use of model files generated by the conversion of clinical imaging data to the .STL file format used by most 3-D printers). Further details regarding the phantom fabrication process are provided in section 2 of the protocol.

The second element of the protocol involves the use of an open-source plug-in for ImageJ to conduct the cross-correlation analyses[9]. This is coupled with the implementation of a simple statistical thresholding scheme (*i.e.*, intensity capping)[10] to improve the image signal prior to cross-correlation, as well as a postcorrelation vector validation scheme, the normalized median test (NMT), to eliminate spurious vectors through a comparison of each to its nearest neighbors[11]. Collectively, this allows imaging to be accomplished using equipment commonly found in many bioengineering laboratories, thus eliminating the need for the acquisition of many of the costly components of typical PIV systems (*e.g.*, pulsed laser, synchronizer, cylindrical optics, and proprietary software). Further details regarding the video collection, image processing, and data analysis are provided in sections 5 and 6 of the protocol.

**Figure 1** illustrates the PIV set-up used in this protocol, which relies upon a fluorescence microscope equipped with a high-speed camera for imaging, as well as an external, continuous white-light source (*i.e.*, metal halide lamp) for through-objective volumetric illumination. A variable-speed gear pump is used to impose the recirculating flow of a transparent mock blood solution through the neurovascular tissue phantoms. The solution is composed of a 60:40 mixture of deionized (DI) water and glycerol, which is a common substitute for blood in hemodynamic studies[12-14], due to a) its similar density and viscosity (*i.e.*, 1080 kg/m$^3$ and 3.5 cP *vs.* 1050 kg/m$^3$ and 3 - 5 cP for blood)[15,16]; b) its transparency in the visible range; c) its similar refractive index as PDMS (1.38 *vs.* 1.42 for PDMS)[17-20], which minimizes optical distortion; d) the ease with which non-Newtonian behavior can be introduced, if needed, *via* the addition of xanthane[21]. Finally, fluorescent polystyrene beads are used as tracer particles (10.3 µm in diameter; 480 nm/501 nm excitation/emission). While neutrally buoyant beads are desired, sourcing tracer particles with optimal fluid mechanical properties (*e.g.*, density, size, composition) and emission wavelength can prove challenging. For example, the beads used herein are slightly less dense than the glycerol solution (1050 kg/m$^3$ *vs.* 1080 kg/m$^3$). However, the hydrodynamic effects, thereof, are negligible, given that the duration of a typical experiment is far shorter than the time scale associated with buoyancy effects (*i.e.*, 5 min and 20 min, respectively). Further details regarding the mock blood solution formulation and *in vitro* circulatory system set-up are provided in sections 3 and 4 of the protocol.

**PROTOCOL:**

**1. ABS-based Sacrificial Mold Fabrication**

1.1. Design an inverse model of the desired tissue phantom using CAD software.

1.2. Print the model using a 3-D printer with ABS as the building material.

**2. PDMS-based Vascular Phantom Fabrication**

**2.1. Mixing**

2.1.1. Mix the PDMS prepolymer base and curing agent in a 10:1 ratio (by weight); a 66 g mixture provides sufficient material for the fabrication of phantoms with volumes up to 50 cm$^3$.

2.1.2. Place the mixture in a vacuum desiccator for 60 min to degas and minimize the bubble entrapment. Use cyclic pressurization/depressurization to facilitate bubble rupture.

**2.2. Casting**

2.2.1. Mount the printed ABS mold on a glass slide using molding putty to seal the interface.

2.2.2. Carefully pour the PDMS mixture into the mold while trying to minimize bubble entrapment. Lingering bubbles can be manually ruptured using a needle.

2.2.3. Cure the cast phantom at room temperature (25 °C) for at least 24 h.

NOTE: At higher temperatures, this process can be accelerated[22].

**2.3. Demolding**

2.3.1. Dissolve the ABS by submerging the phantom in acetone and sonicating for at least 15 min, using powers up to 70 W.

CAUTION: Acetone has a high vapor pressure at room temperature and a low flash point. Consequently, always work under a fume hood and away from potential ignition sources. Wear proper personal protective equipment (*e.g.*, goggles or face shield, lab coat, acetone-resistant gloves).

2.3.2. Thoroughly rinse the phantom with isopropyl alcohol and, then, DI water to remove solvent residues.

NOTE: PDMS swells upon exposure to acetone; however, the swelling subsides once the phantom is rinsed and dried sufficiently[23].

**2.4. Confirmation of phantom fidelity using optical microscopy**

2.4.1. Using an optical microscope with an attached camera and image capture software, capture an image of a critical feature within the phantom under a magnification that maximizes the feature within the field of view.

2.4.2. Capture an image of an appropriate calibration reticle at the same magnification.

2.4.3. Load both images into ImageJ by dragging them onto the **Toolbar**.

2.4.4. Click on the calibration reticle image to make it active and, then, select the **Line** tool. Using the mouse, draw a line along a feature of a known distance and select **Analyze** > **Set Scale** from the ImageJ menu.

NOTE: In the **Set Scale** window, the field labeled **Distance in pixels** should be prepopulated with the length of the drawn line in units of pixels.

2.4.5. Enter the length of the feature in the field labeled **Known Distance**, and its unit in the field labeled **Unit of Length**. Check the box labeled **Global** to apply this calibration factor to all open images.

2.4.6. Make the image of the phantom critical feature active and use the **Line** tool to draw a line along a feature of interest. From the ImageJ menu, select **Analyze** > **Measure** (or press **Ctrl + M**)

221 to measure the length of the line.
222
223 2.4.7. Compare the expected value against the value in the column marked **Length** in the **Results**
224 window to confirm phantom fidelity.
225
226 **3. Mock Blood Solution Formulation**
227
228 3.1. Mix DI water and glycerol in a 60:40 ratio (by volume).
229
230 NOTE: A 100 mL volume is sufficient for the *in vitro* circulatory system described herein.
231
232 3.2. Add 1 mL of 2.5% w/v fluorescent polystyrene bead solution (*i.e.*, tracer particles) to the
233 mock blood solution.
234
235 3.3. Homogenize the mixture on a magnetic stir plate at 400 rpm for 10 min.
236
237 **4. *In Vitro* Circulatory System Set-up**
238
239 **4.1. Pump set-up**
240
241 4.1.1. Use a wire stripper tool to cut off the DC-end plug from the AC-to-DC adapter power
242 source.
243
244 4.1.2. Strip the coating off the power and ground wires and connect them to the input terminal
245 of the pulse width modulation (PWM) voltage regulator.
246
247 4.1.3. Connect the power and ground wires from the pump's DC motor to the output terminal of
248 the PWM voltage regulator.
249
250 NOTE: The PWM's seven-segment display outputs the duty cycle (0% - 100%) used to achieve a
251 variable voltage to the DC motor.
252
253 **4.2. Pump calibration**
254
255 4.2.1. Prepare 200 mL of mock blood solution (see section 3).
256
257 4.2.2. Place tubing from the pump inlet to the beaker holding the mock blood solution.
258
259 4.2.3. Place tubing from the pump outlet to an empty beaker.
260
261 4.2.4. Select a desired duty cycle set point (0% - 100%). Press the **On** button and start a timer.
262
263 4.2.5. Stop the timer once the pump has transferred the entire volume of mock blood solution.
264 Use this time to calculate the volumetric flow rate.

4.2.6. Repeat steps 4.2.1 - 4.2.5 for at least five different duty cycle set points to establish a least-squares regression curve.

NOTE: A minimum of three replicate points per duty cycle set point is recommended. This relationship can be used to correlate the desired flow rate to the required PWM duty cycle.

## 5. Video Collection

### 5.1. Image calibration

5.1.1. Determine the calibration ratio for the video imaging (see section 2).

### 5.2. Apparatus set-up

5.2.1. Place the PDMS phantom on the stage of the fluorescence microscope.

5.2.2. Connect the phantom to the gear pump and introduce the mock blood solution.

NOTE: Optionally, prefill the model with ethanol to facilitate full wetting; then, flush and fill it with the mock blood solution. This may be particularly beneficial for models with smaller vessels and/or blind features.

5.2.3. Set the pump motor controller for the desired flow rate based on the pump calibration curve.

5.2.4. Run the pump for 1 - 5 min prior to the experiment to ensure steady-state conditions.

5.2.5. Turn on the external lamp to illuminate the field of view. Select an appropriate filter based on the excitation wavelength of the fluorescent beads.

5.2.6. Adjust the imaging focal plane to the vessel midplane.

NOTE: This can be achieved by using a focal length that maximizes the imaged vessel cross-section (*e.g.*, when using phantoms with circular vessel cross sections); and/or indexing off of a phantom feature designed to facilitate the identification of the vessel mid-plane.

### 5.3. Video recording

5.3.1. Select the video recording parameters to optimize the signal-to-noise ratio (SNR). Key parameters include exposure time, frame rate, and gain.

NOTE: In this protocol, we use a frame rate of 2,000 fps and a gain of 1.0. However, these parameters may vary based on the application (see the discussion section for further details).

5.3.2. Collect the video and save it in AVI format.

**5.4. Phantom clean-up**

5.4.1. If bead-sticking is observed after an experiment, sonicate the phantom in an aqueous detergent solution using powers up to 70 W.

**6. Image Processing and Data Analysis**

**6.1. Image preprocessing**

6.1.1. Drag the saved AVI file onto the ImageJ window to import it. Select the box marked **Convert to Grayscale**.

6.1.2. From the **ImageJ** menu, select **Analyze** > **Generate Histogram** (or press **Ctrl + H**) to generate a histogram of image pixel intensities. Take note of the mean and standard deviation for the unprocessed image.

NOTE: At high frame rates, it is not unusual for the distribution to be skewed heavily toward zero (*i.e.*, no signal).

6.1.3. From the **ImageJ** menu, select **Image** > **Adjust** > **Brightness and Contrast** (or press **Shift + Ctrl + H**) to apply a brightness/contrast filter.

6.1.4. On the **Brightness and Contrast** menu, press the **Set** button to define the image limits. Set the minimum value to be the mean value plus one standard deviation, and the maximum value to be the maximum intensity of the image (both based on statistics obtained in step 6.1.2).

NOTE: This typically eliminates all but the top 10% of the pixel intensities. The number of standard deviations may be varied depending on the desired distribution of the pixel intensities. A custom macro script for performing the intensity capping operation is provided in the **Supplemental Materials.**

6.1.5. From the **ImageJ** menu, select **Process** > **Noise** > **Despeckle** to reduce the number of saturated pixels.

NOTE: This operation is necessitated by the increased potential for pixel saturation that arises during the optimization of the brightness and contrast, which can produce spurious vectors during subsequent cross-correlation.

6.1.6. From the **ImageJ** menu, select **Process** > **Filters** > **Gaussian Blur** with a radius of 1.5 to reduce artifacts arising from the occasional removal of illuminated pixels in a 3 x 3 neighborhood by the prior despeckling operation.

6.1.7. Click on the **Polygon** tool and, then, click on the image to outline the region of interest (ROI).

6.1.8. From the **ImageJ** menu, select **Edit** > **Clear Outside** to remove sensor noise in locations where no signal is expected (*e.g.*, areas beyond the vessel wall boundary), which can decrease the overall SNR.

**6.2. PIV calculation**

NOTE: This portion of the protocol employs a third-party PIV plug-in for ImageJ, which relies upon Gaussian peak-fitting to enable an estimation of displacement with subpixel accuracy.

6.2.1. From the **ImageJ** menu, select **Plugins** > **Macros** > **Run**… and navigate to the saved macro **Supplemental Code 2.ijjm** to cross-correlate successive image pairs.

NOTE: The macro proceeds as follows. 1) A cross-correlation of the intensity field within consecutive images is first performed to determine the local displacement of advected tracer particles (*i.e.*, the first image pair consists of the first and second images, the second image pair consists of the second and third images, *etc.*). 2) A two-step multipass evaluation is then performed with initial and final interrogation window sizes of 256 x 256 pixels and 128 x 128 pixels, respectively. Finally, 3) the macro performs a temporal average to further reduce the appearance of spurious vectors.

**6.3. Normalized median test (NMT)**

6.3.1. From the **ImageJ** menu, select **Plugins** > **Macros** > **Run…** and navigate to the saved macro **Supplemental Code 3.ijjm** to validate the velocity fields *via* the normalized median test.

NOTE: The macro proceeds as follows. 1) Each vector in an instantaneous vector field is first compared to its eight nearest neighbors to compute the median value. 2) The array of residual errors is then calculated as the difference between each neighboring vector and the calculated median. 3) The difference between the vector under investigation and the median neighboring vector value is then normalized by the median of the residuals. 4) This is then compared to a threshold value (typically, 0.2 pixels), which can be varied based on *a priori* knowledge of noise during the image acquisition. Finally, 5) a temporal average of all validated instantaneous vector fields is performed to produce a composite field, as this has been shown to increase the vector field quality[24].

**REPRESENTATIVE RESULTS:**

**Figure 2** illustrates the PDMS tissue phantom fabrication process. The phantoms designed herein are intended for the study of flow in idealized wide-necked, saccular, intracranial aneurysms, as well as proximal branching perforator arteries. Important additional design features include 1) a common reservoir that all vessels drain into, to ensure unencumbered fluid egress from the

phantom—otherwise, droplet formation may occur at the smaller vessel outlets; 2) a bubble trap, to facilitate bubble removal; 3) an outer cavity wall, to ensure parallelism of the vessel with the horizontal plane, as well as a precise definition of the final phantom slab height, length, and width; 4) the use of a 21 G hypodermic needle shank (820 µm in nominal outer diameter) for the molding of the perforator artery, due to our printer's inability to define such features with sufficient fidelity. Faithful reproduction of all design features is observed throughout.

Representative results of a PIV-based flow characterization performed using the current protocol are presented in **Figure 3** and **Figure 4**. These studies were performed using phantom inlet flow rates of 100 mL/min, data acquisition rates of 2,000 fps, and a temporal averaging over spans of 0.05 s. **Figure 3** shows representative image frames within the perforator artery, before and after intensity capping, as well as corresponding surface plots of the 8-bit pixel intensity values. Both demonstrate that intensity capping significantly increases the peak definition above the noise floor (*i.e.*, increases the SNR), which is critical to ensuring accuracy when performing subsequent cross-correlation. **Figure 4** shows the effects of intensity capping and NMT operations on the velocity vector field. Marked improvement in field uniformity is observed, thus further underscoring the importance of maximizing the SNR to minimize data dropout.

**FIGURE AND TABLE LEGENDS:**

**Figure 1: Particle image velocimetry set-up.** Reliance upon an open-source image analysis and a pre-/postprocessing framework reduces the demand upon the instrumentation for measuring mesoscale flows, thus eliminating the need for many of the costly components of typical PIV systems (*e.g.*, pulsed laser, synchronizer, cylindrical optics, and/or proprietary software).

**Figure 2: PDMS-based tissue phantom fabrication process.** The images illustrate (**a**) a CAD model of the neurovascular phantom mold, (**b**) the printed ABS mold after the removal of the support material, (**c**) the casting and curing of PDMS within the ABS mold, (**d**) partial dissolution of ABS mold material, and (**e**) the completed PDMS phantom, with the inset showing the final dimensions of critical features, as well as the region of interest (ROI) in the perforator artery where the PIV measurements were made.

**Figure 3: Effect of the intensity capping operation on the image SNR.** These panels show representative image frames and the corresponding pixel intensity surface plots within the perforator artery, (**a** and **b**) before and (**c** and **d**) after applying the intensity capping operation.

**Figure 4: Effects of intensity capping and NMT operations on velocity vector fields.** These panels illustrate the representative instantaneous velocity vector field within the perforator artery derived from (**a**) unprocessed image data, (**b**) intensity-capped data, and (**c**) intensity-capped data + NMT postprocessing.

**Figure 5: Effect of interrogation window sizing on correlation quality.** Optimal window sizing occurs when the value of the zero-normalized correlation coefficient is maximized, and the standard deviation is minimized.

**DISCUSSION:**

The protocol described herein outlines a simplified method for performing PIV studies to visualize neurovascular flows at physiologically relevant dimensions and flow conditions *in vitro*. In doing so, it serves to complement protocols reported by others that have also focused on simplifying the quantification of vector fields, but within very different contexts that require the consideration of far larger length scales[25] or lower flow rates[26,27] (*e.g.*, atmospheric or microcirculatory flows), and thus, with a reliance upon schemes that are incompatible with the current application.

The most important considerations for the successful implementation of PIV lie in the minimization of flow field artifacts and the maximization of image quality. Several steps in the tissue phantom fabrication process are critical to both of these criteria. For example, thorough degassing is crucial since air entrained within the PDMS during mixing can lead to bubble formation within the final phantom, which can adversely affect both feature fidelity and optical clarity. Additionally, minimization of surface roughness of the ABS mold is desired, since the PDMS casting process faithfully reproduces even the most minute imperfections (*e.g.*, build lines, surface pores, scratches), thus resulting in surface roughness in the final phantom that can decrease optical clarity and increase the potential for bead accumulation. While the protocol described herein has proven sufficient for the current application, there are numerous reports in the literature of means of reducing such roughness, should there be any need (*e.g.*, acetone vapor smoothing[28] or the optimization of layer thickness and part orientation with respect to the building direction)[29].

The parameter selection for video capture is also critical to ensure a high-fidelity vector field. An optimal SNR is typically achieved at the highest achievable frame rate that still allows sufficient bead exposure (the maximum frame rate being limited by the minimum exposure time). Gain can be used to amplify the signal, but this also increases sensor noise. If the maximum velocity can be estimated from other flow parameters (*e.g.*, inlet volumetric flow rate), then a lower bound on the required frame rate can be estimated using the following relation[30].

$$f_{sampling} > \frac{v_{max} \times c_{calibration}}{h_{interrogation\ window}} \quad (1)$$

Here, $f_{sampling}$ is the camera acquisition rate (Hz), $v_{max}$ is the maximum expected velocity (mm/s), $c_{calibration}$ is the calibration constant (pixels/mm), and $h_{interrogation\ window}$ is the size of the interrogation window (pixels). However, more optimal values can be determined using so-called correlation quality estimation techniques, such as the zero-normalized correlation coefficient[11]. In this technique, the averages of complementary signals from each frame pair are first subtracted and, then, normalized by the standard deviation of their intensities[11]. If a displacement of the original signal exists, such that all peaks and valleys match, the time-shifted value of this signal will be equal to one. Conversely, if there is no displacement that can align these signals, the value will be zero. This information is included in the ImageJ PIV output for each vector, and it can be plotted as its own field to verify whether there are spatial effects

contributing to poor correlation (*e.g.*, uneven lighting). The correlation coefficient can also be averaged over a field as an overall estimate of its quality. Finally, this quantity may also be plotted against varying frame rates or interrogation window sizes to determine an optimum. **Figure 5** illustrates the results from such an analysis using a Monte Carlo-synthesized particle field with displacements consistent with our experimentally measured flows (a typical technique for characterizing correlation quality[11]). The results show that the interrogation window size and frame rate should be chosen such that a particle field is displaced by ≤ 20% of the interrogation window size per frame pair to maximize the correlation coefficient while minimizing its variability.

Although the protocol described herein has proven sufficient for meeting the needs of the current application, it is important to acknowledge its limitations. For example, while contrast enhancement *via* intensity capping offers ease of implementation, transformations of the entire distribution of pixel intensities may improve the SNR further[31]. Similarly, although correlation-based tracking is well established and provides sufficient resolution for reliably estimating first-order flow characteristics relevant to hemodynamics (*e.g.*, intra-aneurysmal velocity), other techniques may offer a higher spatial resolution (*e.g.*, hybrid PIV/PTV, least-squares matching)[32,33] and, thus, greater accuracy when considering characteristics that are more sensitive to the velocity field resolution (*e.g.*, wall shear stress, in-plane vorticity). Likewise, while the NMT provides a means for improving the velocity vector field after cross-correlation, it is important to emphasize that this is just one of many vector validation techniques that could be used[24,34], each with their own unique advantages and disadvantages that may make their use more suitable for applications beyond those described here. Lastly, while the experimental set-up described here seeks to mimic physiologically relevant flow rates and length scales for the neurovasculature, it does not currently allow the analysis of pulsatile flows. This has not been a limitation for the current application, since the range of Womersley numbers in much of the neurovasculature tends to be ≤ 1 (*i.e.*, there is a minimal additive effect of multiple cardiac cycles)[35], which suggests that steady-state conditions are sufficient to recapitulate discrete time points along the cardiac waveform in which the flow rate is comparable. However, for applications where the Womersley number is larger (*e.g.*, vasculature closer to the heart), we envision a potential for introducing pulsatility through the use of an Arduino, which could be used to send the pump a time-varying PWM voltage waveform that enables the mimicking of a cardiac flow profile[36-38].

**ACKNOWLEDGMENTS:**
The authors acknowledge partial support for this project provided by a Collaborative Seed Grant from the Office of Research and Economic Development at UC Riverside.

**DISCLOSURES:**
The authors have nothing to declare.

**REFERENCES**
1. Grant, I. Particle image velocimetry: A review. *Proceedings of the Institution of Mechanical Engineers, Part C: Journal of Mechanical Engineering Science*. **211** (1), 55-76, doi:

10.1243/0954406971521665 (1997).

2. Lindken, R., Rossi, M., Große, S., Westerweel, J. Micro-Particle Image Velocimetry (µPIV): Recent developments, applications, and guidelines. *Lab on a Chip*. **9** (17), 2551, doi: 10.1039/b906558j (2009).

3. Hove, J.R. *et al.* Intracardiac fluid forces are an essential epigenetic factor for embryonic cardiogenesis. *Nature*. **421**, 172 (2003).

4. Ando, J., Yamamoto, K. Vascular Mechanobiology. *Circulation Journal*. **73** (11), 1983-1992, doi: 10.1253/circj.CJ-09-0583 (2009).

5. Conway, D.E. *et al.* Fluid Shear Stress on Endothelial Cells Modulates Mechanical Tension across VE-Cadherin and PECAM-1. *Current Biology*. **23** (11) (2013).

6. Kuhlencordt, P.J. *et al.* Accelerated Atherosclerosis, Aortic Aneurysm Formation, and Ischemic Heart Disease in Apolipoprotein E/Endothelial Nitric Oxide Synthase Double-Knockout Mice. *Circulation*. **104** (4), 448-454, doi: 10.1161/hc2901.091399 (2001).

7. Lieber, B.B., Stancampiano, A.P., Wakhloo, A.K. Alteration of hemodynamics in aneurysm models by stenting: Influence of stent porosity. *Annals of Biomedical Engineering*. **25** (3), 460-469, doi: 10.1007/BF02684187 (1997).

8. Bulusu, K. V., Plesniak, M.W. Experimental Investigation of Secondary Flow Structures Downstream of a Model Type IV Stent Failure in a 180˚ Curved Artery Test Section. *Journal of Visualized Experiments*. (113), e51288, doi: 10.3791/51288 (2016).

9. Tseng, Q. *et al.* Spatial organization of the extracellular matrix regulates cell-cell junction positioning. *Proceedings of the National Academy of Sciences of the United States of America*. **109** (5), 1506-1511, doi: 10.1073/pnas.1106377109 (2012).

10. Shavit, U., Lowe, R.J., Steinbuck, J. V Intensity Capping: a simple method to improve cross-correlation PIV results. *Experiments in Fluids*. **42** (2), 225-240, doi: 10.1007/s00348-006-0233-7 (2007).

11. Raffel, M., Willert, C.E., Werely, S., Kompenhans, J. *Particle Image Velocimetry: a Practical Guide*. Springer. New York, NY (2007).

12. Kerl, H.U. *et al.* Implantation of Pipeline Flow-Diverting Stents Reduces Aneurysm Inflow Without Relevantly Affecting Static Intra-aneurysmal Pressure. *Neurosurgery*. **74** (3), 321-334 (2014).

13. Lieber, B.B., Livescu, V., Hopkins, L.N., Wakhloo, A.K. Particle Image Velocimetry Assessment of Stent Design Influence on Intra-Aneurysmal Flow. *Annals of Biomedical Engineering*. **30** (6),

768-777, doi: 10.1114/1.1495867 (2002).

14. Charonko, J., Karri, S., Schmieg, J., Prabhu, S., Vlachos, P. *In vitro*, time-resolved PIV comparison of the effect of stent design on wall shear stress. *Annals of Biomedical Engineering*. **37** (7), 1310-1321, doi: 10.1007/s10439-009-9697-y (2009).

15. Rand, P.W., Lacombe, E., Hunt, H.E., Austin, W.H. Viscosity of normal human blood under normothermic and hypothermic conditions. *Journal of Applied Physiology*. **19** (1), 117-122, doi: 10.1152/jappl.1964.19.1.117 (1964).

16. Kenner, T., Leopold, H., Hinghofer-Szalkay, H. The continuous high-precision measurement of the density of flowing blood. *Pflügers Archiv European Journal of Physiology*. **370** (1), 25-29, doi: 10.1007/BF00707941 (1977).

17. Hoyt, L.F. New Table of the Refractive Index of Pure Glycerol at 20°C. *Industrial & Engineering Chemistry*. **26** (3), 329-332, doi: 10.1021/ie50291a023 (1934).

18. Cai, Z., Qiu, W., Shao, G., Wang, W. A new fabrication method for all-PDMS waveguides. *Sensors and Actuators A: Physical*. **204**, 44-47 (2013).

19. Bouillot, P. *et al.* Particle imaging velocimetry evaluation of intracranial stents in sidewall aneurysm: hemodynamic transition related to the stent design. *PloS ONE*. **9** (12), e113762, doi: 10.1371/journal.pone.0113762 (2014).

20. Trager, A.L., Sadasivan, C., Lieber, B.B. Comparison of the *in vitro* hemodynamic performance of new flow diverters for bypass of brain aneurysms. *Journal of Biomechanical Engineering*. **134** (8), 084505, doi: 10.1115/1.4006454 (2012).

21. Clauser, J. *et al.* A Novel Plasma-Based Fluid for Particle Image Velocimetry (PIV): *In-Vitro* Feasibility Study of Flow Diverter Effects in Aneurysm Model. *Annals of Biomedical Engineering*. **46** (6), 841-848, doi: 10.1007/s10439-018-2002-1 (2018).

22. Johnston, I.D., McCluskey, D.K., Tan, C.K.L., Tracey, M.C. Mechanical characterization of bulk Sylgard 184 for microfluidics and microengineering. *Journal of Micromechanics and Microengineering*. **24** (3), 035017, doi: 10.1088/0960-1317/24/3/035017 (2014).

23. Lee, J.N., Park, C., Whitesides, G.M. Solvent Compatibility of Poly(dimethylsiloxane)-Based Microfluidic Devices. *Analytical Chemistry*. **75** (23), 6544-6554, doi: 10.1021/ac0346712 (2003).

24. Meinhart, C.D., Wereley, S.T., Santiago, J.G. A PIV Algorithm for Estimating Time-Averaged Velocity Fields. *Journal of Fluids Engineering*. **122** (2), 285, doi: 10.1115/1.483256 (2000).

25. Bosbach, J., Kühn, M., Wagner, C., Raffel, M., Resagk, C. Large-Scale Particle Image Velocimetry of Natural and Mixed Convection. *13th Int Symp on Applications of Laser Techniques*

*to Fluid Mechanics* (2006).

26. Meinhart, C.D., Wereley, S.T., Santiago, J.G. PIV measurements of a microchannel flow. *Experiments in Fluids*. **27** (5), 414-419, doi: 10.1007/s003480050366 (1999).

27. Lima, R. *et al. In vitro* blood flow in a rectangular PDMS microchannel: experimental observations using a confocal micro-PIV system. *Biomedical Microdevices*. **10** (2), 153-167, doi: 10.1007/s10544-007-9121-z (2008).

28. Kuo, C.-C., Mao, R.-C. Development of a Precision Surface Polishing System for Parts Fabricated by Fused Deposition Modeling. *Materials and Manufacturing Processes*. **31** (8), 1113-1118, doi: 10.1080/10426914.2015.1090594 (2016).

29. Kang, K., Oh, S., Yi, H., Han, S., Hwang, Y. Fabrication of truly 3D microfluidic channel using 3D-printed soluble mold. *Biomicrofluidics*. **12** (1), 014105, doi: 10.1063/1.5012548 (2018).

30. Prasad, A.K. Particle Image Velocimetry. *Current Science*. **79** (1), 51-60 (2000).

31. Dellenback, P.A., Macharivilakathu, J., Pierce, S.R. Contrast-enhancement techniques for particle-image velocimetry. *Applied Optics*. **39** (32), 5978-5990, doi: 10.1364/AO.39.005978 (2000).

32. Cowen, E.A., Monismith, S.G. A hybrid digital particle tracking velocimetry technique. *Experiments in Fluids*. **22** (3), 199-211 (1997).

33. Gruen, A.W. Adaptive least squares correlation: a powerful image matching technique. *South African Journal of Photogrammetry, Remote Sensing and Cartography*. **14** (3), 175-187 (1985).

34. Nogueira, J., Lecuona, A., Rodríguez, P.A. Data validation, false vectors correction and derived magnitudes calculation on PIV data. *Measurement Science and Technology*. **8** (12), 1493-1501, doi: 10.1088/0957-0233/8/12/012 (1997).

35. Loudon, C., Tordesillas, A. The Use of the Dimensionless Womersley Number to Characterize the Unsteady Nature of Internal Flow. *Journal of Theoretical Biology*. **191** (1), 63-78 (1998).

36. Drost, S., De Kruif, B.J., Newport, D. Arduino control of a pulsatile flow rig. *Medical Engineering and Physics*. **51**, 67-71, doi: 10.1016/j.medengphy.2017.10.006 (2017).

37. Tsai, W., Savaş, Ö. Flow pumping system for physiological waveforms. *Medical & Biological Engineering & Computing*. **48** (2), 197-201, doi: 10.1007/s11517-009-0573-6 (2010).

38. Kato, T. *et al.* Contrast-enhanced 2D cine phase MR angiography for measurement of basilar artery blood flow in posterior circulation ischemia. *American Journal of Neuroradiology*. **23** (8), 1346-1351 (2002).

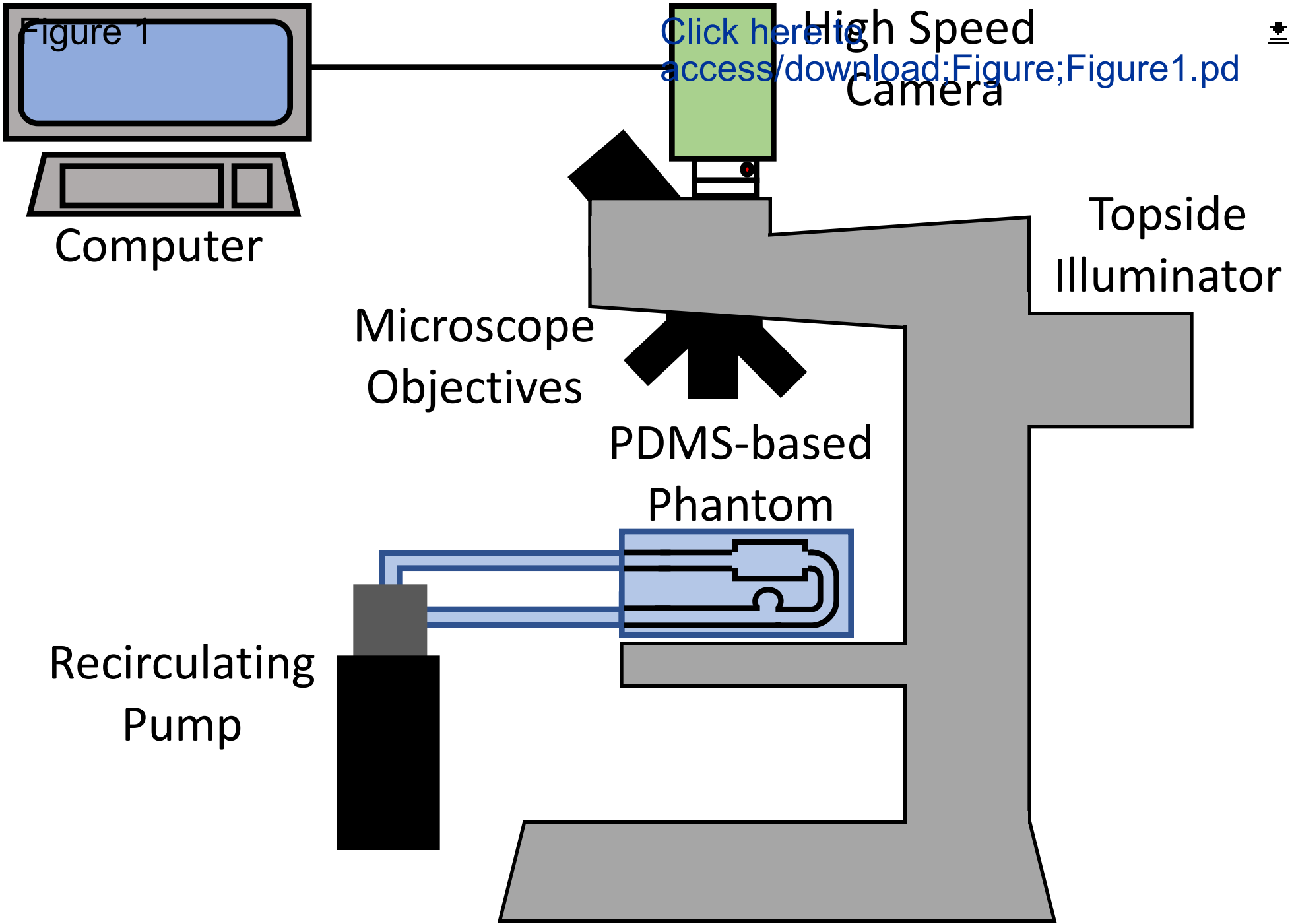
Figure 1
Click here to access/download;Figure;Figure1.pd
High Speed Camera
Computer
Topside Illuminator
Microscope Objectives
PDMS-based Phantom
Recirculating Pump

Figure 2



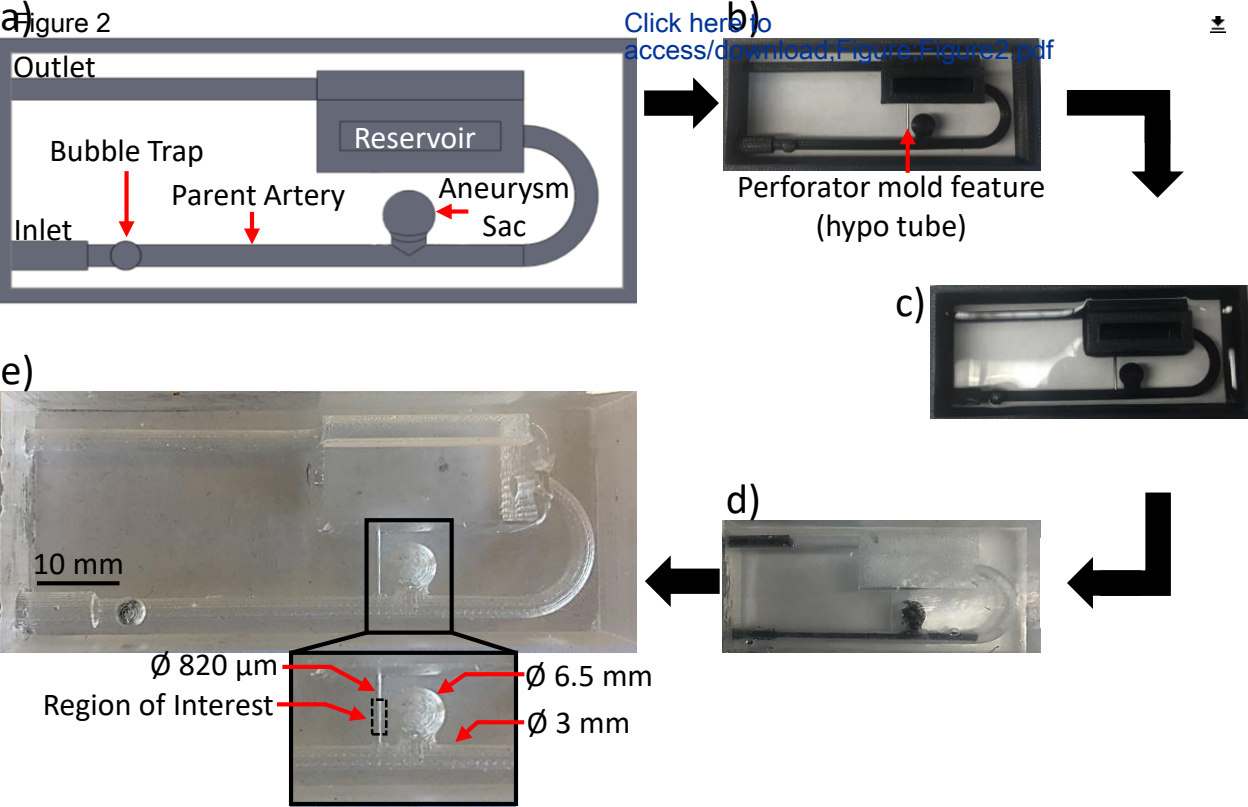

Figure 3



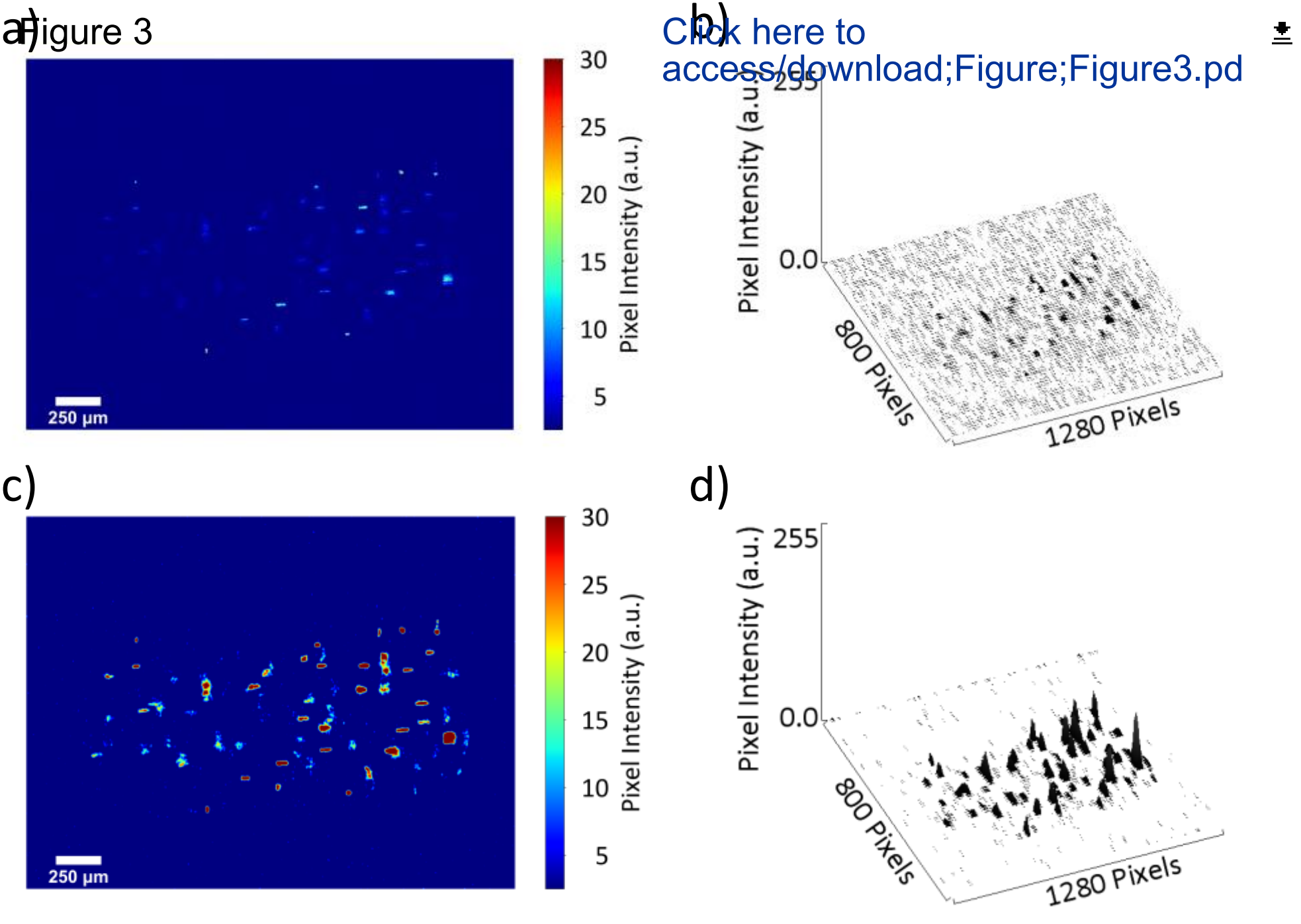

Figure 4



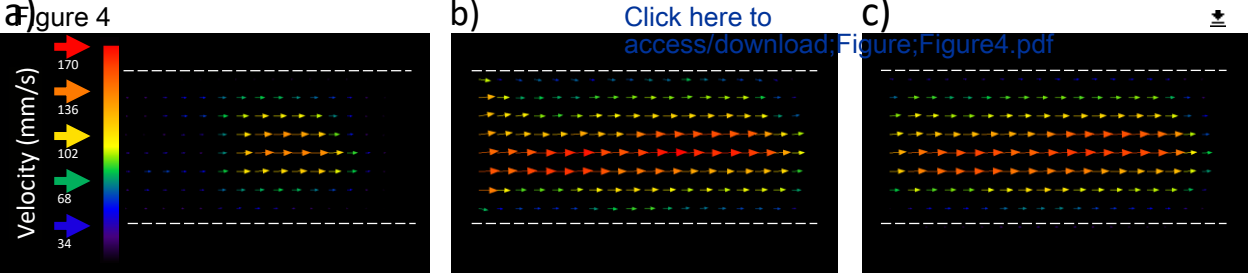

Figure 5



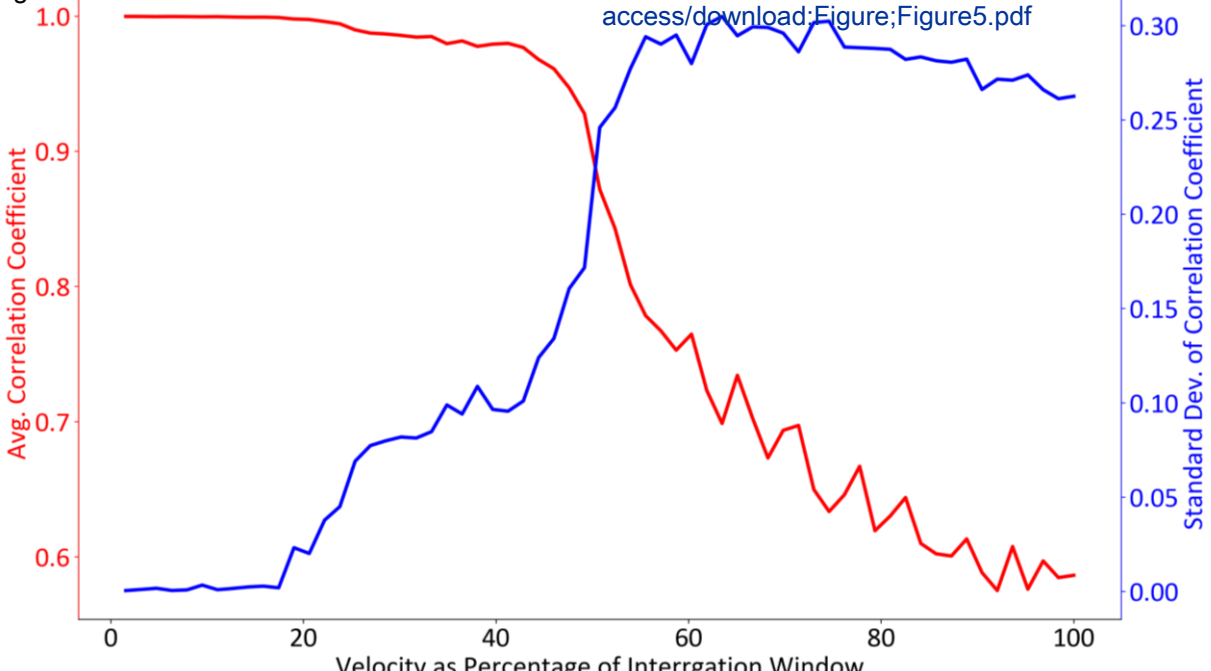

| Name of Material/ Equipment | Company | Catalog Number |
|---|---|---|
| Solidworks 2015 | Dassault Systems | N/A |
| Dow Corning Sylgard 184 Kit | Ellsworth Adhesive | 184 SIL ELAST KIT 3.9KG |
| Stratasys Dimension Elite | Stratasys | 9180-00105 |
| P430 Model Material Cartridge | Stratasys | 340-21202 |
| P400 SR Soluble Support Material Cartridge | Stratasys | 340-30200 |
| CleanStation DT3 | PM3 Technologies | 00-00300R |
| Lindberg Blue M LGO Box Furnace | Thermo Scientific | LB305745M |
| 21G BD PrecisionGlide Needle | Betcon Dickenson | BD 305167 |
| Desiccator (Vacuum) | Polylab | 55205 |
| Branson 1800 Utrasonic Cleaning | Branson | CPX-952-116R |
| Acetone | Fisher Chemical | A9494 |
| Isopropol Alcohol | Fisher Chemical | A4514 |
| Glycerol | Fisher Chemical | GW33500 |
| 10um Polystyrene Yellow-Green Fluorescent Particles | Magsphere | PSF-010UM |
| Phantom Miro | Vision Research | Miro M310 |
| Micropump | Cole-Parmer | 81101 |
| Leica DM2000 | Leica Microsystems | DM2000 |
| Leica 10X Objective | Leica Microsystems | 506259 |
| Leica 2.5X Objective | Leica Microsystems | 11506083 |
| Leica Blue Filter Cube L5 | Leica Microsystems | 513840 |
| Leica EL6000 | Leica Microsystems | 11504115 |
| Alconox | Alconox Inc | 1104-1 |
| ImageJ | NIH | N/A |
| Particle Image Velocimetry PIV Plugin | Qingson Tseng | N/A |

| | Comments/Description |
|---|---|
| CAD Software | |
| PDMS Kit | |
| 3D printer | |
| ABS build material | |
| Support material | |
| Base bath | |
| Oven | |
| Branching perforator mold segment | |
| Desiccator | |
| Sonicator | |
| Acetone | |
| Isopropol Alcohol | |
| Glycerol | |
| Fluorescent beads | |
| High speed camera | |
| Recirculating pump | |
| Fluorescent Microscope | |
| Objective for perforator | |
| Objective aneurysm sac | |
| Blue filter cube | |
| Light source | |
| Detergent | |
| Open source image analysis software | |
| https://sites.google.com/site/qingzongtseng/piv | |

1 Alewife Center #200
Cambridge, MA 02140
tel. 617.945.9051
www.jove.com

# ARTICLE AND VIDEO LICENSE AGREEMENT

| | |
|---|---|
| Title of Article: | Simplified protocol for meso-scale particle image velocimetry studies of neurovascular flows in vitro |
| Author(s): | Ryan A. Peck, Edver Bahena, Reza Jahan, Guillermo Aguilar, Hideaki Tsutsui Marko Princevac, Monica M. Wilhelmus, and Masaru P. Rao |

Item 1: The Author elects to have the Materials be made available (as described at http://www.jove.com/publish) via:

☑ Standard Access ☐ Open Access

Item 2: Please select one of the following items:

☑ The Author is **NOT** a United States government employee.

☐ The Author is a United States government employee and the Materials were prepared in the course of his or her duties as a United States government employee.

☐ The Author is a United States government employee but the Materials were NOT prepared in the course of his or her duties as a United States government employee.

## ARTICLE AND VIDEO LICENSE AGREEMENT

1. **Defined Terms.** As used in this Article and Video License Agreement, the following terms shall have the following meanings: "**Agreement**" means this Article and Video License Agreement; "**Article**" means the article specified on the last page of this Agreement, including any associated materials such as texts, figures, tables, artwork, abstracts, or summaries contained therein; "**Author**" means the author who is a signatory to this Agreement; "**Collective Work**" means a work, such as a periodical issue, anthology or encyclopedia, in which the Materials in their entirety in unmodified form, along with a number of other contributions, constituting separate and independent works in themselves, are assembled into a collective whole; "**CRC License**" means the Creative Commons Attribution-Non Commercial-No Derivs 3.0 Unported Agreement, the terms and conditions of which can be found at: http://creativecommons.org/licenses/by-nc-nd/3.0/legalcode; "**Derivative Work**" means a work based upon the Materials or upon the Materials and other pre-existing works, such as a translation, musical arrangement, dramatization, fictionalization, motion picture version, sound recording, art reproduction, abridgment, condensation, or any other form in which the Materials may be recast, transformed, or adapted; "**Institution**" means the institution, listed on the last page of this Agreement, by which the Author was employed at the time of the creation of the Materials; "**JoVE**" means MyJove Corporation, a Massachusetts corporation and the publisher of The Journal of Visualized Experiments; "**Materials**" means the Article and / or the Video; "**Parties**" means the Author and JoVE; "**Video**" means any video(s) made by the Author, alone or in conjunction with any other parties, or by JoVE or its affiliates or agents, individually or in collaboration with the Author or any other parties, incorporating all or any portion of the Article, and in which the Author may or may not appear.

2. **Background.** The Author, who is the author of the Article, in order to ensure the dissemination and protection of the Article, desires to have the JoVE publish the Article and create and transmit videos based on the Article. In furtherance of such goals, the Parties desire to memorialize in this Agreement the respective rights of each Party in and to the Article and the Video.

3. **Grant of Rights in Article.** In consideration of JoVE agreeing to publish the Article, the Author hereby grants to JoVE, subject to **Sections 4** and **7** below, the exclusive, royalty-free, perpetual (for the full term of copyright in the Article, including any extensions thereto) license (a) to publish, reproduce, distribute, display and store the Article in all forms, formats and media whether now known or hereafter developed (including without limitation in print, digital and electronic form) throughout the world, (b) to translate the Article into other languages, create adaptations, summaries or extracts of the Article or other Derivative Works (including, without limitation, the Video) or Collective Works based on all or any portion of the Article and exercise all of the rights set forth in (a) above in such translations, adaptations, summaries, extracts, Derivative Works or Collective Works and(c) to license others to do any or all of the above. The foregoing rights may be exercised in all media and formats, whether now known or hereafter devised, and include the right to make such modifications as are technically necessary to exercise the rights in other media and formats. If the "Open Access" box has been checked in **Item 1** above, JoVE and the Author hereby grant to the public all such rights in the Article as provided in, but subject to all limitations and requirements set forth in, the CRC License.

4. **Retention of Rights in Article.** Notwithstanding the exclusive license granted to JoVE in **Section 3** above, the Author shall, with respect to the Article, retain the non-exclusive right to use all or part of the Article for the non-commercial purpose of giving lectures, presentations or teaching classes, and to post a copy of the Article on the Institution's website or the Author's personal website, in each case provided that a link to the Article on the JoVE website is provided and notice of JoVE's copyright in the Article is included. All non-copyright intellectual property rights in and to the Article, such as patent rights, shall remain with the Author.

5. **Grant of Rights in Video – Standard Access.** This **Section 5** applies if the "Standard Access" box has been checked in **Item 1** above or if no box has been checked in **Item 1** above. In consideration of JoVE agreeing to produce, display or otherwise assist with the Video, the Author hereby acknowledges and agrees that, Subject to **Section 7** below, JoVE is and shall be the sole and exclusive owner of all rights of any nature, including, without limitation, all copyrights, in and to the Video. To the extent that, by law, the Author is deemed, now or at any time in the future, to have any rights of any nature in or to the Video, the Author hereby disclaims all such rights and transfers all such rights to JoVE.

6. **Grant of Rights in Video – Open Access.** This **Section 6** applies only if the "Open Access" box has been checked in **Item 1** above. In consideration of JoVE agreeing to produce, display or otherwise assist with the Video, the Author hereby grants to JoVE, subject to **Section 7** below, the exclusive, royalty-free, perpetual (for the full term of copyright in the Article, including any extensions thereto) license (a) to publish, reproduce, distribute, display and store the Video in all forms, formats and media whether now known or hereafter developed (including without limitation in print, digital and electronic form) throughout the world, (b) to translate the Video into other languages, create adaptations, summaries or extracts of the Video or other Derivative Works or Collective Works based on all or any portion of the Video and exercise all of the rights set forth in (a) above in such translations, adaptations, summaries, extracts, Derivative Works or Collective Works and (c) to license others to do any or all of the above. The foregoing rights may be exercised in all media and formats, whether now known or hereafter devised, and include the right to make such modifications as are technically necessary to exercise the rights in other media and formats. For any Video to which this **Section 6** is applicable, JoVE and the Author hereby grant to the public all such rights in the Video as provided in, but subject to all limitations and requirements set forth in, the CRC License.

7. **Government Employees.** If the Author is a United States government employee and the Article was prepared in the course of his or her duties as a United States government employee, as indicated in **Item 2** above, and any of the licenses or grants granted by the Author hereunder exceed the scope of the 17 U.S.C. 403, then the rights granted hereunder shall be limited to the maximum rights permitted under such statute. In such case, all provisions contained herein that are not in conflict with such statute shall remain in full force and effect, and all provisions contained herein that do so conflict shall be deemed to be amended so as to provide to JoVE the maximum rights permissible within such statute.

8. **Protection of the Work.** The Author(s) authorize JoVE to take steps in the Author(s) name and on their behalf if JoVE believes some third party could be infringing or might infringe the copyright of either the Author's Article and/or Video.

9. **Likeness, Privacy, Personality.** The Author hereby grants JoVE the right to use the Author's name, voice, likeness, picture, photograph, image, biography and performance in any way, commercial or otherwise, in connection with the Materials and the sale, promotion and distribution thereof. The Author hereby waives any and all rights he or she may have, relating to his or her appearance in the Video or otherwise relating to the Materials, under all applicable privacy, likeness, personality or similar laws.

10. **Author Warranties.** The Author represents and warrants that the Article is original, that it has not been published, that the copyright interest is owned by the Author (or, if more than one author is listed at the beginning of this Agreement, by such authors collectively) and has not been assigned, licensed, or otherwise transferred to any other party. The Author represents and warrants that the author(s) listed at the top of this Agreement are the only authors of the Materials. If more than one author is listed at the top of this Agreement and if any such author has not entered into a separate Article and Video License Agreement with JoVE relating to the Materials, the Author represents and warrants that the Author has been authorized by each of the other such authors to execute this Agreement on his or her behalf and to bind him or her with respect to the terms of this Agreement as if each of them had been a party hereto as an Author. The Author warrants that the use, reproduction, distribution, public or private performance or display, and/or modification of all or any portion of the Materials does not and will not violate, infringe and/or misappropriate the patent, trademark, intellectual property or other rights of any third party. The Author represents and warrants that it has and will continue to comply with all government, institutional and other regulations, including, without limitation all institutional, laboratory, hospital, ethical, human and animal treatment, privacy, and all other rules, regulations, laws, procedures or guidelines, applicable to the Materials, and that all research involving human and animal subjects has been approved by the Author's relevant institutional review board.

11. **JoVE Discretion.** If the Author requests the assistance of JoVE in producing the Video in the Author's facility, the Author shall ensure that the presence of JoVE employees, agents or independent contractors is in accordance with the relevant regulations of the Author's institution. If more than one author is listed at the beginning of this Agreement, JoVE may, in its sole

discretion, elect not take any action with respect to the Article until such time as it has received complete, executed Article and Video License Agreements from each such author. JoVE reserves the right, in its absolute and sole discretion and without giving any reason therefore, to accept or decline any work submitted to JoVE. JoVE and its employees, agents and independent contractors shall have full, unfettered access to the facilities of the Author or of the Author's institution as necessary to make the Video, whether actually published or not. JoVE has sole discretion as to the method of making and publishing the Materials, including, without limitation, to all decisions regarding editing, lighting, filming, timing of publication, if any, length, quality, content and the like.

12. **Indemnification.** The Author agrees to indemnify JoVE and/or its successors and assigns from and against any and all claims, costs, and expenses, including attorney's fees, arising out of any breach of any warranty or other representations contained herein. The Author further agrees to indemnify and hold harmless JoVE from and against any and all claims, costs, and expenses, including attorney's fees, resulting from the breach by the Author of any representation or warranty contained herein or from allegations or instances of violation of intellectual property rights, damage to the Author's or the Author's institution's facilities, fraud, libel, defamation, research, equipment, experiments, property damage, personal injury, violations of institutional, laboratory, hospital, ethical, human and animal treatment, privacy or other rules, regulations, laws, procedures or guidelines, liabilities and other losses or damages related in any way to the submission of work to JoVE, making of videos by JoVE, or publication in JoVE or elsewhere by JoVE. The Author shall be responsible for, and shall hold JoVE harmless from, damages caused by lack of sterilization, lack of cleanliness or by contamination due to the making of a video by JoVE its employees, agents or independent contractors. All sterilization, cleanliness or decontamination procedures shall be solely the responsibility of the Author and shall be undertaken at the Author's expense. All indemnifications provided herein shall include JoVE's attorney's fees and costs related to said losses or damages. Such indemnification and holding harmless shall include such losses or damages incurred by, or in connection with, acts or omissions of JoVE, its employees, agents or independent contractors.

13. **Fees.** To cover the cost incurred for publication, JoVE must receive payment before production and publication the Materials. Payment is due in 21 days of invoice. Should the Materials not be published due to an editorial or production decision, these funds will be returned to the Author. Withdrawal by the Author of any submitted Materials after final peer review approval will result in a US$1,200 fee to cover pre-production expenses incurred by JoVE. If payment is not received by the completion of filming, production and publication of the Materials will be suspended until payment is received.

14. **Transfer, Governing Law.** This Agreement may be assigned by JoVE and shall inure to the benefits of any of JoVE's successors and assignees. This Agreement shall be governed and construed by the internal laws of the Commonwealth of Massachusetts without giving effect to any conflict of law provision thereunder. This Agreement may be executed in counterparts, each of which shall be deemed an original, but all of which together shall be deemed to me one and the same agreement. A signed copy of this Agreement delivered by facsimile, e-mail or other means of electronic transmission shall be deemed to have the same legal effect as delivery of an original signed copy of this Agreement.

A signed copy of this document must be sent with all new submissions. Only one Agreement is required per submission.

**CORRESPONDING AUTHOR**

| | |
|---|---|
| Name: | Masaru P. Rao |
| Department: | Mechanical Engineering |
| Institution: | University of California, Riverside |
| Title: | Associate Professor |
| Signature: | |
| Date: | 08/01/2018 |

Please submit a **signed** and **dated** copy of this license by one of the following three methods:

1. Upload an electronic version on the JoVE submission site
2. Fax the document to +1.866.381.2236
3. Mail the document to JoVE / Attn: JoVE Editorial / 1 Alewife Center #200 / Cambridge, MA 02140

UC RIVERSIDE UNIVERSITY OF CALIFORNIA

*Bourns College of Engineering*
*Department of Mechanical Engineering*

September 14, 2018

Philip Steindel, Ph.D.
Review Editor
JoVE

Re: Manuscript revision (JoVE 58902)

Dear Dr. Steindel,

We thank you for your efforts on our behalf. We also thank the Reviewers for their insightful comments, and the time they invested in reviewing our manuscript.

We have revised the manuscript to address the Editorial and Reviewers' comments and we provide a point-by-point response in the following pages. We have uploaded copies of the final manuscript in both MS Word and PDF formats, and both unmarked (JoVE58902R1) and marked up (JoVE58902R1_MARKED) versions.

We believe that the manuscript has been strengthened as a result of the feedback, and as such, we look forward to its publication.

Best regards,

Masaru P. Rao
Associate Professor
Department of Mechanical Engineering
Department of Bioengineering *(Participating Faculty)*
Materials Science & Engineering Program *(Core Faculty)*
University of California, Riverside
Tel: (951) 827-5870
Email: mprao@engr.ucr.edu
URL: http://www.engr.ucr.edu/~mprao

***Editorial and Reviewers' comments and Author responses (JoVE 58902)***

The Editorial and Reviewers' comments are italicized below. They are included verbatim and in their entirety. Our corresponding responses are bolded.

**Editorial comments and Author responses:**

*"1. Please take this opportunity to thoroughly proofread the manuscript to ensure that there are no spelling or grammar issues."*

**Done.**

*"2. Please provide an email address for each author."*

**Done.**

*"3. Please adjust the numbering of the Protocol to follow the JoVE Instructions for Authors. For example, 1 should be followed by 1.1 and then 1.1.1 and 1.1.2 if necessary. Please refrain from using bullets, dashes, or indentations."*

**Done. Please note that this required wholesale revision of the protocol section. As such, the other changes made in this section in response to the Editorial & Reviewer's comments are not distinguishable from the original text in the marked up copy of the revised manuscript (i.e., entire protocol section is marked as changed).**

*"4. Please revise the protocol to contain only action items that direct the reader to do something (e.g., "Do this," "Ensure that," etc.). The actions should be described in the imperative tense in complete sentences wherever possible. Avoid usage of phrases such as "could be," "should be," and "would be" throughout the Protocol. Any text that cannot be written in the imperative tense may be added as a "Note." Please include all safety procedures and use of hoods, etc. However, notes should be used sparingly and actions should be described in the imperative tense wherever possible."*

**Done.**

*"5. Please add more details to your protocol steps. There should be enough detail in each step to supplement the actions seen in the video so that viewers can easily replicate the protocol. Please ensure you answer the "how" question, i.e., how is the step performed? Alternatively, add references to published material specifying how to perform the protocol action. See examples below:*

*"1.1: Unclear what we can film here. Please describe the specific actions that are being performed here, otherwise please do not highlight this step for filming."*

**We have elected to remove the CAD model design and 3D printing portions from the filming segment to allow for more detailed elaboration of the other aspects of the protocol.**

*"Line 120: Is the ratio by weight or by volume? Please specify the volume/mass of the mixture prepared here."*

**We have provided further details in this regard in Section 2.1.1 of the revised manuscript.**

*"Line 140: Please describe how to confirm fidelity. What are observed here?"*

**We have provided further details in this regard in Section 2.4 of the revised manuscript.**

*"3.2: How many fluorescent polystyrene beads are added and where are they added?"*

**We have provided further details in this regard in Section 3.2 of the revised manuscript.**

*"Line 166: What is used to capture an image?"*

**We have provided further details in this regard in Section 5.1 of the revised manuscript.**

*"Line 211: What detergent is used? Please also mention the sonication power used."*

**The detergent (Alconox) was specified in the Table of Materials document included in the original manuscript package. However, this may have been missed, since the table's description column was pushed to the second page of the document.**

**Sonication power is not user-definable for the ultrasonic cleaner used herein. However, the stated maximum sonication power for this system is 70 W. We have provided further details in this regard in Section 5.4.1 of the revised manuscript.**

*"6. Lines 157-163, 188-208, etc.: The Protocol should contain only action items that direct the reader to do something. Please write the text in the imperative tense and move the discussion about the protocol to the Discussion."*

**Done.**

*"7. Lines 214-280: Software must have a GUI (graphical user interface) and software steps must be more explicitly explained ('click', 'select', etc.). Please add more specific details (e.g. button clicks for software actions, numerical values for settings, etc.) to your protocol steps."*

**We have provided further details in this regard wherever appropriate in the protocol of the revised manuscript.**

*"8. Please include single-line spaces between all paragraphs, headings, steps, etc."*

**Done.**

*"9. After you have made all the recommended changes to your protocol (listed above), please highlight 2.75 pages or less of the Protocol (including headings and spacing) that identifies the essential steps of the protocol for the video, i.e., the steps that should be visualized to tell the most cohesive story of the Protocol."*

**Done.**

*"10. Please highlight complete sentences (not parts of sentences). Please ensure that the highlighted part of the step includes at least one action that is written in imperative tense."*

**Done.**

*"11. Please include all relevant details that are required to perform the step in the highlighting. For example: If step 2.5 is highlighted for filming and the details of how to perform the step are given in steps 2.5.1 and 2.5.2, then the sub-steps where the details are provided must be highlighted."*

**Done.**

*"12. JoVE article does not have a Conclusion section. Please move information in the Conclusion section to Results or Discussion section."*

**This portion was eliminated, to reduce redundancy.**

**REVIEWER #1 comments and Author responses:**

*"Manuscript Summary:*
*This manuscript presents a protocol for the evaluation of vascular flows in vitro. The protocol description comprises 3 major blocks: (1+2) Fabrication of the phantom, (3) preparation of the working fluid, (4) Video recording, and (5) Particle Image Velocimetry (PIV) analysis.*
*The part of mold fabrication (1+2) is interesting and provides numerous practical insights and advices, the preparation of the working fluid and recording (3+4) is more standard but can be useful. The PIV analysis (5) is less accurate and includes arbitrary subjective choices."*

*"Major Concerns:*
*My major concern is that the protocol describes in depth some steps of a more complete procedure, where some parts are not mentioned, some are faced very superficially while some others are analyzed in depth. I think that this structure can be misleading.*
*In summary, I advise to limit the protocol to phantom fabrication (1+2) with indication of image recording (3+4). Possibly mentioning how this fits into a complete in-vitro modelling of vascular systems (which include, at least, imaging/design, circulation system)."*

*"Below are my detailed comments:"*

*"1) The part of PIV analysis combines pre-filtering of images, regular PIV calculation (performed by an external package) and post-filtering/validation of the results. I find this part very superficial and not useful. There are numerous PIV packages available (that include pre/post filtering) whose optimization depends on numerous details, including image properties and calculation objectives, that cannot be covered here. Therefore, I suggest to remove this part and simply refer to a general PIV processing. Otherwise, if authors want to keep this part, I suggest that they present it as made of 3 sub-phases. One is pre-filtering (5.1, where they clarify that and their choices are possible proposal -not necessarily the optimal- among numerous others). A second is PIV calculation (where cross-correlation is one option, while there are others that more now common because better performing). The third is validation or filtering of results (NMT is one option -not necessarily the optimal- among many others)."*

**The image analysis section of the Protocol has been reformatted as suggested in the revised manuscript. In the Discussion section, we have also clarified that each of the methods described represents just one of several potential options. While we agree that other techniques may achieve higher performance (e.g., least-squares matching, hybrid PIV/PTV), this level of sophistication was deemed unnecessary for determining first-order approximations of the characteristics of current interest (i.e., intra-aneurysmal velocity fields). However, since other researchers may be interested in characteristics that are more sensitive to velocity field resolution (e.g., wall shear stress or vorticity), we have added further discussion in this regard, as well as citations to more authoritative work in this area.**

*"2) The part of preparation of the geometry for the vessel is completely missing. It comprises its design within CAD that can be based on images (which type, how recorded...?) or based on combination/deformation of simple geometric models. This preliminary phase (which would be before phase 1) is not reported or mentioned."*

**We have clarified in the Introduction of the revised manuscript that the fabricated phantom geometries are based upon idealized representations of neurovascular structures (which are generated using a common CAD software package). We have also clarified that fabrication of more complex, patient-specific geometries should be possible as well (e.g., via use of model files**

**generated by conversion of clinical imaging data into the .STL file format used by most 3D printers). However, we believe that further elaboration in this regard lies beyond the scope of the current protocol.**

*"3) Similarly to the previous point, the in-vitro circulatory system is not described. This challenging experimental aspect is not mentioned here."*

**We have provided further details in this regard in Sections 4 and 5.2 of the revised manuscript.**

*"Minor Concerns:"*
*"4) p.1 l.79. Specify the cost >$100k, or eliminate explicit figure. Because it looks a lot, if you do not consider the laser that can be easily substituted by simpler illumination systems."*

**It's been our experience that the base cost of commercial turn-key 2D PIV systems often runs well beyond $100k (not including fluorescence microscope or other ancillary equipment), hence the inclusion of this figure in the original manuscript. However, we acknowledge that there may be potential for significant variation in system configuration depending on specific users' needs, so we have eliminated this figure in the Introduction of the revised manuscript.**

*"5) The protocol is limited to steady-state conditions, which represents an important limitation for vascular vessels of pathological interest. This limitation does not appear necessary to the protocol (image recording is made with high frame rate and the experimental circulatory system is not described). Please clarify."*

**Synchronization of the video to the desired temporal positions in the waveform would be required, which would increase setup cost and complexity. Since steady-state conditions have been sufficient for the needs of our application thus far, we have not explored these avenues further.**

**<u>Reviewer #2 comments and Author responses</u>:**
*"Manuscript Summary: The authors report a method to perform PIV measurements in mm-scale phantoms of the human vascular system, claiming this to be a cheap(er) option.*

*Major Concerns: the authors claim to have a cheap way to circumvent several tools that are needed for PIV measurements. However, when using a continuous laser source (instead of pulsed) there is no need to sync the laser and the camera, this is already available in classical textbooks about PIV. Furthermore the authors do not elaborate about the light source they are using in the reported method. I think the authors should remove this claim, as the needed components are still costly (3D printer, high speed camera, microscope, light source, ultrasonic cleaner etc.)"*

**The specifics of the light source were detailed in the Table of Materials document of the original manuscript (i.e., external metal halide continuous white light source for through-objective, volumetric illumination). However, the Reviewer's comment suggests that it would've been better to also include this information within the manuscript body itself. As such, we have remedied this omission in the Introduction of the revised manuscript.**

**The intent of the protocol is not to demonstrate the most inexpensive PIV system possible, but rather to demonstrate a means for implementing PIV using resources already at the disposal of many bioengineering researchers. In doing so, this reduces the need for acquisition of some of the more costly components of a typical PIV system, thus lowering the barrier to entry for non-experts. We have clarified this point throughout the revised manuscript.**

*"Minor Concerns:"*

*"page 2, line 114, the use of acetone fumes (which is mentioned in the discussion) is a very good addition to the protocol, we do this in our lab for all flow phantoms we make to ensure a smooth surface, and also seal the print, to prevent air that resides in the phantom from entering the PDMS. Furthermore, report about the thickness of your print, and refer to printing hollow to have a good circulation of the acetone to promote dissolving the ABS. The container you pour the PDMS into should have nice flat and smooth surfaces to prevent reflection of the light source."*

**We have clarified in the Introduction of the revised manuscript that our models are based on solid prints, since this best ensures mold integrity, particularly for our most diminutive features. However, we have also added brief discussion of the virtues of hollow models as well.**

**While we acknowledge the potential advantages of acetone smoothing, our experience thus far has not shown the necessity for this operation, hence its omission from the current protocol.**

*"page 2, line 127, you can also cure in a stove to speed up the process (be done in 1 or 2 hours)."*

**We have provided further details in this regard in Section 2.2.3 of the revised manuscript.**

*"page 3, line 142, only water and glycerol will not match the refractive index with PDMS (unless you add a lot of glycerol, making the viscosity very unrealistic), you should introduce a salt, like Sodium iodide, to truly match the refractive index"*

**As discussed in the original manuscript, the 60:40 DI/glycerol mock blood solution is used widely in the experimental hemodynamics community, and the references cited make no mention of salt. This therefore suggests that perfect index matching may not be a necessity for applications such as those considered here (i.e., neurovascular flows). We have added further citations in this regard in the revised manuscript, including:**

- **Bouillot, P., Brina, O., Ouared, R., Lovblad, K.-O., Farhat, M., Pereira, V.M. Particle Imaging Velocimetry Evaluation of Intracranial Stents in Sidewall Aneurysm: Hemodynamic Transition Related to the Stent Design. *PLoS ONE*. 9 (12), e113762, doi: 10.1371/journal.pone.0113762 (2014).**
- **Trager, A.L., Sadasivan, C., Lieber, B.B. Comparison of the in vitro hemodynamic performance of new flow diverters for bypass of brain aneurysms. *Journal of biomechanical engineering.* 134 (8), 084505, doi: 10.1115/1.4006454 (2012).**

*"page, 4, line 177, elaborate about the used light source, no sheet? What about out of plane motion?"*

**As discussed earlier, the specifics of the light source were detailed in the Table of Materials document of the original manuscript (i.e., external metal halide continuous white light source for through-objective, volumetric illumination), and this information has now been added in the Introduction of the revised manuscript.**

**Volumetric illumination is chosen in the current protocol to simplify implementation. It is also commonly used in micro-PIV, since the depth of focus approaches the thickness of typical light sheets. Since the depth of focus is small at higher magnifications, out of plane motions that are large relative to the focal depth will result in potential correlation error due to mismatching, similar to that which would be seen for a light sheet. Smaller out of plane motions will contribute to cosine-error, as is also commonly encountered with light sheets.**

*"page 4, line 216, other tools like Pivlab, built in the Matlab environment is a good and versatile tool"*

**ImageJ was chosen for ease of implementation, as well as its broad familiarity to the bioengineering community.**

*"page 6, line 295, these images lack a reference, were in the phantom are these images taken? what is the scale? add vessel walls as a reference. How did you mask the images?"*

**The location of the images presented in Figs. 3 and 4 was detailed in the Representative Results section in the original manuscript (i.e., within the perforator artery). However, the Reviewer's comment suggests that it would've been better to also include this information within the captions as well. We have remedied this omission in the revised manuscript. Scale bars have also been added to these figures, as have dotted lines to demarcate the vessel walls. Finally, the location of the ROI for these measurements has been added to Figure 2.**

JOURNAL OF VISUALIZED EXPERIMENTS
1 Alewife Center #200
Cambridge, MA 02140
tel. 617.945.9051
www.jove.com

**TITLE:** Simplified protocol for meso-scale particle image velocimetry studies of neurovascular flows *in vitro*

**AUTHORS AND AFFILIATIONS:**
Ryan A. Peck[1*], Edver Bahena[1*], Reza Jahan[2], Guillermo Aguilar[1,3,4], Hideaki Tsutsui[1,4], Marko Princevac[1], Monica M. Wilhelmus[1], and Masaru P. Rao[1,3,4]

[1] Department of Mechanical Engineering, University of California, Riverside, CA, USA
[2] Division of Interventional Neuroradiology, University of California, Los Angeles, California, USA
[3] Materials Science and Engineering Program, University of California, Riverside, CA, USA
[4] Department of Bioengineering, University of California, Riverside, CA, USA

*Contributed Equally

Authors:
Ryan A. Peck: rpeck003@ucr.edu
Edver Bahena: ebahe002@ucr.edu
Reza Jahan: rjahan@mednet.ucla.edu
Guillermo Aguilar: gaguilar@engr.ucr.edu
Hideaki Tsutsui: htsutsui@engr.ucr.edu
Marko Princevac: marko@engr.ucr.edu
Monica M. Wilhelmus: monicamo@engr.ucr.edu

Corresponding Author:
Masaru P. Rao
mprao@engr.ucr.edu

**KEYWORDS:**
Particle Image Velocimetry, PDMS Tissue Phantom, 3D Printing, Fluid Mechanics, Signal Processing, Neurovascular.

**SUMMARY:**
Within this protocol we detail simplified methods for fabricating transparent neurovascular phantoms and characterizing flow therein. We highlight several important parameters and demonstrate their relationship to field accuracy.

**ABSTRACT:**
Particle Image Velocimetry (PIV) is used in a wide variety of fields, due to the opportunity it provides for precisely visualizing and quantifying flows across a large spatiotemporal range. However, its implementation typically requires use of expensive and specialized instrumentation, which limits its broader utility. Moreover, within the field of bioengineering, *in vitro* flow visualization studies are also often further limited by the high cost of commercially-sourced tissue phantoms that recapitulate desired anatomical structures, particularly for those that span the

meso-scale regime (i.e., sub-mm to mm length-scales). Herein, we present a simplified experimental protocol developed to address these limitations, the key elements of which include: 1) a relatively low-cost method for fabricating meso-scale tissue phantoms using 3D printing and silicone casting; and 2) an open-source image analysis and processing framework that reduces demand upon the instrumentation for measuring meso-scale flows (i.e., velocities up to tens of mm/s). Collectively, this lowers the barrier to entry for non-experts by leveraging resources already at the disposal of many bioengineering researchers. We demonstrate the applicability of this protocol within the context of neurovascular flow characterization; however, it is expected to be relevant to a broader range of meso-scale applications in bioengineering and beyond.

**INTRODUCTION:**

Particle image velocimetry (PIV) is widely used in experimental fluid mechanics for flow visualization and quantitative investigations of fluid motion that vary in length-scale from atmospheric to microcirculatory flows[1–3]. While the specifics of its implementation can vary as widely as its applications, one aspect common to nearly all PIV studies is the use of video imaging of tracer particles seeded within the working fluid, followed by pair-wise analysis of consecutive image frames to extract desired flow characteristics. Typically, this is accomplished by first sub-dividing each image frame into smaller regions termed interrogation windows. As a consequence of the random positions of the dispersed particles, each interrogation window contains a unique distribution of pixel intensities. If the window size and data acquisition rate are chosen appropriately, cross-correlation of the intensity signal in each window can be used to estimate the average displacement within that region. Finally, given that the magnification and frame rate are known experimental parameters, an instantaneous velocity vector field can be readily computed.

A major advantage of PIV over single-point measurement techniques is its ability to map vector fields across a two- or three-dimensional domain. Hemodynamic applications, in particular, have benefited from this capability, since it allows a thorough investigation of local flows, which are known to play a significant role in vascular disease or remodeling (e.g., atherosclerosis, angiogenesis)[4–6]. This has also been true for the evaluation of neurovascular flows, and the interactions thereof with endovascular devices (e.g., flow diverters, stents, intra-saccular coils, etc.), since the relevant lengths-scales in such applications can often span one or more orders of magnitude (e.g., micrometer to mm-scale), and device geometry and placement can significantly impact the local fluid mechanics[7].

Most groups conducting PIV-based hemodynamics studies have relied on experimental setups that closely mimic some of the earliest investigations of stent influence on vascular flow[7, 8]. Typically, these include: a) pulsed lasers and high-speed cameras, to capture high velocity flows; b) synchronizers, to prevent aliasing between the pulse frequency of the laser and the camera acquisition frame rate; c) cylindrical optics, to form a light sheet, and thus, minimize background fluorescence from tracer particles above and below the interrogation plane; and d) in the case of commercial turn-key systems, proprietary software packages, to perform the cross-correlation analyses. However, while some applications require the performance and/or versatility collectively afforded by these components, many others do not. Moreover, the high cost of

commercially-sourced tissue phantoms that recapitulate desired vascular structures can also prove limiting for many *in vitro* studies, particularly for phantoms with features that bridge the meso-scale regime (> $500/phantom). Herein, we report the development of a simplified protocol for implementing PIV for *in vitro* visualization of neurovascular flows, which typically lie both spatially and temporally within the meso-scale regime (i.e., length-scales ranging from sub-mm to mm, and velocities up to tens of mm/s). The protocol seeks to leverage resources already at the disposal of many bioengineering researchers, thus lowering the barrier to entry for non-experts.

The first element of this protocol involves the use of an investment casting technique to enable in-house fabrication of transparent, polydimethylsiloxane (PDMS)-based tissue phantoms from 3D-printed sacrificial molds. By leveraging the increasing availability of 3D printers in recent years, particularly those in shared/multi-user facilities (e.g., institutional facilities or public makerspaces), this methodology cuts cost significantly (e.g., < $100/phantom in our case), while enabling rapid turnaround for fabrication of a wide variety of designs and geometries. In the current protocol, a fused deposition modeling system is used with acrylonitrile butadiene styrene (ABS) as the build material, and the printed part serves as a sacrificial mold for the subsequent phantom casting. Our experience has shown that ABS is well-suited for such use, since it is soluble in common solvents (e.g., acetone), and it has sufficient strength and rigidity to maintain mold integrity after removal of the support material (e.g., to prevent deformation or fracture of diminutive mold features). In the current protocol, mold integrity is further ensured through the use of solid printed models, although this comes at the expense of increased dissolution time. Use of hollow models may also possible in some cases, to enhance solvent access, and thus, reduce dissolution time. However, careful consideration should be given to the effect this may have on mold integrity. Finally, while the phantoms fabricated herein are based upon idealized representations of neurovascular structures generated using a common CAD software package, the protocol is expected to be amenable to the fabrication of more complex, patient-specific geometries as well (e.g., via use of model files generated by conversion of clinical imaging data into the .STL file format used by most 3D printers). Further details regarding the phantom fabrication process are provided in Section 2 of the Protocol.

The second element of the protocol involves the use of an open-source plug-in for ImageJ to conduct the cross-correlation analyses[9]. This is coupled with the implementation of a simple statistical thresholding scheme (i.e. intensity capping)[10] to improve image signal prior to cross-correlation, as well as a post-correlation vector validation scheme, the normalized median test (NMT), to eliminate spurious vectors through comparison of each to its nearest neighbors[11]. Collectively, this allows imaging to be accomplished using equipment commonly found in many bioengineering laboratories, thus eliminating the need for acquisition of many of the costly components of typical PIV systems (e.g., pulsed laser, synchronizer, cylindrical optics, and proprietary software). Further details regarding the video collection, image processing, and data analysis are provided in Sections 5 and 6 of the Protocol.

Figure 1 illustrates the PIV setup used in this protocol, which relies upon a fluorescence microscope equipped with a high-speed camera for imaging, as well as an external, continuous

white-light source (i.e., metal halide lamp) for through-objective volumetric illumination. A variable-speed gear pump is used to impose recirculating flow of a transparent mock blood solution through the neurovascular tissue phantoms. The solution is composed of a 60:40 mixture of DI water and glycerol, which is a common substitute for blood in hemodynamics studies[12–14], due to: a) its similar density and viscosity, i.e. 1080 kg/m$^3$ & 3.5 cP, vs. 1050 kg/m$^3$ & 3.0 – 5.0 cP for blood[15, 16]; b) its transparency in the visible range; c) its similar refractive index as PDMS (1.38 vs. 1.42 for PDMS)[17–20] , which minimizes optical distortion; and d) the ease with which non-Newtonian behavior can be introduced, if needed, via the addition of xanthane[21]. Finally, fluorescent polystyrene beads are used as tracer particles (10.3 µm diameter; 480 nm/501 nm excitation/emission). While neutrally-buoyant beads are desired, sourcing tracer particles with optimal fluid mechanical properties (e.g., density, size, composition) and emission wavelength can prove challenging. For example, the beads used herein are slightly less dense than the glycerol solution (1050 kg/m$^3$ vs. 1080 kg/m$^3$). However, the hydrodynamic effects thereof are negligible, given that the duration of a typical experiment is far shorter than the time scale associated with buoyancy effects (i.e., 5 min & 20 min, respectively). Further details regarding the mock blood solution formulation and *in vitro* circulatory system setup are provided in Sections 3 and 4 of the Protocol.

**PROTOCOL:**

1. ABS-BASED SACRIFICIAL MOLD FABRICATION
    - 1.1. Design an inverse model of the desired tissue phantom using CAD software.
    - 1.2. Print the model using a 3D printer with ABS as the build material.
2. PDMS-BASED VASCULAR PHANTOM FABRICATION
    - 2.1. Mixing
        - 2.1.1. Mix the PDMS prepolymer base and curing agent in a 10:1 ratio (by weight). A 66 g mixture provides sufficient material for fabrication of phantoms with volumes up to 50 cm$^3$.
        - 2.1.2. Place the mixture in a vacuum desiccator for 60 min to degas and minimize bubble entrapment. Use cyclic pressurization/depressurization to facilitate bubble rupture.
    - 2.2. Casting
        - 2.2.1. Mount the printed ABS mold on a glass slide using molding putty to seal the interface.
        - 2.2.2. Carefully pour the PDMS mixture into the mold while trying to minimize bubble entrapment. Lingering bubbles can be manually ruptured using a needle.
        - 2.2.3. Cure the cast phantom at room temperature (25°C) for at least 24 h. At higher temperatures this process can be accelerated[22].
    - 2.3. Demolding
        - 2.3.1. Dissolve the ABS by submerging the phantom in acetone and sonicating for at least 15 min using powers up to 70 W.

            CAUTION: Acetone has high vapor pressure at room temperature and low flash point. Consequently, always work under a fume hood and away from potential ignition sources. Wear proper personal protective equipment (e.g., goggles or face shield, lab coat, acetone-resistant gloves, etc.).

2.3.2. Thoroughly rinse the phantom with isopropyl alcohol, and then DI water to remove solvent residues.

NOTE: PDMS swells upon exposure to acetone; however, swelling subsides once the phantom is rinsed and dried sufficiently[23].

2.4. Confirm phantom fidelity using optical microscopy

2.4.1. Using an optical microscope with attached camera and image capture software, capture an image of a critical feature within the phantom under a magnification that maximizes the feature within the field of view.

2.4.2. Capture an image of an appropriate calibration reticle at the same magnification.

2.4.3. Load both images into ImageJ by dragging them onto the "Toolbar".

2.4.4. Click on the calibration reticle image to make it active, and then select the "Line" tool. Using the mouse, draw a line along a feature of a known distance and select "Analyze" > "Set Scale…" from the ImageJ menu.

2.4.5. In the "Set Scale" window, the field labeled "Distance in pixels" should be pre-populated with the length of the drawn line in units of pixels. Enter the length of the feature in the field labeled "Known Distance", and its units in the field labeled "Unit of Length". Check the box labeled "Global" to apply this calibration factor to all open images.

2.4.6. Make the image of the phantom critical feature active and use the "Line" tool to draw a line along a feature of interest.

2.4.7. From the ImageJ menu, select "Analyze" > "Measure" (or press Ctrl + M) to measure the length of the line.

2.4.8. Compare the expected value against the value in the column marked "Length" in the "Results" window to confirm phantom fidelity.

3. MOCK BLOOD SOLUTION FORMULATION

3.1. Mix DI water and glycerol in a 60:40 ratio (by volume). A 100 mL volume is sufficient for the *in vitro* circulatory system described herein.

3.2. Add 1 mL of 2.5% w/v fluorescent polystyrene bead solution (i.e., tracer particles) to the mock blood solution.

3.3. Homogenize the mixture on a magnetic stir plate at 400 rpm for 10 min.

4. *IN VITRO* CIRCULATORY SYSTEM SETUP

4.1. Pump Setup

4.1.1. Use a wire stripper tool to cut off the DC-end plug from the AC to DC adapter power source.

4.1.2. Strip the coating off the power and ground wires and connect them to the input terminal of the pulse width modulation (PWM) voltage regulator.

4.1.3. Connect the power and ground wires from the pump's DC motor to the output terminal of the PWM voltage regulator. The PWM's 7-segment display outputs the duty cycle (0% - 100%) used to achieve a variable voltage to the DC motor.

4.2. Pump Calibration

4.2.1. Prepare 200 mL of mock blood solution (see Section 3).

4.2.2. Place tubing from the pump inlet to the beaker holding the mock blood solution.

4.2.3. Place tubing from the pump outlet to an empty beaker.

4.2.4. Select a desired duty cycle set-point (0% - 100%). Press the "On" button and start a timer.

4.2.5. Stop the timer once the pump has transferred the entire volume of mock blood solution. Use this time to calculate the volumetric flow rate.

4.2.6. Repeat steps 4.2.1 – 4.2.5 for at least 5 different duty cycle set-points to establish a least-squares regression curve. A minimum of three replicate points per duty cycle set-point is recommended. This relationship can be used to correlate the desired flow rate to the required PWM duty cycle.

## 5. VIDEO COLLECTION

### 5.1. Image calibration

5.1.1. Determine calibration ratio for the video imaging (see Section 2).

### 5.2. Apparatus set up

5.2.1. Place the PDMS phantom on the stage of the fluorescence microscope.

5.2.2. Connect the phantom to the gear pump and introduce the mock blood solution.

*(Optional)* Pre-fill the model with ethanol to facilitate full wetting, then flush and fill with mock blood solution. This may be particularly beneficial for models with smaller vessels and/or blind features.

5.2.3. Set the pump motor controller for the desired flow rate based on the pump calibration curve.

5.2.4. Run the pump for 1 - 5 min prior to the experiment to ensure steady-state conditions.

5.2.5. Turn on the external lamp to illuminate the field of view. Select an appropriate filter based upon the excitation wavelength of the fluorescent beads.

5.2.6. Adjust the imaging focal plane to the vessel mid-plane. This can be achieved by using a focal length that maximizes the imaged vessel cross-section (e.g., when using phantoms with circular vessel cross sections); and/or indexing off of a phantom feature designed to facilitate identification of the vessel mid-plane.

### 5.3. Video recording

5.3.1. Select the video recording parameters to optimize signal-to-noise ratio (SNR). Key parameters include exposure time, frame rate, and gain. In this protocol we use a frame rate of 2000 fps, and a gain of 1.0. However, these parameters may vary based on application (see Discussion section for further details).

5.3.2. Collect video and save in AVI format.

### 5.4. Phantom clean up

5.4.1. If bead-sticking is observed after an experiment, sonicate the phantom in an aqueous detergent solution using powers up to 70 W.

## 6. IMAGE PROCESSING AND DATA ANALYSIS

### 6.1. Image pre-processing

6.1.1. Drag the saved AVI file onto the ImageJ window to import it. Select the box marked "Convert to Grayscale".

6.1.2. From the “ImageJ” menu, select “Analyze” > “Generate Histogram” (or press Ctrl + H) to generate a histogram of image pixel intensities. Take note of the mean and standard deviation for the unprocessed image.

NOTE: At high frame rates, it is not unusual for the distribution to be skewed heavily toward zero (i.e., no signal).

6.1.3. From the “ImageJ” menu, select “Image” > “Adjust”> “Brightness and Contrast” (or press Shift + Ctrl + H) to apply a brightness/contrast filter.

6.1.4. On the “Brightness and Contrast” menu, press the “Set” button to define the image limits. Set the minimum value to be the mean value plus one standard deviation, and the maximum value to be the maximum intensity of the image (both based on statistics obtained in Section 6.1.2).

NOTE: This typically eliminates all but the top 10% of pixel intensities. The number of standard deviations may be varied depending on the desired distribution of pixel intensities. A custom macro script for performing the intensity capping operation is provided in the Supplemental Material.

6.1.5. From the “ImageJ” menu, select “Process” > “Noise” > “Despeckle” to reduce the number of saturated pixels.

NOTE: This operation is necessitated by the increased potential for pixel saturation that arises during optimization of brightness and contrast, which can produce spurious vectors during subsequent cross-correlation.

6.1.6. From the “ImageJ” menu, select “Process” > “Filters” > “Gaussian Blur” with a radius of 1.5 to reduce artifacts arising from the occasional removal of illuminated pixels in a 3x3 neighborhood by the prior despeckling operation.

6.1.7. Click on the “Polygon” tool, and then click within the image to outline the region of interest (ROI).

6.1.8. From the “ImageJ” menu, select “Edit” > “Clear Outside” to remove sensor noise in locations where no signal is expected (e.g., areas beyond vessel wall boundary), which can decrease overall SNR.

6.2. PIV Calculation

NOTE: This portion of the protocol employs a third-party PIV plug-in for ImageJ, which relies upon Gaussian peak-fitting to enable estimation of displacement with sub-pixel accuracy.

6.2.1. From the “ImageJ” menu, select “Plugins” > “Macros” > “Run…” and navigate to the saved macro “Supplemental Code 2.ijjm” to cross-correlate successive image pairs.

NOTE: The macro proceeds as follows:1) Cross-correlation of the intensity field

within consecutive images is first performed to determine the local displacement of advected tracer particles, i.e. the first image pair consists of the first and second images, the second image pair consists of the second and third images, etc.; 2) a two-step multi-pass evaluation is then performed with initial and final interrogation window sizes of 256 x 256 pixels and 128 x 128 pixels, respectively; and finally, 3) the macro performs a temporal average to further reduce the appearance of spurious vectors.

6.3. Normalized median test (NMT)

6.3.1. From the "ImageJ" menu, select "Plugins" > "Macros" > "Run…" and navigate to the saved macro "Supplemental Code 3.ijjm" to validate the velocity fields via the normalized median test.

NOTE: The macro proceeds as follows: 1) each vector in an instantaneous vector field is first compared to its eight nearest neighbors to compute the median value; 2) the array of residual errors is then calculated as the difference between each neighboring vector and the calculated median; 3) the difference between the vector under investigation and the median neighboring vector value is then normalized by the median of the residuals; 4) this is then compared to a threshold value (typically 0.2 pixels), which can be varied based on *a priori* knowledge of noise during image acquisition; and finally, 5) a temporal average of all validated instantaneous vector fields is performed to produce a composite field, as this has been shown to increase the vector field quality[24].

**REPRESENTATIVE RESULTS:**

Figure 2 illustrates the PDMS tissue phantom fabrication process. The phantoms designed herein are intended for the study of flow in idealized wide-necked, saccular, intracranial aneurysms, as well as proximal branching perforator arteries. Important additional design features include: 1) a common reservoir that all vessels drain into, to ensure unencumbered fluid egress from the phantom, otherwise droplet formation may occur at the smaller vessel outlets; 2) a bubble trap, to facilitate bubble removal; 3) an outer cavity wall, to ensure parallelism of the vessel with the horizontal plane, as well as precise definition of the final phantom slab height, length and width; and 4) use of a 21 gauge hypodermic needle shank (820 µm nominal outer diameter) for molding of the perforator artery, due to our printer's inability to define such features with sufficient fidelity. Faithful reproduction of all design features is observed throughout.

Representative results for PIV-based flow characterization performed using the current protocol are presented in Figures 3 and 4. These studies were performed using phantom inlet flow rates of 100 mL/min, data acquisition rates of 2000 fps, and temporal averaging over spans of 0.05 s. Figure 3 shows representative image frames within the perforator artery, before and after intensity capping as well as corresponding surface plots of the 8-bit pixel intensity values. Both demonstrate that intensity capping significantly increases peak definition above the noise floor (i.e., increases SNR), which is critical to ensuring accuracy when performing subsequent cross-correlation. Figure 4 shows the effects of intensity capping and NMT operations on the velocity

vector field. Marked improvement in field uniformity is observed, thus further underscoring the importance of maximizing SNR to minimize data dropout.

**FIGURE AND TABLE LEGENDS:**

**Figure 1: Particle image velocimetry setup.** Reliance upon an open-source image analysis and pre/post-processing framework reduces demand upon the instrumentation for measuring meso-scale flows, thus eliminating the need for many of the costly components of typical PIV systems (e.g., pulsed laser, synchronizer, cylindrical optics, &/or proprietary software).

**Figure 2: PDMS-based tissue phantom fabrication process:** a) CAD model of neurovascular phantom mold; b) Printed ABS mold, after removal of support material; c) Casting and curing of PDMS within the ABS mold; d) Partial dissolution of ABS mold material; and e) Completed PDMS phantom, with inset showing final dimensions of critical features, as well as the region of interest (ROI) in the perforator artery where the PIV measurements were made.

**Figure 3: Effect of intensity capping operation on image SNR.** Representative image frame and corresponding pixel intensity surface plots within the perforator artery, before (a, b) and after applying the intensity capping operation (c, d).

**Figure 4: Effects of intensity capping and NMT operations on velocity vector fields:** Representative instantaneous velocity vector field within the perforator artery derived from: a) unprocessed image data; b) intensity capped data; and c) intensity capped data + NMT post-processing.

**Figure 5: Effect of interrogation window sizing on correlation quality.** Optimal window sizing occurs when the value of the zero-normalized correlation coefficient is maximized, and the standard deviation is minimized.

**DISCUSSION:**

The protocol described herein outlines a simplified method for performing PIV studies to visualize neurovascular flows at physiologically-relevant dimensions and flow conditions *in vitro*. In doing so, it serves to complement protocols reported by others that have also focused on simplifying the quantification of vector fields, but within very different contexts that require consideration of far larger length-scales[25] or lower flow rates[26, 27](e.g. atmospheric or microcirculatory flows), and thus, reliance upon schemes that are incompatible with the current application.

The most important considerations for successful implementation of PIV lie in the minimization of flow field artifacts and maximization of image quality. Several steps in the tissue phantom fabrication process are critical to both of these criteria. For example, thorough degassing is crucial since air entrained within the PDMS during mixing can lead to bubble formation within the final phantom, which can adversely affect both feature fidelity and optical clarity. Additionally, minimization of surface roughness of the ABS mold is desired, since the PDMS casting process faithfully reproduces even the most minute imperfections (e.g., build lines, surface pores,

scratches, etc.), thus resulting in surface roughness in the final phantom that can decrease optical clarity and increase potential for bead accumulation. While the protocol described herein has proven sufficient for the current application, there are numerous reports in the literature of means for reducing such roughness, should there be need (e.g., acetone vapor smoothing[28], or optimization of layer thickness and part orientation with respect to build direction)[29].

Parameter selection for video capture is also critical to ensure a high-fidelity vector field. Optimal SNR is typically achieved at the highest achievable frame rate that still allows sufficient bead exposure (maximum frame rate being limited by minimum exposure time). Gain can be used to amplify the signal, but this also increases sensor noise. If the maximum velocity can be estimated from other flow parameters (e.g., inlet volumetric flow rate), then a lower bound on the required frame rate can be estimated using the following relation[30]:

$$f_{sampling} > \frac{v_{max} \cdot c_{calibration}}{h_{interrogation\ window}} \quad \textbf{(1)}$$

where $f_{sampling}$ is the camera acquisition rate (Hz), $v_{max}$ is the maximum expected velocity (mm/s), $c_{calibration}$ is the calibration constant (pixels/mm), and $h_{interrogation\ window}$ is the size of the interrogation window (pixels). However, more optimal values can be determined using so-called correlation quality estimation techniques, such as the zero-normalized correlation coefficient[11]. In this technique, the averages of complementary signals from each frame-pair are first subtracted, and then normalized by the standard deviation of their intensities[11]. If a displacement of the original signal exists, such that all peaks and valleys match, the time-shifted value of this signal will be equal to one. Conversely, if there is no displacement that can align these signals, the value will be zero. This information is included in the ImageJ PIV output for each vector, and it can be plotted as its own field to verify whether there are spatial effects contributing to poor correlation (e.g., uneven lighting). The correlation coefficient can also be averaged over a field as an overall estimate of its quality. Finally, this quantity may also be plotted against varying frame rates or interrogation window sizes to determine an optimum. Figure 5 illustrates the results from such an analysis using a Monte-Carlo synthesized particle field with displacements consistent with our experimentally-measured flows (a typical technique for characterizing correlation quality[11]). The results show that the interrogation window size and frame rate should be chosen such that a particle field is displaced by ≤ 20% of the interrogation window size per frame-pair to maximize the correlation coefficient, while minimizing its variability.

Although the protocol described herein has proven sufficient for meeting the needs of the current application, it is important to acknowledge its limitations. For example, while contrast enhancement via intensity capping offers ease of implementation, transformations of the entire distribution of pixel intensities may improve SNR further[31]. Similarly, although correlation-based tracking is well-established and provides sufficient resolution for reliably estimating first-order flow characteristics relevant to hemodynamics (e.g., intra-aneurysmal velocity), other techniques may offer higher spatial resolution (e.g., hybrid PIV/PTV, least squares matching)[32, 33], and thus greater accuracy when considering characteristics that are more sensitive to velocity field resolution (e.g., wall shear stress, in-plane vorticity). Likewise, while the NMT provides a means

for improving the velocity vector field after cross-correlation, it is important to emphasize that this is just one of many vector validation techniques that could be used[24, 34], each with their own unique advantages and disadvantages that may make their use more suitable for applications beyond those described here. Lastly, while our experimental setup seeks to mimic physiologically-relevant flow rates and length scales for the neurovasculature, it does not currently allow the analysis of pulsatile flows. This has not been a limitation for our current application, since the range of Womersely numbers in much of the neurovasculature tends to be ≤ 1 (i.e., there is minimal additive effect of multiple cardiac cycles)[35], which suggests that steady-state conditions are sufficient to recapitulate discrete time points along the cardiac waveform in which the flow rate is comparable. However, for applications where the Womersely number is larger (e.g., vasculature closer to the heart), we envision potential for introducing pulsatility through the use of an Arduino, which could be used to send the pump a time-varying PWM voltage waveform that enables mimicking of a cardiac flow profile[36–38].

**ACKNOWLEDGMENTS:**

The authors acknowledge partial support for this project provided by a Collaborative Seed Grant from the Office of Research and Economic Development at UC Riverside.

**DISCLOSURES:**

The authors declare no competing financial interests.

**REFERENCES**

1. Grant, I. Particle image velocimetry: A review. *Proceedings of the Institution of Mechanical Engineers, Part C: Journal of Mechanical Engineering Science*. **211** (1), 55–76, doi: 10.1243/0954406971521665 (1997).
2. Lindken, R., Rossi, M., Große, S., Westerweel, J. Micro-Particle Image Velocimetry (µPIV): Recent developments, applications, and guidelines. *Lab on a Chip*. **9** (17), 2551, doi: 10.1039/b906558j (2009).
3. Hove, J.R., Köster, R.W., Forouhar, A.S., Acevedo-Bolton, G., Fraser, S.E., Gharib, M. Intracardiac fluid forces are an essential epigenetic factor for embryonic cardiogenesis. *Nature*. **421**, 172, at <http://dx.doi.org/10.1038/nature01282> (2003).
4. Ando, J., Yamamoto, K. Vascular Mechanobiology. *Circulation Journal*. **73** (11), 1983–1992, doi: 10.1253/circj.CJ-09-0583 (2009).
5. Conway, D.E., Breckenridge, M.T., Hinde, E., Gratton, E., Chen, C.S., Schwartz, M.A. *Fluid Shear Stress on Endothelial Cells Modulates Mechanical Tension across VE-Cadherin and PECAM-1*. *Current Biology*. **23** (11), at <http://www.sciencedirect.com/science/article/pii/S0960982213004909>. (2013).
6. Kuhlencordt, P.J. *et al.* Accelerated Atherosclerosis, Aortic Aneurysm Formation, and Ischemic Heart Disease in Apolipoprotein E/Endothelial Nitric Oxide Synthase Double-Knockout Mice. *Circulation*. **104** (4), 448–454, doi: 10.1161/hc2901.091399 (2001).
7. Lieber, B.B., Stancampiano, A.P., Wakhloo, A.K. Alteration of hemodynamics in aneurysm models by stenting: Influence of stent porosity. *Annals of Biomedical Engineering*. **25** (3), 460–469, doi: 10.1007/BF02684187 (1997).
8. Bulusu, K. V., Plesniak, M.W. Experimental Investigation of Secondary Flow Structures

Downstream of a Model Type IV Stent Failure in a 180˚ Curved Artery Test Section. *Journal of Visualized Experiments*. (113), e51288–e51288, doi: 10.3791/51288 (2016).

9. Tseng, Q. *et al.* Spatial organization of the extracellular matrix regulates cell-cell junction positioning. *Proceedings of the National Academy of Sciences of the United States of America*. **109** (5), 1506–11, doi: 10.1073/pnas.1106377109 (2012).
10. Shavit, U., Lowe, R.J., Steinbuck, J. V Intensity Capping: a simple method to improve cross-correlation PIV results. *Experiments in Fluids*. **42** (2), 225–240, doi: 10.1007/s00348-006-0233-7 (2007).
11. M. Raffel, C. Willert, S. Werely, J.K. *Particle Image Velocimetry: a Practical Guide*. Springer. New York. (2007).
12. Kerl, H.U. *et al.* Implantation of Pipeline Flow-Diverting Stents Reduces Aneurysm Inflow Without Relevantly Affecting Static Intra-aneurysmal Pressure. *Neurosurgery*. **74** (3), 321–334, at <http://dx.doi.org/10.1227/NEU.0000000000000253> (2014).
13. Lieber, B.B., Livescu, V., Hopkins, L.N., Wakhloo, A.K. Particle Image Velocimetry Assessment of Stent Design Influence on Intra-Aneurysmal Flow. *Annals of Biomedical Engineering*. **30** (6), 768–777, doi: 10.1114/1.1495867 (2002).
14. Charonko, J., Karri, S., Schmieg, J., Prabhu, S., Vlachos, P. *In vitro*, time-resolved PIV comparison of the effect of stent design on wall shear stress. *Annals of biomedical engineering*. **37** (7), 1310–21, doi: 10.1007/s10439-009-9697-y (2009).
15. Rand, P.W., Lacombe, E., Hunt, H.E., Austin, W.H. Viscosity of normal human blood under normothermic and hypothermic conditions. *Journal of Applied Physiology*. **19** (1), 117–122, doi: 10.1152/jappl.1964.19.1.117 (1964).
16. Kenner, T., Leopold, H., Hinghofer-Szalkay, H. The continuous high-precision measurement of the density of flowing blood. *Pflügers Archiv European Journal of Physiology*. **370** (1), 25–29, doi: 10.1007/BF00707941 (1977).
17. Hoyt, L.F. New Table of the Refractive Index of Pure Glycerol at 20°C. *Industrial & Engineering Chemistry*. **26** (3), 329–332, doi: 10.1021/ie50291a023 (1934).
18. Cai, Z., Qiu, W., Shao, G., Wang, W. A new fabrication method for all-PDMS waveguides. *Sensors and Actuators A: Physical*. **204**, 44–47, doi: https://doi.org/10.1016/j.sna.2013.09.019 (2013).
19. Bouillot, P., Brina, O., Ouared, R., Lovblad, K.-O., Farhat, M., Pereira, V.M. Particle imaging velocimetry evaluation of intracranial stents in sidewall aneurysm: hemodynamic transition related to the stent design. *PloS one*. **9** (12), e113762, doi: 10.1371/journal.pone.0113762 (2014).
20. Trager, A.L., Sadasivan, C., Lieber, B.B. Comparison of the *in vitro* hemodynamic performance of new flow diverters for bypass of brain aneurysms. *Journal of biomechanical engineering*. **134** (8), 084505, doi: 10.1115/1.4006454 (2012).
21. Clauser, J. *et al.* A Novel Plasma-Based Fluid for Particle Image Velocimetry (PIV): *In-Vitro* Feasibility Study of Flow Diverter Effects in Aneurysm Model. *Annals of Biomedical Engineering*. **46** (6), 841–848, doi: 10.1007/s10439-018-2002-1 (2018).
22. Johnston, I.D., McCluskey, D.K., Tan, C.K.L., Tracey, M.C. Mechanical characterization of bulk Sylgard 184 for microfluidics and microengineering. *Journal of Micromechanics and Microengineering*. **24** (3), 035017, doi: 10.1088/0960-1317/24/3/035017 (2014).
23. Lee, J.N., Park, C., Whitesides, G.M. Solvent Compatibility of Poly(dimethylsiloxane)-Based

Microfluidic Devices. *Analytical Chemistry*. **75** (23), 6544–6554, doi: 10.1021/ac0346712 (2003).

24. Meinhart, C.D., Wereley, S.T., Santiago, J.G. A PIV Algorithm for Estimating Time-Averaged Velocity Fields. *Journal of Fluids Engineering*. **122** (2), 285, doi: 10.1115/1.483256 (2000).
25. Bosbach, J., Kühn, M., Wagner, C., Raffel, M., Resagk, C. Large-Scale Particle Image Velocimetry of Natural and Mixed Convection. *13th Int Symp on Applications of Laser Techniques to Fluid Mechanics* (2006).
26. Meinhart, C.D., Wereley, S.T., Santiago, J.G. PIV measurements of a microchannel flow. *Experiments in Fluids*. **27** (5), 414–419, doi: 10.1007/s003480050366 (1999).
27. Lima, R. *et al. In vitro* blood flow in a rectangular PDMS microchannel: experimental observations using a confocal micro-PIV system. *Biomedical Microdevices*. **10** (2), 153–167, doi: 10.1007/s10544-007-9121-z (2008).
28. Kuo, C.-C., Mao, R.-C. Development of a Precision Surface Polishing System for Parts Fabricated by Fused Deposition Modeling. *Materials and Manufacturing Processes*. **31** (8), 1113–1118, doi: 10.1080/10426914.2015.1090594 (2016).
29. Kang, K., Oh, S., Yi, H., Han, S., Hwang, Y. Fabrication of truly 3D microfluidic channel using 3D-printed soluble mold. *Biomicrofluidics*. **12** (1), 014105, doi: 10.1063/1.5012548 (2018).
30. Prasad, A.K. Particle Image Velocimetry. *Current Science*. **79** (1), 51–60 (2000).
31. Dellenback, P.A., Macharivilakathu, J., Pierce, S.R. Contrast-enhancement techniques for particle-image velocimetry. *Applied Optics*. **39** (32), 5978–5990, doi: 10.1364/AO.39.005978 (2000).
32. Cowen, E.A., Monismith, S.G. A hybrid digital particle tracking velocimetry technique. *Experiments in fluids*. **22** (3), 199–211 (1997).
33. Gruen, A.W. Adaptive least squares correlation: a powerful image matching technique. *South African Journal of Photogrammetry, Remote Sensing and Cartography*. **14** (3), 175–187, at <http://citeseerx.ist.psu.edu/viewdoc/summary;jsessionid=8478C7133B070BA354E5DED2EFF60262?doi=10.1.1.93.6891\nhttp://www.idb.arch.ethz.ch/files/alsm_awgruen.pdf> (1985).
34. Nogueira, J., Lecuona, A., Rodríguez, P.A. Data validation, false vectors correction and derived magnitudes calculation on PIV data. *Measurement Science and Technology*. **8** (12), 1493–1501, doi: 10.1088/0957-0233/8/12/012 (1997).
35. Loudon, C., Tordesillas, A. The Use of the Dimensionless Womersley Number to Characterize the Unsteady Nature of Internal Flow. *Journal of Theoretical Biology*. **191** (1), 63–78, doi: https://doi.org/10.1006/jtbi.1997.0564 (1998).
36. Drost, S., De Kruif, B.J., Newport, D. Arduino control of a pulsatile flow rig. *Medical Engineering and Physics*. **51**, 67–71, doi: 10.1016/j.medengphy.2017.10.006 (2017).
37. Tsai, W., Savaş, Ö. Flow pumping system for physiological waveforms. *Medical & Biological Engineering & Computing*. **48** (2), 197–201, doi: 10.1007/s11517-009-0573-6 (2010).
38. Kato, T., Indo, T., Yoshida, E., Iwasaki, Y., Sone, M., Sobue, G. Contrast-enhanced 2D cine phase MR angiography for measurement of basilar artery blood flow in posterior circulation ischemia. *AJNR. American journal of neuroradiology*. **23** (8), 1346–51, at <http://www.ncbi.nlm.nih.gov/pubmed/12223376> (2002).

jove JOURNAL OF VISUALIZED EXPERIMENTS
1 Alewife Center #200
Cambridge, MA 02140
tel. 617.945.9051
www.jove.com

**TITLE:** Simplified protocol for meso-scale particle image velocimetry studies of neurovascular flows ~~*in vitro*~~*in vitro*

Formatted: Font: Italic

**AUTHORS AND AFFILIATIONS:**
Ryan A. Peck[1*], Edver Bahena[1*], Reza Jahan[2], Guillermo Aguilar[1,3,4], Hideaki Tsutsui[1,4], Marko Princevac[1], Monica M. Wilhelmus[1], and Masaru P. Rao[1,3,4]

[1] Department of Mechanical Engineering, University of California, Riverside, CA, USA
[2] Division of Interventional Neuroradiology, University of California, Los Angeles, California, USA
[3] Materials Science and Engineering Program, University of California, Riverside, CA, USA
[4] Department of Bioengineering, University of California, Riverside, CA, USA

*Contributed Equally

Authors:
Ryan A. Peck: rpeck003@ucr.edu
Edver Bahena: ebahe002@ucr.edu
Reza Jahan: rjahan@mednet.ucla.edu
Guillermo Aguilar: gaguilar@engr.ucr.edu
Hideaki Tsutsui: htsutsui@engr.ucr.edu
Marko Princevac: marko@engr.ucr.edu
Monica M. Wilhelmus: monicamo@engr.ucr.edu

Corresponding Author:
Masaru P. Rao
mprao@engr.ucr.edu

**KEYWORDS:**
Particle Image Velocimetry, PDMS Tissue Phantom, 3D Printing, Fluid Mechanics, Signal Processing, Neurovascular.

**SUMMARY:**
Within this protocol we detail simplified methods for fabricating transparent neurovascular phantoms and characterizing flow therein. We highlight several important parameters and demonstrate their relationship to field accuracy.

**ABSTRACT:**
Particle Image Velocimetry (PIV) is used in a wide variety of fields, due to the opportunity it provides for precisely visualizing and quantifying flows across a large spatiotemporal range. However, its implementation typically requires use of expensive and specialized instrumentation, which limits its broader utility. Moreover, within the field of bioengineering, *in vitro* flow

visualization studies are also often further limited by the high cost of commercially-sourced tissue phantoms that recapitulate desired anatomical structures, particularly for those that span the meso-scale regime (i.e., sub-mm to mm length-scales). Herein, we present a simplified experimental protocol developed to address these limitations, the key elements of which include: 1) a relatively low-cost method for fabricating meso-scale tissue phantoms using 3D printing and silicone casting; and 2) an open-source image analysis and ~~pre/post-~~processing framework that reduces demand upon the instrumentation for measuring meso-scale flows (i.e., velocities up to tens of mm/s). Collectively, this lowers the barrier to entry for non-experts by leveraging resources already at the disposal of many bioengineering researchers. ~~, thus circumventing the~~ applicability of this protocol within the context of neurovascular flow characterization; however, it is expected to be relevant to a broader range of meso-scale applications in bioengineering and beyond.

**INTRODUCTION:**

Particle image velocimetry (PIV) is widely used in experimental fluid mechanics for flow visualization and quantitative investigations of fluid motion that vary in length-scale from atmospheric to microcirculatory flows[1–3]. While the specifics of its implementation can vary as widely as its applications, one aspect common to nearly all PIV studies is the use of video imaging of tracer particles seeded within the working fluid, followed by pair-wise analysis of consecutive image frames to extract desired flow characteristics. Typically, this is accomplished by first sub-dividing each image frame into smaller regions termed interrogation windows. As a consequence of the random positions of the dispersed particles, each interrogation window contains a unique distribution of pixel intensities. If the window size and data acquisition rate are chosen appropriately, cross-correlation of the intensity signal in each window can be used to estimate the average displacement within that region. Finally, given that the magnification and frame rate are known experimental parameters, an instantaneous velocity vector field can be readily computed.

A major advantage of PIV over single-point measurement techniques is its ability to map vector fields across a two- or three-dimensional domain. Hemodynamic applications, in particular, have benefited from this capability, since it allows a thorough investigation of local flows, which are known to play a significant role in vascular disease or remodeling (e.g., atherosclerosis, angiogenesis)[4–6]. This has also been true for the evaluation of neurovascular flows, and the interactions thereof with endovascular devices (e.g., flow diverters, stents, intra-saccular coils, etc.), since the relevant lengths-scales in such applications can often span one or more orders of magnitude (e.g., micrometer to mm-scale), and device geometry and placement can significantly impact the local fluid mechanics[7].

Most groups conducting PIV-based hemodynamics studies have relied on experimental setups that closely mimic some of the earliest investigations of stent influence on vascular flow[7, 8]. Typically, these include: a) pulsed lasers and high-speed cameras, to capture high velocity flows; b) synchronizers, to prevent aliasing between the pulse frequency of the laser and the camera acquisition frame rate; c) cylindrical optics, to form a light sheet, and thus, minimize background fluorescence from tracer particles above and below the interrogation plane; and d) in the case of

commercial turn-key systems, proprietary software packages, to perform the cross-correlation analyses. However, while some applications require the performance and/or versatility collectively afforded by these components, many others do not~~, thus making it sometimes difficult to justify the high cost of such systems.~~ ~~(which can reach up to > $100k)~~. ~~-~~Moreover, the high cost of commercially-sourced tissue phantoms that recapitulate desired vascular structures can also prove limiting for many ~~*in vitro*~~*in vitro* studies, particularly for phantoms with features that bridge the meso-scale regime (> $500/phantom). ~~It must be emphasized that the intent of this protocol is to outline a methodology to perform PIV with lab components that are already accessible to bioengineering laboratories. It is out of the scope of this document to provide a detailed guide on PIV and the reader is referred to comprehensive texts for variations on the method (CITE). Here, we lay out a fail-proof framework that can be readily applied even if one lacks experience with this measurement technique.~~ Herein, we report the development of a simplified~~e~~ ~~and low-cost~~ protocol for implementing PIV for *in vitro* visualization of neurovascular flows, which typically lie both spatially and temporally within the meso-scale regime (i.e., length-scales ranging from sub-mm to mm, and velocities up to tens of mm/s). The protocol seeks to leverage resources already at the disposal of many bioengineering researchers, thus lowering the barrier to entry for non-experts.

~~It must be emphasized that the intent of this protocol is to outline a methodology to perform PIV~~ in-house fabrication of transparent, polydimethylsiloxane (PDMS)~~silicone~~-based tissue phantoms from 3D-printed sacrificial ~~acrylonitrile butadiene styrene (ABS)~~ molds. By leveraging the increasing availability of 3D printers in recent years, particularly those in shared/multi-user facilities (e.g., institutional facilities or public makerspaces), this methodology cuts cost significantly (e.g., < $100/phantom in our case), while enabling rapid turnaround for fabrication of a wide variety of designs and geometries. In the current protocol, a fused deposition modeling system is used with acrylonitrile butadiene styrene (ABS) as the build material, and the printed part serves as a sacrificial mold for the subsequent phantom casting. Our experience has shown that ABS is well-suited for such use, since it is soluble in common solvents (e.g., acetone), and it has sufficient strength and rigidity to maintain mold integrity after removal of the support material (e.g., to prevent deformation or fracture of diminutive mold features). In the current protocol, mold integrity is further ensured through the use of solid printed models, although this comes at the expense of increased dissolution time. Use of hollow models may also possible in some cases, to enhance solvent access, and thus, reduce dissolution time. However, careful consideration should be given to the effect this may have on mold integrity. Finally, while the phantoms fabricated herein are based upon idealized representations of neurovascular structures generated using a common CAD software package, the protocol is expected to be amenable to the fabrication of more complex, patient-specific geometries as well (e.g., via use of model files generated by conversion of clinical imaging data into the .STL file format used by most 3D printers). Further details regarding the phantom fabrication process are provided in ~~Protocol~~ Section ~~s 1 and~~ 2 of the Protocol.

The second element of the protocol involves the use of an open-source plug-in for ImageJ to conduct the cross-correlation analyses[9]. This is coupled with the implementation of a simple statistical thresholding scheme (i.e. intensity capping)[10] to improve image signal prior to cross-

Field Code Changed

Field Code Changed

correlation, ~~and~~ as well as a post-correlation vector validation scheme, the normalized median (NMT), to eliminate spurious vectors through comparison of each to its nearest neighbors[11]. Collectively, this allows imaging to be accomplished using equipment commonly found in many bioengineering laboratories ~~(e.g., fluorescence microscope with filtered, continuous white light)~~, thus eliminating the need for acquisition of many of the costly components of typical PIV systems (e.g., pulsed laser, synchronizer, cylindrical optics, and proprietary software). Further details regarding the video collection, image processing, and data analysis are provided in Sections 5 and 6 of the Protocol.

Figure 1 illustrates ~~the various components of~~ the PIV setup used in this ~~study~~protocol, which relies upon a fluorescence microscope equipped with a high-speed camera for imaging, as well as an external, continuous white-light source (i.e., metal halide lamp) for through-objective volumetric illumination. A ~~, which also includes a~~ variable-speed gear pump is used to ~~to enable~~impose recirculating flow of a transparent mock blood solution ~~of a transparent mock blood solution~~ through ~~PDMS-based~~the neurovascular tissue phantoms. The solution ~~–~~is composed of a 60:40 mixture of DI water and glycerol, which is a common substitute for blood in hemodynamics studies[12–14], due to: a) its similar density and viscosity, i.e. 1080 kg/m$^3$ & 3.5 cP, vs. 1050 kg/m$^3$ & 3.0 – 5.0 cP for blood[15, 16]; b) its transparency in the visible range; c) its similar refractive index as PDMS (1.38 vs. 1.42 for PDMS)[17–20] ~~20, 21~~, which minimizes optical and d) the ease with which non-Newtonian behavior can be introduced, if needed, via the addition of xanthane[21]. Finally, fluorescent polystyrene beads are used as tracer particles (10.3 µm diameter; 480 nm/501 nm excitation/emission). While neutrally-buoyant beads are desired, sourcing tracer particles with optimal fluid mechanical properties (e.g., density, size, composition) and emission wavelength can prove challenging. For example, the beads used herein are slightly less dense than the glycerol solution (1050 kg/m$^3$ vs. 1080 kg/m$^3$). However, the hydrodynamic effects thereof are negligible, given that the duration of a typical experiment is far shorter than the time scale associated with buoyancy effects (i.e., 5 min & 20 min, respectively). Further details regarding the mock blood solution formulation and ~~,~~ *in vitro* circulatory system setup~~video collection, image processing, and data analysis~~ are provided in Sections 3 and 4 of the Protocol ~~Sections 3 to 5~~.

**PROTOCOL:**

1. ABS-BASED SACRIFICIAL MOLD FABRICATION
   - 1.1. Design an inverse model of the desired tissue phantom using CAD software.
   - ~~1.~~1.2. Print the model using a 3D printer with ABS as the build material.
   - ~~Design inverse model of desired tissue phantom using CAD software. The design used in~~
   - 2.1. Mixing
     - 2.1.1. ~~In a disposable weigh boat,~~ Mix the PDMS prepolymer base and curing agent in a mixture provides sufficient material for fabrication of phantoms with volumes up to 50~~XXX~~ ~~m~~cm$^3$ ~~of 60g base to 6g curing agent for 5 to 10 min~~.
     - Place the mixture in a vacuum desiccator for 60 min to degas and minimize bubble entrapment. Use cyclic pressurization/depressurization to facilitate bubble
   - Casting
     - 2.2.1. Mount the printed ABS mold on a glass slide using molding putty to seal the

Field Code Changed

Formatted: Highlight

Commented [A5]: Where do I mix it? What type of container? Does it need to be flat, deep?

Formatted: Highlight

Formatted: Highlight

Formatted: Highlight

Formatted: Highlight

interfaceMount printed ABS mold on a 75mm x 25mm glass slide such so that the top

Carefully pour the PDMS mixture into the mold while trying to minimize bubble entrapment. Lingering bubbles can be manually ruptured using a needlePour PDMS

2.2. Curing

temperatures this process can be accelerated[22].

2.3. Demolding

2.3.1. Dissolve the ABS by submerging the phantom in acetone and sonicating for at least 15 min using powers up to 70 W.

Place in ultrasonicaultrasonic bath to facilitate the dissolving of the ABS.

2.3.2. Thoroughly rinse the phantom with isopropyl alcohol, and then DI water to remove solvent residuesRinse phantom with isopropyl alcohol and DI water and check to

phantom is rinsed and dried sufficiently[23].

2.4. Phantom fidelity verification

2.4.1. Using an optical microscope with attached camera and image capture software, capture an image of a critical feature within the phantom under a magnification that maximizes the feature within the field of view.

Save the imagean image of the phantom under magnification. (For the example data

2.4.3. Load both images into ImageJ by dragging them onto the "ImageJ Ttoolbar".

2.4.4. MakeClick on -the calibration reticle image to make it active, and then select the "Lline" tool. Using the mouse, d Draw a line along a feature of a known distance and select "Analyze" > "Set Scale…" from the ImageJ menu.

2.4.5. In the "Sset Sscale" window, the field labeled "Distance in pixels" should be pre-populated with the length of the drawn line in units of pixels. Enter the length of the feature on the calibration window in the field labeled "Known Ddistance", and its units in the field labeled "Unit of Llength". Check the box labeled "Global" to apply this calibration factor to all open images.

2.4.6. Make the image of the phantom critical feature active and use the "Lline" tool to draw a line along a feature of interest.

2.4.7. From the ImageJ menu, select "Analyze" > "Measure" (or press Ctrl + M) to measure the length of the line.

Compare the expected value against the value in the column marked "Llength" in the the "Results" window to confirm phantom fidelity.

3. MOCK BLOOD SOLUTION FORMULATION

3.1. Mix DI water and glycerol in a 60:40 ratio (by volume). A 100 mL volume is sufficient for the *in vitro* circulatory system described herein Mix 100 mL of 60:40 solution of DI water

3.1.

mock blood solution.

3.2. 3.3. n and Hhomogenize the mixture on a magnetic stir plateplate at 400 rpm for 10 min.

*10.3 µm diameter beads with 480 nm/501 nm excitation/emission wavelengths*

**Formatted:** Highlight

**Formatted:** Font: (Default) +Body (Calibri), Font color: Auto

**Formatted:** Highlight

**Formatted:** Font: (Default) +Body (Calibri), Font color: Auto

**Formatted:** Highlight

**Commented [A11]:** Are there any specs I need to know about?

**Commented [RP12R11]:** We're looking into power. I don't believe that power is variable in the tabletop sonicators we use.

**Formatted:** Font: (Default) +Body (Calibri), Font color: Auto

**Formatted:** Highlight

**Formatted:** Font: (Default) +Body (Calibri), Font color: Auto

**Formatted:** Normal, Indent: Left: 0.75", No bullets or numbering

**Field Code Changed**

**Commented [A14]:** You should add which magnification you used to do this (maybe as a note).

**Formatted:** Font: (Default) +Body (Calibri), Font color: Auto

**Formatted:** Highlight

**Formatted:** Normal, No bullets or numbering

**Formatted:** Highlight

**Formatted:** Highlight

**Formatted:** Highlight

**Formatted:** Highlight

**Formatted:** Highlight

**Formatted:** Indent: Left: 0.55", No bullets or numbering

4.1. Pump Setup

4.1.1. Use a wire stripper tool to cut off the DC-end plug from the A~~/~~C to DC adapter source.

4.1.2. Strip the coating off the power and ground wires and connect them to the input terminal of the pulse width modulation (PWM) voltage regulator.

4.1.3. Connect the power and ground wires from the pump's DC motor to the output terminal of the PWM voltage regulator. The PWM's 7-segment -display outputs the duty cycle (0% - 100%) used to achieve a variable voltage to the DC motor.

4.2. Pump Calibration

4.2.1. ~~In a 500mL beaker,~~P~~-P~~~~p~~repare ~~1~~200 mL of mock blood solution (see S~~as outlined in~~

4.2.2. Place tubing from the pump inlet to the beaker holding the mock blood solution.

4.2.3. Place tubing from the pump outlet to an empty ~~500 mL~~ beaker.~~r. from the volume.~~

4.2.4. Select a desired ~~range of duty cycle values to~~ duty cycle set-point (0% - 100%). ~~and~~ timer. ~~and collect~~

4.2.5. Stop the timer once the pump has transferred ~~all~~the entire volume of ~~of the~~ mock solution. Use this time to calculate the volumetric flow rate.

~~-~~4.2.6. Repeat steps 4.2.1 – 4.2.5 for at least 5 different ~~varying flow rates~~duty cycle set-a least-squares regression curve. A minimum of three replicate points per duty cycle set-point is recommended. This relationship can be used to correlate the desired flow rate to the required PWM duty cycle.

~~4.~~5. VIDEO COLLECTION

~~-~~Image calibration

~~-~~Determine calibration ratio for the video imaging (see Section 2).~~Within the PCC~~

~~- Import this image into ImageJ to estimate the calibration constant (e.g., pixels/mm).~~

~~-~~Place the PDMS phantom on the stage of the ~~upright~~ fluorescence microscope.

5.2.2. Connect the phantom to the~~a~~ gear pump and introduce the mock blood solution.

~~o~~

with mock blood solution~~.~~. ~~, which~~ This may be particularly beneficial for models with vessels and/or blind features ~~(e.g., small perforators and aneurysm sacs, respectively)~~.

~~o~~

5.2.3. Set the pump motor controller for the desired flow rate based on the pump calibration curve.

~~-~~Run the pump for 1 ~~to~~ - 5 min~~utes~~ prior to the experiment to ensure steady-state conditions.

~~-~~Turn on the ~~Mg-Halide~~external lamp to ~~I~~illuminate the field of view ~~of the camera according~~ based upon the ~~to the~~ excitation wavelength of the fluorescent beads.

~~-~~Adjust the imaging focal plane to the vessel mid-plane. This can be achieved by ~~:~~

~~-~~

phantoms with circular vessel cross sections); and/or

feature designed to facilitate identification of the vessel mid-plane~~. In the example~~

~~4.1.~~ Video recording

~~-~~Select the video recording parameters to optimize signal-to-noise ratio (SNR). parameters include exposure time, frame rate, and gain.

**Formatted:** Not Highlight

**Formatted:** Not Highlight

**Formatted:** Not Highlight

**Formatted:** Not Highlight

**Formatted:** Outline numbered + Level: 3 + Numbering Style: 1, 2, 3, … + Start at: 1 + Alignment: Left + Aligned at: 0.5" + Indent at: 0.75"

**Formatted:** Not Highlight

**Formatted:** Outline numbered + Level: 3 + Numbering Style: 1, 2, 3, … + Start at: 1 + Alignment: Left + Aligned at: 0.5" + Indent at: 0.75"

**Formatted:** Font: (Default) +Body (Calibri), Font color: Auto

frame rate of 2000 ~~frames~~fps~~/s~~, and a gain of 1.0. However, these parameters may on application (see~~; refer to~~ D~~d~~iscussion section for ~~more~~further details).

~~o 1.1.1. Gain can be used to amplify the signal, but this also increases sensor noise.~~

- Phantom clean up
  - If bead-sticking is observed after an experiment, sonicate the phantom in an aqueous aqueous ~~Alconox~~ detergent solution using powers up to 70 W.

## ~~5.~~6. IMAGE PROCESSING AND DATA ANALYSIS

- Image pre~~-filtering~~processing~~processing~~
  - o Drag the saved AVI file onto the I~~i~~mageJ window to ~~i~~import it. ~~AVI file into ImageJ in~~ "C~~c~~onvert to G~~g~~rayscale".
  - From the "ImageJ" m~~M~~enu, ~~S~~select "Analyze" > "Generate Histogram" (or press ~~c~~Ctrl H) to ~~Intensity capping~~ standard deviation for the unprocessed image.

    NOTE: At high frame rates, it is not unusual for the distribution to be heavily toward zero (i.e., no signal).

  6.1.3. From the "ImageJ" ~~ImageJ~~ m~~M~~enu, ~~S~~select "Image" > "Adjust"> "Brightness and press Shift + Ctrl + H) to ~~A~~apply a brightness/contrast filter.

  6.1.4. On the "B~~b~~rightness and C~~c~~ontrast" menu, ~~P~~press the "Set" button to define the limits. ~~Choose~~Set the minimum value to be ~~such that the intensity limits are set by set~~ the maximum value to be the maximum intensity of the image (both based on statistics obtained in Section ~~5.1~~6.1.2).

    o NOTE: ~~obtained in step 5.1.2.~~ This typically eliminates all but the top 10% of standard deviations may be varied depending on the desired distribution of pixel intensities.
    operation is provided in the Supplemental Material.

  - From the "ImageJ" ~~ImageJ~~ m~~M~~enu, ~~S~~select "Process" > "Noise" > "Despeckle" ~~.~~ number of saturated pixels.

    NOTE: This operation is necessitated by the increased potential for pixel saturation that arises during optimization of brightness and contrast, which can produce spurious vectors during subsequent cross-correlation.

  - From the "ImageJ" ~~ImageJ~~ m~~M~~enu, ~~S~~select "Process" > "Filters" > "~~-~~Gaussian Blur" radius of 1.5 to reduce artifacts arising from the ~~. Select the radius to be 1.5. This value~~ pixels in a 3x3 neighborhood by the prior despeckling operation.
  - o Click on the "P~~p~~olygon" tool, and then click within the image to outline the ~~The~~ interest (ROI).
  - From the "ImageJ" ~~ImageJ~~ m~~M~~enu, select "Edit" > "Clear Outside" ~~definition~~to locations where no signal is expected (e.g., areas beyond vessel wall boundary), which can decrease overall SNR.

~~The ImageJ *ROI Definition* function, followed by the *Clear Outside* function, can~~

NOTE: This portion of the protocol ~~e section below~~ employs a third-party PIV plug-in for ImageJ~~ for conducting PIV analyses~~, ~~. Ensure the plug-in has been installed before implementing any of the operations below.~~which relies upon Gaussian peak-fitting to enable estimation of displacement with sub-pixel accuracy.

6.2.1. From the "ImageJ" ~~ImageJ~~ m~~M~~enu, ~~Cross correlation~~Sselect "Plugins" > "Macros" saved macro "Supplemental Cod~~d~~e 2.ijjm" to ~~perform a batched correlation on~~cross-

NOTE: The ~~code performs an algorithm~~macro ~~is~~proceeds as follows: within consecutive images is first performed to determine the local displacement of advected tracer particles, i.e. ~~(i.e.~~ the first image pair ~~is~~consists of the first and images~~images #1 and #2~~, ~~and~~ the second image pair ~~pair is~~consists of the second two-step multi-pass evaluation ~~was adopted~~is then performed with initial and interrogation window sizes of 256 x 256 pixels and 128 x 128 pixels, respectively; and finally, 3) ~~. After the correlation is performed for all image pairs,~~ the macro ~~potential for introduction~~appearance of spurious vectors.

6.3. Normalized median test (NMT)

6.3.1. From the "ImageJ" ~~ImageJ~~ m~~M~~enu, select "Plugins" > "Macros" > "Run…" and saved macro "Supplemental Code 3.ijjm" to ~~perform a batched vector validation~~ normalized median test.

NOTE: The macro ~~algorithm performs~~is proceeds as follows: 1) ~~Perform~~ field is first compared to its eight nearest neighbors ~~and~~to compute the median 2) ~~.~~ neighboring vector and the ~~median vector magnitude~~calculated median; ~~.~~3) t vector under investigation and the median neighboring vector value is then normalized by the median of the residuals; 4) ~~.~~ value (typically 0.2 pixels), which can be varied based on *a priori* knowledge of noise during image acquisition; and finally, 5) ~~.~~ instantaneous vector fields ~~before averaging them, since~~ is performed to produce a composite field, as this has been shown to increase the vector field quality[24].

**REPRESENTATIVE RESULTS:**

Figure 2 illustrates the PDMS tissue phantom fabrication process. The phantoms designed herein are intended for the study of flow in idealized wide-necked, saccular, intracranial aneurysms, as well as proximal branching perforator arteries. Important additional design features include: 1) a common reservoir that all vessels drain into, to ensure unencumbered fluid egress from the phantom, otherwise droplet formation may occur at the smaller vessel outlets; 2) a bubble trap, to facilitate bubble removal; 3) an outer cavity wall, to ensure parallelism of the vessel with the horizontal plane, as well as precise definition of the final phantom slab height, length and width; and 4) use of a 21 gauge hypodermic needle shank (820 µm nominal outer diameter) for molding

**Formatted:** Font: (Default) +Body (Calibri), Font color: Auto

**Formatted:** List Paragraph, Outline numbered + Level: 2 + Numbering Style: 1, 2, 3, … + Start at: 1 + Alignment: Left + Aligned at: 0.25" + Indent at: 0.55"

**Formatted:** Font: (Default) +Body (Calibri), Not Bold, Font color: Auto

**Formatted:** Font: (Default) +Body (Calibri), Font color: Auto

**Formatted:** Left, Outline numbered + Level: 3 + Numbering Style: 1, 2, 3, … + Start at: 1 + Alignment: Left + Aligned at: 0.5" + Indent at: 0.75"

of the perforator artery, due to our printer's inability to define such features with sufficient fidelity. Faithful reproduction of all design features is observed throughout.

Representative results for PIV-based flow characterization performed using the current protocol are presented in Figures 3 and 4. These studies were performed using phantom inlet flow rates of 100 mL/min, data acquisition rates of 2000 fps, and temporal averaging over spans of 0.05 s. Figure 3 shows representative image frames within the perforator artery, before and after intensity capping as well as corresponding surface plots of the 8-bit pixel intensity values. Both demonstrate that intensity capping significantly increases peak definition above the noise floor (i.e., increases SNR), which is critical to ensuring accuracy when performing subsequent cross-correlation. Figure 4 shows the effects of intensity capping and NMT operations on the velocity vector field. Marked improvement in field uniformity is observed, thus further underscoring the importance of maximizing SNR to minimize data dropout.

**FIGURE AND TABLE LEGENDS:**

**Figure 2: PDMS-based tissue phantom fabrication process:** a) CAD model of neurovascular phantom mold; b) Printed ABS mold, after removal of support material; c) Casting and curing of PDMS within the ABS mold; d) Partial dissolution of ABS mold material; and e) Completed PDMS phantom, with inset showing final dimensions of ~~key~~ critical features, as well as the region of interest (ROI) in the perforator artery where the PIV measurements were made. ~~.~~

**Figure 3: Effect of intensity capping operation on image SNR.** Representative image frame and corresponding pixel intensity surface plots within the perforator artery, before (a, b) and after applying the intensity capping operation (c, d).

**Figure 4: Effects of intensity capping and NMT operations on velocity vector fields:** Representative instantaneous velocity vector field within the perforator artery derived from: ~~(~~a) unprocessed image data; ~~(~~b) intensity capped data; and ~~(~~c) intensity capped data + NMT post-processing.

**Figure 5: Effect of interrogation window sizing on correlation quality.** Optimal window sizing occurs when the value of the zero-normalized correlation coefficient is maximized, and the standard deviation is minimized.

**DISCUSSION:**

The protocol described herein outlines a simplified~~e~~ ~~and relatively low-cost~~ method for performing PIV studies to visualize neurovascular flows at physiologically-relevant dimensions and flow conditions ~~*in vitro*~~*in vitro*. In doing so, it serves to complement protocols reported by others that have also focused on simplifying the quantification of ~~ying~~ vector fields, but within very different contexts that require consideration of far larger length-scales[25~~23~~] or lower flow rates[26, 27](e.g. atmospheric or microcirculatory flows), and thus, reliance upon ~~simplification~~

schemes that are incompatible with the current application.

The most important considerations for successful implementation of PIV lie in the of flow field artifacts and maximization of image quality. Several steps in the tissue phantom fabrication process are critical to both of these criteria. For example, thorough degassing is crucial since air entrained within the PDMS during mixing can lead to bubble formation within the final phantom, which can adversely affect both feature fidelity and optical clarity. Additionally, minimization of surface roughness of the ABS mold is desired, since the PDMS casting process faithfully reproduces even the most minute imperfections (e.g., build lines, surface pores, scratches, etc.), thus resulting in surface roughness in the final phantom that can decrease optical clarity and increase potential for bead accumulation. While the protocol described herein has proven sufficient for the current application~~beyond the scope of the current protocol, ,~~ there are means for reducing such roughness, should there be need (e.g., acetone vapor smoothing[28], or optimization of layer thickness and part orientation with respect to build direction)[29]~~)~~.

$$f_{sampling} > \frac{v_{max} \cdot c_{calibration}}{h_{interrogation\ window}} \qquad \mathbf{(1)}$$

where $f_{sampling}$ is the camera acquisition rate (Hz), $v_{max}$ is the maximum expected velocity (mm/s), $c_{calibration}$ is the calibration constant (pixels/mm), and $h_{interrogation\ window}$ is the size of the interrogation window (pixels)~~.~~

correlation quality estimation techniques, such as the zero-normalized correlation coefficient[11]. In this technique, the averages of complementary signals from each frame-pair are first subtracted, and then normalized by the standard deviation of their intensities[11]. If a displacement of the original signal exists, such that all peaks and valleys match, the time-shifted value of this signal will be equal to one. Conversely, if there is no displacement that can align these signals, the value will be zero. This information is included in the ImageJ PIV output for each vector, and it can be plotted as its own field to ~~see if~~verify whether there are spatial effects contributing to correlation (e.g., uneven lighting). The correlation coefficient can also be averaged over a field as an overall estimate of its quality. Finally, this quantity may also be plotted against varying frame rates or interrogation window sizes to determine an optimum. Figure 5 illustrates the results from such an analysis using a Monte-Carlo synthesized particle field with displacements consistent with our experimentally-measured flows (a typical technique for characterizing correlation quality[11]). The results show that the interrogation window size and frame rate should be chosen such that a particle field is displaced by ≤ 20% of the interrogation window size per frame-pair to maximize the correlation coefficient, while minimizing its variability.

**Formatted:** Font: (Default) Cambria Math, Font color: Auto, Not Highlight

**Formatted:** Font: (Default) Cambria Math, Font color: Auto, Not Highlight

**Formatted:** Font: (Default) Cambria Math, Font color: Auto, Not Highlight

**Formatted:** Font: (Default) Cambria Math, Font color: Auto, Not Highlight

**Formatted:** Font: (Default) Cambria Math, Font color: Auto, Not Highlight

**Formatted:** Font: (Default) Cambria Math, Font color: Auto, Not Highlight

**Formatted:** Font: (Default) Cambria Math, Font color: Auto, Not Highlight

**Formatted:** Font: (Default) Cambria Math, Font color: Auto, Not Highlight

**Formatted:** Font: (Default) Cambria Math, Font color: Auto, Not Highlight

**Formatted:** Font: (Default) Cambria Math, Font color: Auto, Not Highlight

**Formatted:** Font color: Auto, Not Highlight

**ACKNOWLEDGMENTS:**

The authors acknowledge partial support for this project provided by a Collaborative Seed Grant from the Office of Research and Economic Development at UC Riverside.

**DISCLOSURES:**

The authors declare no competing financial interests.

**REFERENCES**


1. Grant, I. Particle image velocimetry: A review. *Proceedings of the Institution of Mechanical Engineers, Part C: Journal of Mechanical Engineering Science*. **211** (1), 55–76, doi: 10.1243/0954406971521665 (1997).
2. Lindken, R., Rossi, M., Große, S., Westerweel, J. Micro-Particle Image Velocimetry (µPIV): Recent developments, applications, and guidelines. *Lab on a Chip*. **9** (17), 2551, doi: 10.1039/b906558j (2009).
3. Hove, J.R., Köster, R.W., Forouhar, A.S., Acevedo-Bolton, G., Fraser, S.E., Gharib, M. Intracardiac fluid forces are an essential epigenetic factor for embryonic cardiogenesis. *Nature*. **421**, 172, at <http://dx.doi.org/10.1038/nature01282> (2003).
4. Ando, J., Yamamoto, K. Vascular Mechanobiology. *Circulation Journal*. **73** (11), 1983–1992, doi: 10.1253/circj.CJ-09-0583 (2009).
5. Conway, D.E., Breckenridge, M.T., Hinde, E., Gratton, E., Chen, C.S., Schwartz, M.A. *Fluid Shear Stress on Endothelial Cells Modulates Mechanical Tension across VE-Cadherin and PECAM-1*. *Current Biology*. **23** (11), at <http://www.sciencedirect.com/science/article/pii/S0960982213004909>. (2013).
6. Kuhlencordt, P.J. *et al.* Accelerated Atherosclerosis, Aortic Aneurysm Formation, and Ischemic Heart Disease in Apolipoprotein E/Endothelial Nitric Oxide Synthase Double-Knockout Mice. *Circulation*. **104** (4), 448–454, doi: 10.1161/hc2901.091399 (2001).
7. Lieber, B.B., Stancampiano, A.P., Wakhloo, A.K. Alteration of hemodynamics in aneurysm models by stenting: Influence of stent porosity. *Annals of Biomedical Engineering*. **25** (3), 460–469, doi: 10.1007/BF02684187 (1997).
8. Bulusu, K. V., Plesniak, M.W. Experimental Investigation of Secondary Flow Structures Downstream of a Model Type IV Stent Failure in a 180˚ Curved Artery Test Section. *Journal of Visualized Experiments*. (113), e51288–e51288, doi: 10.3791/51288 (2016).
9. Tseng, Q. *et al.* Spatial organization of the extracellular matrix regulates cell-cell junction positioning. *Proceedings of the National Academy of Sciences of the United States of America*. **109** (5), 1506–11, doi: 10.1073/pnas.1106377109 (2012).
10. Shavit, U., Lowe, R.J., Steinbuck, J. V Intensity Capping: a simple method to improve cross-correlation PIV results. *Experiments in Fluids*. **42** (2), 225–240, doi: 10.1007/s00348-006-0233-7 (2007).
11. M. Raffel, C. Willert, S. Werely, J.K. *Particle Image Velocimetry: a Practical Guide*. Springer. New York. (2007).
12. Kerl, H.U. *et al.* Implantation of Pipeline Flow-Diverting Stents Reduces Aneurysm Inflow Without Relevantly Affecting Static Intra-aneurysmal Pressure. *Neurosurgery*. **74** (3), 321–334, at <http://dx.doi.org/10.1227/NEU.0000000000000253> (2014).
13. Lieber, B.B., Livescu, V., Hopkins, L.N., Wakhloo, A.K. Particle Image Velocimetry Assessment of Stent Design Influence on Intra-Aneurysmal Flow. *Annals of Biomedical Engineering*. **30** (6), 768–777, doi: 10.1114/1.1495867 (2002).
14. Charonko, J., Karri, S., Schmieg, J., Prabhu, S., Vlachos, P. *In vitro*, time-resolved PIV

comparison of the effect of stent design on wall shear stress. *Annals of biomedical engineering*. **37** (7), 1310–21, doi: 10.1007/s10439-009-9697-y (2009).

15. Rand, P.W., Lacombe, E., Hunt, H.E., Austin, W.H. Viscosity of normal human blood under normothermic and hypothermic conditions. *Journal of Applied Physiology*. **19** (1), 117–122, doi: 10.1152/jappl.1964.19.1.117 (1964).
16. Kenner, T., Leopold, H., Hinghofer-Szalkay, H. The continuous high-precision measurement of the density of flowing blood. *Pflügers Archiv European Journal of Physiology*. **370** (1), 25–29, doi: 10.1007/BF00707941 (1977).
17. Hoyt, L.F. New Table of the Refractive Index of Pure Glycerol at 20°C. *Industrial & Engineering Chemistry*. **26** (3), 329–332, doi: 10.1021/ie50291a023 (1934).
18. Cai, Z., Qiu, W., Shao, G., Wang, W. A new fabrication method for all-PDMS waveguides. *Sensors and Actuators A: Physical*. **204**, 44–47, doi: https://doi.org/10.1016/j.sna.2013.09.019 (2013).
19. Bouillot, P., Brina, O., Ouared, R., Lovblad, K.-O., Farhat, M., Pereira, V.M. Particle imaging velocimetry evaluation of intracranial stents in sidewall aneurysm: hemodynamic transition related to the stent design. *PloS one*. **9** (12), e113762, doi: 10.1371/journal.pone.0113762 (2014).
20. Trager, A.L., Sadasivan, C., Lieber, B.B. Comparison of the *in vitro* hemodynamic performance of new flow diverters for bypass of brain aneurysms. *Journal of biomechanical engineering*. **134** (8), 084505, doi: 10.1115/1.4006454 (2012).
21. Clauser, J. *et al.* A Novel Plasma-Based Fluid for Particle Image Velocimetry (PIV): *In-Vitro* Feasibility Study of Flow Diverter Effects in Aneurysm Model. *Annals of Biomedical Engineering*. **46** (6), 841–848, doi: 10.1007/s10439-018-2002-1 (2018).
22. Johnston, I.D., McCluskey, D.K., Tan, C.K.L., Tracey, M.C. Mechanical characterization of bulk Sylgard 184 for microfluidics and microengineering. *Journal of Micromechanics and Microengineering*. **24** (3), 035017, doi: 10.1088/0960-1317/24/3/035017 (2014).
23. Lee, J.N., Park, C., Whitesides, G.M. Solvent Compatibility of Poly(dimethylsiloxane)-Based Microfluidic Devices. *Analytical Chemistry*. **75** (23), 6544–6554, doi: 10.1021/ac0346712 (2003).
24. Meinhart, C.D., Wereley, S.T., Santiago, J.G. A PIV Algorithm for Estimating Time-Averaged Velocity Fields. *Journal of Fluids Engineering*. **122** (2), 285, doi: 10.1115/1.483256 (2000).
25. Bosbach, J., Kühn, M., Wagner, C., Raffel, M., Resagk, C. Large-Scale Particle Image Velocimetry of Natural and Mixed Convection. *13th Int Symp on Applications of Laser Techniques to Fluid Mechanics* (2006).
26. Meinhart, C.D., Wereley, S.T., Santiago, J.G. PIV measurements of a microchannel flow. *Experiments in Fluids*. **27** (5), 414–419, doi: 10.1007/s003480050366 (1999).
27. Lima, R. *et al. In vitro* blood flow in a rectangular PDMS microchannel: experimental observations using a confocal micro-PIV system. *Biomedical Microdevices*. **10** (2), 153–167, doi: 10.1007/s10544-007-9121-z (2008).
28. Kuo, C.-C., Mao, R.-C. Development of a Precision Surface Polishing System for Parts Fabricated by Fused Deposition Modeling. *Materials and Manufacturing Processes*. **31** (8), 1113–1118, doi: 10.1080/10426914.2015.1090594 (2016).
29. Kang, K., Oh, S., Yi, H., Han, S., Hwang, Y. Fabrication of truly 3D microfluidic channel using 3D-printed soluble mold. *Biomicrofluidics*. **12** (1), 014105, doi: 10.1063/1.5012548 (2018).

30. Prasad, A.K. Particle Image Velocimetry. *Current Science*. **79** (1), 51–60 (2000).
31. Dellenback, P.A., Macharivilakathu, J., Pierce, S.R. Contrast-enhancement techniques for particle-image velocimetry. *Applied Optics*. **39** (32), 5978–5990, doi: 10.1364/AO.39.005978 (2000).
32. Cowen, E.A., Monismith, S.G. A hybrid digital particle tracking velocimetry technique. *Experiments in fluids*. **22** (3), 199–211 (1997).
33. Gruen, A.W. Adaptive least squares correlation: a powerful image matching technique. *South African Journal of Photogrammetry, Remote Sensing and Cartography*. **14** (3), 175–187, at <http://citeseerx.ist.psu.edu/viewdoc/summary;jsessionid=8478C7133B070BA354E5DED2EFF60262?doi=10.1.1.93.6891\nhttp://www.idb.arch.ethz.ch/files/alsm_awgruen.pdf> (1985).
34. Nogueira, J., Lecuona, A., Rodríguez, P.A. Data validation, false vectors correction and derived magnitudes calculation on PIV data. *Measurement Science and Technology*. **8** (12), 1493–1501, doi: 10.1088/0957-0233/8/12/012 (1997).
35. Loudon, C., Tordesillas, A. The Use of the Dimensionless Womersley Number to Characterize the Unsteady Nature of Internal Flow. *Journal of Theoretical Biology*. **191** (1), 63–78, doi: https://doi.org/10.1006/jtbi.1997.0564 (1998).
36. Drost, S., De Kruif, B.J., Newport, D. Arduino control of a pulsatile flow rig. *Medical Engineering and Physics*. **51**, 67–71, doi: 10.1016/j.medengphy.2017.10.006 (2017).
37. Tsai, W., Savaş, Ö. Flow pumping system for physiological waveforms. *Medical & Biological Engineering & Computing*. **48** (2), 197–201, doi: 10.1007/s11517-009-0573-6 (2010).
38. Kato, T., Indo, T., Yoshida, E., Iwasaki, Y., Sone, M., Sobue, G. Contrast-enhanced 2D cine phase MR angiography for measurement of basilar artery blood flow in posterior circulation ischemia. *AJNR. American journal of neuroradiology*. **23** (8), 1346–51, at <http://www.ncbi.nlm.nih.gov/pubmed/12223376> (2002).

jove JOURNAL OF VISUALIZED EXPERIMENTS
1 Alewife Center #200
Cambridge, MA 02140
tel. 617.945.9051
www.jove.com

**TITLE:** Simplified protocol for meso-scale particle image velocimetry studies of neurovascular flows ~~*in vitro*~~*in vitro*

Formatted: Italic

**AUTHORS AND AFFILIATIONS:**
Ryan A. Peck[1*], Edver Bahena[1*], Reza Jahan[2], Guillermo Aguilar[1,3,4], Hideaki Tsutsui[1,4], Marko Princevac[1], Monica M. Wilhelmus[1], and Masaru P. Rao[1,3,4]

[1] Department of Mechanical Engineering, University of California, Riverside, CA, USA
[2] Division of Interventional Neuroradiology, University of California, Los Angeles, California, USA
[3] Materials Science and Engineering Program, University of California, Riverside, CA, USA
[4] Department of Bioengineering, University of California, Riverside, CA, USA

*Contributed Equally

Authors:
Ryan A. Peck: rpeck003@ucr.edu
Edver Bahena: ebahe002@ucr.edu
Reza Jahan: rjahan@mednet.ucla.edu
Guillermo Aguilar: gaguilar@engr.ucr.edu
Hideaki Tsutsui: htsutsui@engr.ucr.edu
Marko Princevac: marko@engr.ucr.edu
Monica M. Wilhelmus: monicamo@engr.ucr.edu

Corresponding Author:
Masaru P. Rao
mprao@engr.ucr.edu

**KEYWORDS:**
Particle Image Velocimetry, PDMS Tissue Phantom, 3D Printing, Fluid Mechanics, Signal Processing, Neurovascular.

**SUMMARY:**
Within this protocol we detail simplified methods for fabricating transparent neurovascular phantoms and characterizing flow therein. We highlight several important parameters and demonstrate their relationship to field accuracy.

**ABSTRACT:**
Particle Image Velocimetry (PIV) is used in a wide variety of fields, due to the opportunity it provides for precisely visualizing and quantifying flows across a large spatiotemporal range. However, its implementation typically requires use of expensive and specialized instrumentation, which limits its broader utility. Moreover, within the field of bioengineering, *in vitro* flow

visualization studies are also often further limited by the high cost of commercially-sourced tissue phantoms that recapitulate desired anatomical structures, particularly for those that span the meso-scale regime (i.e., sub-mm to mm length-scales). Herein, we present a simplified experimental protocol developed to address these limitations, the key elements of which include: 1) a relatively low-cost method for fabricating meso-scale tissue phantoms using 3D printing and silicone casting; and 2) an open-source image analysis and ~~pre/post-~~processing framework that reduces demand upon the instrumentation for measuring meso-scale flows (i.e., velocities up to tens of mm/s). Collectively, this lowers the barrier to entry for non-experts by leveraging resources already at the disposal of many bioengineering researchers. ~~, thus circumventing the need to implement many of the more costly components in standard PIV systems.~~ We demonstrate the applicability of this protocol within the context of neurovascular flow characterization; however, it is expected to be relevant to a broader range of meso-scale applications in bioengineering and beyond.

**Formatted:** Font: 12 pt, Not Bold, Not Highlight

**INTRODUCTION:**

Particle image velocimetry (PIV) is widely used in experimental fluid mechanics for flow visualization and quantitative investigations of fluid motion that vary in length-scale from atmospheric to microcirculatory flows[1–3]. While the specifics of its implementation can vary as widely as its applications, one aspect common to nearly all PIV studies is the use of video imaging of tracer particles seeded within the working fluid, followed by pair-wise analysis of consecutive image frames to extract desired flow characteristics. Typically, this is accomplished by first sub-dividing each image frame into smaller regions termed interrogation windows. As a consequence of the random positions of the dispersed particles, each interrogation window contains a unique distribution of pixel intensities. If the window size and data acquisition rate are chosen appropriately, cross-correlation of the intensity signal in each window can be used to estimate the average displacement within that region. Finally, given that the magnification and frame rate are known experimental parameters, an instantaneous velocity vector field can be readily computed.

A major advantage of PIV over single-point measurement techniques is its ability to map vector fields across a two- or three-dimensional domain. Hemodynamic applications, in particular, have benefited from this capability, since it allows a thorough investigation of local flows, which are known to play a significant role in vascular disease or remodeling (e.g., atherosclerosis, angiogenesis)[4–6]. This has also been true for the evaluation of neurovascular flows, and the interactions thereof with endovascular devices (e.g., flow diverters, stents, intra-saccular coils, etc.), since the relevant lengths-scales in such applications can often span one or more orders of magnitude (e.g., micrometer to mm-scale), and device geometry and placement can significantly impact the local fluid mechanics[7].

Most groups conducting PIV-based hemodynamics studies have relied on experimental setups that closely mimic some of the earliest investigations of stent influence on vascular flow[7, 8]. Typically, these include: a) pulsed lasers and high-speed cameras, to capture high velocity flows; b) synchronizers, to prevent aliasing between the pulse frequency of the laser and the camera acquisition frame rate; c) cylindrical optics, to form a light sheet, and thus, minimize background

fluorescence from tracer particles above and below the interrogation plane; and d) in the case of commercial turn-key systems, proprietary software packages, to perform the cross-correlation analyses. However, while some applications require the performance and/or versatility collectively afforded by these components, many others do not~~, thus making it sometimes difficult to justify the high cost of such systems. (which can reach up to > $100k)~~. ~~-~~Moreover, the high cost of commercially-sourced tissue phantoms that recapitulate desired vascular structures can also prove limiting for many ~~*in vitro*~~*in vitro* studies, particularly for phantoms with features that bridge the meso-scale regime (> $500/phantom). ~~It must be emphasized that the intent of this protocol is to outline a methodology to perform PIV with lab components that are already accessible to bioengineering laboratories. It is out of the scope of this document to provide a detailed guide on PIV and the reader is referred to comprehensive texts for variations on the method (CITE). Here, we lay out a fail-proof framework that can be readily applied even if one lacks experience with this measurement technique.~~ Herein, we report the development of a simplified~~e~~ ~~and low-cost~~ protocol for implementing PIV for *in vitro* visualization of neurovascular flows, which typically lie both spatially and temporally within the meso-scale regime (i.e., length-scales ranging from sub-mm to mm, and velocities up to tens of mm/s). The protocol seeks to leverage resources already at the disposal of many bioengineering researchers, thus lowering the barrier to entry for non-experts.

~~It must be emphasized that the intent of this protocol is to outline a methodology to perform PIV with lab components that are already accessible to bioengineering laboratories. It is out of the scope of this document to provide a detailed guide on PIV and the reader is referred to comprehensive texts for variations on the method and optimization[9, 10] (CITE). HereIn this protocol, we lay out a fail-proof framework that can be readily applied even if one lacks experience performing measurements with this technique.~~

The first element of this protocol involves the use of an investment casting technique to enable in-house fabrication of transparent, polydimethylsiloxane (PDMS)~~silicone~~-based tissue phantoms from 3D-printed sacrificial ~~acrylonitrile butadiene styrene (ABS)~~ molds. By leveraging the increasing availability of 3D printers in recent years, particularly those in shared/multi-user facilities (e.g., institutional facilities or public makerspaces), this methodology cuts cost significantly (e.g., < $100/phantom in our case), while enabling rapid turnaround for fabrication of a wide variety of designs and geometries. In the current protocol, a fused deposition modeling system is used with acrylonitrile butadiene styrene (ABS) as the build material, and the printed part serves as a sacrificial mold for the subsequent phantom casting. Our experience has shown that ABS is well-suited for such use, since it is soluble in common solvents (e.g., acetone), and it has sufficient strength and rigidity to maintain mold integrity after removal of the support material (e.g., to prevent deformation or fracture of diminutive mold features). In the current protocol, mold integrity is further ensured through the use of solid printed models, although this comes at the expense of increased dissolution time. Use of hollow models may also possible in some cases, to enhance solvent access, and thus, reduce dissolution time. However, careful consideration should be given to the effect this may have on mold integrity. Finally, while the phantoms fabricated herein are based upon idealized representations of neurovascular structures generated using a common CAD software package, the protocol is expected to be

**Formatted:** Highlight

**Formatted:** Highlight

**Formatted:** Highlight

amenable to the fabrication of more complex, patient-specific geometries as well (e.g., via use of model files generated by conversion of clinical imaging data into the .STL file format used by most 3D printers). Further details regarding the phantom fabrication process are provided in ~~Protocol~~ Section ~~s 1 and~~ 2 of the Protocol.

The second element of the protocol involves the use of an open-source plug-in for ImageJ to conduct the cross-correlation analyses[9]. This is coupled with the implementation of a simple statistical thresholding scheme (i.e. intensity capping)[10] to improve image signal prior to cross-correlation, ~~and~~ as well as a post-correlation vector validation scheme, the normalized median test (NMT), to eliminate spurious vectors through comparison of each to its nearest neighbors[11]. Collectively, this allows imaging to be accomplished using equipment commonly found in many bioengineering laboratories ~~(e.g., fluorescence microscope with filtered, continuous white light)~~, thus eliminating the need for acquisition of many of the costly components of typical PIV systems (e.g., pulsed laser, synchronizer, cylindrical optics, and proprietary software). Further details regarding the video collection, image processing, and data analysis are provided in Sections 5 and 6 of the Protocol.

Figure 1 illustrates ~~the various components of~~ the PIV setup used in this ~~study~~protocol, which relies upon a fluorescence microscope equipped with a high-speed camera for imaging, as well as an external, continuous white-light source (i.e., metal halide lamp) for through-objective volumetric illumination. A ~~, which also includes a~~ variable-speed gear pump is used to ~~to enable~~impose recirculating flow of a transparent mock blood solution ~~of a transparent mock blood solution~~ through ~~PDMS-based~~the neurovascular tissue phantoms. The solution ~~–~~is composed of a 60:40 mixture of DI water and glycerol, which is a common substitute for blood in hemodynamics studies[12–14], due to: a) its similar density and viscosity, i.e. 1080 kg/m$^3$ & 3.5 cP, vs. 1050 kg/m$^3$ & 3.0 – 5.0 cP for blood[15, 16]; b) its transparency in the visible range; c) its similar refractive index as PDMS (1.38 vs. 1.42 for PDMS)[17–20] ~~20, 21~~, which minimizes optical distortion; and d) the ease with which non-Newtonian behavior can be introduced, if needed, via the addition of xanthane[21]. Finally, fluorescent polystyrene beads are used as tracer particles (10.3 µm diameter; 480 nm/501 nm excitation/emission). While neutrally-buoyant beads are desired, sourcing tracer particles with optimal fluid mechanical properties (e.g., density, size, composition) and emission wavelength can prove challenging. For example, the beads used herein are slightly less dense than the glycerol solution (1050 kg/m$^3$ vs. 1080 kg/m$^3$). However, the hydrodynamic effects thereof are negligible, given that the duration of a typical experiment is far shorter than the time scale associated with buoyancy effects (i.e., 5 min & 20 min, respectively). Further details regarding the mock blood solution formulation and ~~,~~ *in vitro* circulatory system setup~~video collection, image processing, and data analysis~~ are provided in Sections 3 and 4 of the Protocol ~~Sections 3 to 5~~.

**PROTOCOL:**

1. ABS-BASED SACRIFICIAL MOLD FABRICATION
   - 1.1. Design an inverse model of the desired tissue phantom using CAD software.
   - ~~1.~~1.2. Print the model using a 3D printer with ABS as the build material.
   - ~~Design inverse model of desired tissue phantom using CAD software. The design used in~~

Field Code Changed
Field Code Changed
Field Code Changed
Formatted: Not Highlight
Formatted: Not Highlight
Formatted: Not Highlight
Formatted: Not Highlight
Formatted: Not Highlight
Formatted: Not Highlight
Formatted: Not Highlight
Formatted: Not Highlight
Formatted: Not Highlight
Formatted: Not Highlight
Formatted: Not Highlight
Formatted: Not Highlight
Formatted: Not Highlight
Formatted: Not Highlight
Formatted: Not Highlight
Formatted: Font: (Default) Calibri
Formatted: Not Highlight
Formatted
Formatted: Not Highlight
Formatted: Not Highlight
Formatted: Not Highlight
Formatted: Not Highlight
Formatted: Not Highlight
Formatted: Highlight

~~this protocol is an idealized sidewall aneurysm model.~~

~~1.1. Saved desired CAD model in .STL format for import to 3-D Printing software.Other groups have shown the potential~~

~~Turn on printer and allow it to warm up.~~

~~While the printer is warming up, open CatalystEX.~~

~~Once CatalystEX has loaded, click on File, then from the drop-down menu click "Open STL".~~

~~Locate the .STL file you wish to print from the computer directory and click "Load".~~

~~Once the .STL file has been imported click on the General Tab~~

~~On the right hand side under Properties select layer resolution and click .0070~~

~~Click on Model Interior and select Sparse (High density)~~

~~NOTE: Sparse (Low Density) uses less material and creates a more porous modelhas more voids inside the model,. Tthis is good for a first pass print to ensure the model will work. Sparse (High Density) fills up some of the voids that would be present in the Low Density settinis less porousg,. this is the preferred option for printing the sacrificial mold s as it reduces the probability of releasing trapped used to print the model that will be cast as it will contain less voids that could potentially release air bubbles during the casting. Solid is not need when it comes to printing the model, it adds more ABS but also takes longer to dissolve out~~

~~Modify field marked Modify Leave the field " Number of copies" with desired number of copiesto 1~~

~~Select the desired unit scale used when making the STL file. In this case the unit of measure is millimeter.~~

~~Leave field marked "Scale" as default value (1). Leave scale at 1~~

~~Click on the Orientation Tab~~

~~Click on Auto Orient on the right hand side.~~

~~NOTE: If not satisfied with the auto orient function you may use the XYZ axis to rotate it to your preference.~~

~~Click "Process STL ". After and once that's been completed click "Add to Pack"~~

~~Click on the Pack Tab~~

~~You will see an outlineThe software will display of the print area as well as an outline of the model. You may can click and drag the model to any spot on the print area.~~

~~NOTE: If you'd like to make duplicates, click Copy for number of copies you'd like and arrange them on the print area so they don't overlap.~~

~~When you are ready, click print to send the STL file to the 3D printer~~

~~On the printer itself, it will show that the STL file has been loaded.~~

~~Open the printer door and load the baseboard. Then lock it in place by turning the tabs at the front up~~

**Formatted:** Font: (Default) +Body (Calibri), Font color: Auto, Highlight

**Formatted**

**Formatted:** Highlight

**Formatted:** Font: (Default) +Body (Calibri), Font color: Auto, Highlight

**Formatted:** Justified, Space After: 0 pt, Line spacing: single, No widow/orphan control, Don't adjust space between Latin and Asian text, Don't adjust space between Asian text and numbers

**Commented [MR1]:** Describe clicking sequences in all software portions in a consistent manner throughout protocol. The scheme used in the Image Processing section seems most efficient.

**Formatted:** Font: (Default) +Body (Calibri), Font color: Auto, Highlight

**Formatted:** Justified, Space After: 0 pt, Line spacing: single, No widow/orphan control, Don't adjust space between Latin and Asian text, Don't adjust space between Asian text and numbers

**Formatted:** Font: (Default) +Body (Calibri), Font color: Auto, Highlight

**Formatted:** Font: (Default) +Body (Calibri), Font color: Auto, Highlight

**Formatted:** Justified, Space After: 0 pt, Line spacing: single, No widow/orphan control, Don't adjust space between Latin and Asian text, Don't adjust space between Asian text and numbers

**Commented [RP2]:** Where on the printer?

**Formatted:** Default Paragraph Font, Font: (Default) +Body (Calibri), Font color: Auto, Highlight

**Formatted:** Font: (Default) +Body (Calibri), Font color: Auto, Highlight

~~Close the door, and on display press the button next to the prompt asking ifg the baseboard has been loaded. This will initiate the calibration step and also warm up the printer.~~

~~Once the printer has reached operating temperature it will automatically start the print~~

~~You may place the printer on Auto Shutdown by pressing the button next to the prompt and turning off the printer using the power switch~~

~~Once the print is complete open the door, unlock the baseboard, and remove it from the printer~~

~~Put on googles, lab coat, and rubber gloves~~

~~Take the baseboard with the model and place it in the NaOH base bath~~

~~Turn on the base bath and let it sit for 5 hours. This will dissolve out the support material and free the model. If after 5 hours the support material hasn't fully dissolved, leave it in for another 5 hours.~~

~~Put on googles, lab coat, and rubber gloves~~

~~Remove the baseboard and model from the base bath and place in the sink. Leave the faucet running for about 15 minutes to ensure no base solution is left on the model or baseboard. You may then dry the model and baseboard.~~

~~1.2. Print model using 3D printer.~~

~~A fused deposition modeling system is used herein, with ABS as the build material (0.635 mm resolution in build plane, and 0.178 mm layer resolution).~~

~~ABS is well-suited for use as sacrificial mold material, since it has sufficient strength and rigidity to maintain structural integrity after removal of the support material, and it is soluble in common solvents (e.g., acetone).~~

2. PDMS-BASED VASCULAR PHANTOM FABRICATION

2.1. Mixing

2.1.1. ~~In a disposable weigh boat,~~ Mix the PDMS prepolymer base and curing agent in a 10:1 ratio (by weight). ~~Mmix PDMS monomer base and curing agent in 10:1 weight ratio~~A 66 g mixture provides sufficient material for fabrication of phantoms with volumes up to 50~~XXX~~ ~~mc~~m$^3$ ~~of 60g base to 6g curing agent for 5 to 10 min~~.

Place the mixture in a vacuum desiccator for 60 min to degas and minimize bubble entrapment. Use cyclic pressurization/depressurization to facilitate bubble rupture.

~~2.1.1.~~2.1.2. ~~*(Optional)* Manually, Ccycleic pressurization/depressurization by turning the vacuum on and off may be used to facilitate bubble rupture.~~

Casting

2.2.

2.2.1. Mount the printed ABS mold on a glass slide using molding putty to seal the interface~~Mount printed ABS mold on a 75mm x 25mm glass slide, such so that the top is open to atmosphere. using Use molding putty to seal interface~~.

Carefully pour the PDMS mixture into the mold while trying to minimize bubble entrapment. Lingering bubbles can be manually ruptured using a needle~~Pour PDMS mixture to fill into the mold and rupture any bubbles that form.~~

2.2.2. ~~afterward~~.

~~2.2. Curing~~

**Commented [A3]:** Even if you remove it from video, I think this needs more detail: what is the resolution at which you printed, the material, do you need a special type of printer?

**Commented [A4]:** Need Edver to add detail about how to use Stratsys software to orient part, etc.

**Formatted:** Highlight

**Formatted:** Highlight

**Formatted** ...

**Commented [A5]:** Where do I mix it? What type of container? Does it need to be flat, deep?

**Formatted:** Highlight

**Formatted:** Highlight

**Formatted** ...

**Commented [A6]:** For how long and at what rate? Specs of pressure/depress?

**Commented [RP7R6]:** This is a manual cycling of the vacuum line on under the laminar flow hood so it's not well-controlled enough to prescribe rates, etc. I've updated to reflect this.

**Formatted:** Highlight

**Formatted:** Outline numbered + Level: 2 + Numbering Style: 1, 2, 3, … + Start at: 1 + Alignment: Left + Aligned at: 0.25" + Indent at: 0.55"

**Formatted:** Highlight

**Formatted** ...

**Formatted:** Outline numbered + Level: 3 + Numbering Style: 1, 2, 3, … + Start at: 1 + Alignment: Left + Aligned at: 0.5" + Indent at: 0.75"

**Commented [A8]:** Dimensions?

**Formatted** ...

**Formatted** ...

**Commented [A9]:** Do I rupture them as I pour or do I wait and do it afterwards?

**Commented [RP10R9]:** Updated

**Formatted:** Highlight

**Formatted** ...

Cure the cast phantom at room temperature (25°C) for at least 24 h. At higher temperatures this process can be accelerated[22].

~~2.3. Demolding~~

~~Submerge phantom in acetone bath for 15 min to dissolve ABS.~~

2.2.3.

2.3. Demolding

2.3.1. Dissolve the ABS by submerging the phantom in acetone and sonicating for at least 15 min using powers up to 70 W.

~~Place in ultrasonicaultrasonic bath to facilitate the dissolving of the ABS.~~

~~Refresh the acetone bath with fresh acetone once every 30 minutes.~~

~~o Dissolution may be facilitated by ultrasonic agitation and/or periodic refreshing of acetone bath.~~

CAUTION: Acetone has high vapor pressure at room temperature and low flash point. Consequently, always work under a fume hood and away from potential ignition sources. Wear proper personal protective equipment (e.g., goggles or face shield, lab coat, acetone-resistant gloves, etc.).

2.3.2. Thoroughly rinse the phantom with isopropyl alcohol, and then DI water to remove solvent residues~~Rinse phantom with isopropyl alcohol and DI water and check to ensure no ABS residue is left from the 3D printed model~~.

NOTE: PDMS swells upon exposure to acetone; however, swelling subsides once the phantom is rinsed and dried sufficiently[23].

~~o~~

~~2.4. Phantom fidelity verification~~

2.4. Confirm phantom fidelity using optical microscopy

2.4.1. Using an optical microscope with attached camera and image capture software, capture an image of a critical feature within the phantom under a magnification that maximizes the feature within the field of view.

~~Save the imagean image of the phantom under magnification. (For the example data we've used 10x, but this value may vary based on application).~~

2.4.2. ~~At the same magnification,~~ Ccapture an ~~a still~~ image of an ~~the~~appropriate

Formatted
Formatted
Formatted
Formatted
Formatted
Formatted
Formatted
Formatted
Formatted
Commented [A11]: Are there any specs I need to know
Commented [RP12R11]: We're looking into power. I
Formatted
Formatted
Formatted
Formatted
Commented [A13]: What do you mean by refresh?
Formatted
Formatted
Formatted
Formatted
Formatted
Formatted
Formatted
Formatted
Formatted
Field Code Changed
Formatted
Formatted
Formatted
Formatted
Formatted
Formatted
Formatted
Formatted
Commented [A14]: You should add which magnificatio
Formatted
Formatted
Formatted
Formatted
Formatted
Formatted

~~resolution target or~~ calibration reticle at the same magnification.~~save a reference image whose length is known~~

2.4.3. Load both images into ImageJ by dragging them onto the "~~ImageJ~~ ~~T~~toolbar".

2.4.4. ~~Make~~Click on ~~-~~the calibration reticle image to make it active, and then select the "~~L~~line" tool. Using the mouse, d~~D~~raw a line along a feature of a known distance and select "Analyze" > "Set Scale…" from the ImageJ menu.

2.4.5. In the "~~S~~set ~~S~~scale" window, the field labeled "Distance in pixels" should be pre-populated with the length of the drawn line in units of pixels. Enter the length of the feature ~~on the calibration window~~ in the field labeled "Known ~~D~~distance", and its units in the field labeled "Unit of ~~L~~length". Check the box labeled "Global" to apply this calibration factor to all open images.

2.4.6. Make the image of the phantom critical feature active and use the "~~L~~line" tool to draw a line along a feature of interest.

2.4.7. From the ImageJ menu, select "Analyze" > "Measure" (or press Ctrl + M) to measure the length of the line.

Compare the expected value against the value in the column marked "~~L~~length" in the "Results" window to confirm phantom fidelity.

~~Note: The steps above should be repeated for any measurement using a different microscope objective.~~

~~-~~2.4.8. ~~Verify that no or other techniques. Check to see if any ABS residue film is in the parent artery or aneurysm sac. Excess residue may be removed with an additional acetone/Isopropyl alcohol rinse.~~

3. MOCK BLOOD SOLUTION FORMULATION

3.1. Mix DI water and glycerol in a 60:40 ratio (by volume). A 100 mL volume is sufficient for the *in vitro* circulatory system described herein~~Mix 100 mL of 60:40 solution of DI water and glycerol, respectively~~.

~~3.1.~~

~~NOTE:~~

~~- This is the standard blood substitute in hemodynamics studies[15–17], due to its:~~

~~o density and viscosity (1080 kg/m³ and 3.5 cP, respectively, compared to 1050 kg/m³ and 3.0 – 5.0 cP for blood)[18, 19];~~

~~o transparency in the visible range; and~~

~~o similar refractive index as PDMS (1.41 38 compared to 1.42 for PDMS)[20, 21], which minimizes optical distortion. N~~

~~Non-Newtonian behavior can be achieved with addition of xanthane, if needed[22].~~

3.2. Add 1 mL of 2.5% w~~eight~~/v~~olume~~ fluorescent polystyrene bead solution~~s~~ (i.e.~~,~~ tracer particles) to the mock blood solution.

~~3.2.~~3.3. ~~n and~~ H~~h~~omogenize the mixture on a magnetic stir plate~~plate~~ at 400 rpm for 10 min.

~~10.3 µm diameter beads with 480 nm/501 nm excitation/emission wavelengths are used in this study.~~

**Formatted:** Font: (Default) +Body (Calibri), Font color: Auto

**Formatted** ...

**Formatted** ...

**Formatted** ...

**Formatted** ...

**Formatted:** Font: (Default) Calibri, Font color: Black

**Formatted** ...

**Formatted:** Outline numbered + Level: 3 + Numbering Style: 1, 2, 3, … + Start at: 1 + Alignment: Left + Aligned at: 0.5" + Indent at: 0.75"

**Formatted** ...

**Formatted:** Font: (Default) +Body (Calibri), Font color: Auto

**Commented [A15]:** What do I do if I have residue? Do I start over?

**Formatted:** Highlight

**Formatted:** Highlight

**Formatted:** Outline numbered + Level: 2 + Numbering Style: 1, 2, 3, … + Start at: 1 + Alignment: Left + Aligned at: 0.25" + Indent at: 0.55"

**Formatted** ...

**Formatted:** Highlight

**Formatted:** Indent: Left: 0.55", No bullets or numbering

**Field Code Changed**

**Formatted** ...

**Field Code Changed**

**Formatted** ...

**Formatted:** Highlight

**Formatted:** Highlight

**Field Code Changed**

**Formatted** ...

**Commented [A16]:** According to editor's notes: shouldn't this be added as a note?

**Formatted** ...

**Formatted** ...

**Formatted** ...

**Formatted:** Font: Italic, Not Highlight

**Formatted:** Normal, Indent: Left: 0.5", No bullets or numbering

- *An optimal bead volume fraction of 1% was determined empirically for the current application. Lower volume fractions may be possible with larger interrogation windows.*
- *While neutrally buoyant beads are desired, sourcing tracer particles with optimal fluid mechanical properties (e.g., density, size, composition) and emission wavelength can prove challenging. In this study, beads slightly less dense than the glycerol solution were used (1050 kg/m3 compared to 1080 kg/m3). However, the hydrodynamic effects thereof are negligible, given that the duration of a typical experiment is far shorter than the time scale associated with buoyancy effects (i.e., 5 min and 20 min, respectively).*

4. *SHOULD WE ADD SETTING IT UP TO COVER THE IN VITRO PART THEY ASKED?PUMP SETUPIN-VITRO* CIRCULATORY SYSTEM SETUP

4.1. Pump Setup

4.1.1. Use a wire stripper tool to cut off the DC-end plug from the A/C to DC adapter power source.

4.1.2. Strip the coating off the power and ground wires and connect them to the input terminal of the pulse width modulation (PWM) voltage regulator.

4.1.3. Connect the power and ground wires from the pump's DC motor to the output terminal of the PWM voltage regulator. The PWM's 7-segment -display outputs the duty cycle (0% - 100%) used to achieve a variable voltage to the DC motor.

4.2. Pump Calibration

4.2.1. In a 500mL beaker,P-Pprepare 1200 mL of mock blood solution (see Sas outlined in section 3). (More volume may be required for calibrating over a range of larger flow rates)

4.2.2. Place tubing from the pump inlet to the beaker holding the mock blood solution.

4.2.3. Place tubing from the pump outlet to an empty 500 mL beaker.r. from the volume.

4.2.4. Select a desired range of duty cycle values to duty cycle set-point (0% - 100%). and pPress the "On" button. and Sstart a timer. and collect

4.2.5. Stop the timer once the pump has transferred allthe entire volume of of the mock blood from the inlet beaker Apply to the outlet beaker solution. Use this time to calculate the volumetric flow rate.

4.2.6. Repeat steps 4.2.1 – 4.2.5 for at least 5 different varying flow ratesduty cycle set-points -to establish a least-squares regression curve. A minimum of three replicate points per duty cycle set-point is recommended. This relationship can be used to correlate the desired flow rate to the required PWM duty cycle.

4.5. VIDEO COLLECTION

Image calibration

5.1.

Determine calibration ratio for the video imaging (see Section 2).Within the PCC software, click the camera icon to Ccapture a still image of the resolution target or calibration reticle.

5.1.1. Follow steps as outlined in 2.7 to obtain the calibration ratio.

Import this image into ImageJ to estimate the calibration constant (e.g., pixels/mm).

Apparatus set up

5.2.

Place the PDMS phantom on the stage of the upright fluorescence microscope.

Formatted ...
Formatted: Font: Italic, Not Highlight
Formatted: Outline numbered + Level: 1 + Numbering Style: 1, 2, 3, … + Start at: 1 + Alignment: Left + Aligned at: 0" + Indent at: 0.25"
Formatted ...
Formatted ...
Formatted: Outline numbered + Level: 2 + Numbering Style: 1, 2, 3, … + Start at: 1 + Alignment: Left + Aligned at: 0.25" + Indent at: 0.55"
Formatted ...
Formatted: Outline numbered + Level: 3 + Numbering Style: 1, 2, 3, … + Start at: 1 + Alignment: Left + Aligned at: 0.5" + Indent at: 0.75"
Formatted ...
Formatted ...
Formatted: Outline numbered + Level: 2 + Numbering Style: 1, 2, 3, … + Start at: 1 + Alignment: Left + Aligned at: 0.25" + Indent at: 0.55"
Formatted: Outline numbered + Level: 3 + Numbering Style: 1, 2, 3, … + Start at: 1 + Alignment: Left + Aligned at: 0.5" + Indent at: 0.75"
Formatted ...
Commented [A17]: This should be added as a note. I ...
Formatted: Not Highlight
Formatted: Not Highlight
Formatted ...
Formatted ...
Formatted: Not Highlight
Commented [A18]: You mention a beaker here: ho w ...
Commented [MR19R18]: Seems unnecessary.
Formatted ...
Formatted ...
Formatted ...
Formatted ...
Formatted ...
Commented [A20]: Is this mounted on the microscope?
Commented [RP21R20]: No, this is just a slide with ...
Formatted: Highlight
Formatted ...
Formatted ...
Formatted ...
Formatted ...
Formatted ...

5.2.1.

5.2.2. Connect the phantom to the~~a~~ gear pump and introduce the mock blood solution.

~~o~~

~~*As an optional step,* (Optional) *the* phantom may be pre-filled~~Pre-fill the model with ethanol to facilitate full wetting, then flush and fill with mock blood solution~~.~~. ~~which~~ This may be particularly beneficial for models with smaller vessels and/or blind features ~~(e.g., small perforators and aneurysm sacs, respectively)~~.

~~o~~

5.2.3. Set the pump motor controller for the desired flow rate based on the pump calibration curve.

~~-~~Run the pump for 1 ~~to~~ 5 min~~utes~~ prior to the experiment to ensure steady-state conditions.

5.2.4.

~~-~~Turn on the ~~Mg-Halide~~external lamp to ~~i~~illuminate the field of view ~~of the camera from the top with a through-objective illumination source~~. Select ~~the~~ an appropriate filter ~~according~~ based upon the ~~to the~~ excitation wavelength of the fluorescent beads.

5.2.5.

~~-~~Adjust the imaging focal plane to the vessel mid-plane. This can be achieved by ~~:~~

~~o~~ using a focal length that maximizes the imaged vessel cross-section (e.g., when using phantoms with circular vessel cross sections); and/or

~~o~~5.2.6. indexing off of a phantom feature designed to facilitate identification of the vessel mid-plane~~. In the example provided a 10x objective is used~~.

~~4.1.~~ Video recording

5.3.

~~-~~Select the video recording parameters to optimize signal-to-noise ratio (SNR).

~~o~~ Key parameters include exposure time, frame rate, and gain.

~~Optimal SNR is typically achieved at the highest achievable frame rate that still allows sufficient bead exposure (maximum frame rate being limited by minimum exposure time).~~ In this protocol we use ~~an exposure time of XX of XX,~~ a frame rate of 2000 ~~frames~~fps~~/s,~~, and a gain of 1.0. However, these parameters may vary based on application (see~~; refer to~~ Ddiscussion section for ~~more~~further details).

5.3.1.

~~o1.1.1. Gain can be used to amplify the signal, but this also increases sensor noise.~~

~~o If the maximum velocity can be estimated from other flow parameters (e.g., inlet volumetric flow rate), then a lower bound on the required frame rate can be estimated using the following relation[21]:~~

$$f_{sampling} > \frac{v_{max} \cdot c_{calibration}}{h_{interrogation\ window}} \quad (1)$$

~~where $f_{sampling}$ is the camera acquisition rate (Hz), $v_{max}$ is the maximum expected velocity~~

~~(mm/s), $c_{calibration}$ is the calibration constant (pixels/mm), and $h_{interrogation\ window}$ is the size of the interrogation window (pixels).~~

~~o If the sampling frame rate matches $f_{sampling}$, maximum local velocities are not captured via cross-correlation of image pairs, since the distance traveled by tracer particles in between frames exactly matches the length scale of the interrogation windows. Therefore, the camera should be set to acquire images at a higher frame rate.~~

~~o For the current application, it was found that cross-correlation is optimized when tracer particles travel ≤ 20% of the interrogation window width per frame pair (see Discussion section for further details).~~

5.3.2. Collect video and save in AVI format.

Phantom clean up

5.4.

If bead-sticking is observed after an experiment, sonicate the phantom in an aqueous ~~Alconox~~ detergent solution using powers up to 70 W.

5.4.1. ~~*(Optional)* Use of a pipe cleaner with matching diameter can also to facilitate cleaning. Note: This must be done carefully, although care must be taken take care to ensure the phantom is not damaged.~~

~~5.~~6. IMAGE PROCESSING AND DATA ANALYSIS

Image pre-~~filtering~~processing~~processing~~

6.1.

~~o~~ Drag the saved AVI file onto the ~~I~~imageJ window to ~~I~~import it. ~~AVI file into ImageJ in grayscale format.~~

6.1.1. Select the box marked "~~C~~convert to ~~G~~grayscale".

From the "ImageJ" m~~M~~enu, ~~S~~select "Analyze" > "Generate Histogram" (or press ~~c~~Ctrl + H) to ~~Intensity capping~~

~~o To increase the quality of the signal correlation, the difference between the peaks and valleys (i.e. contrast) of the input signals should be maximized[11].~~

~~o~~ ~~G~~generate a histogram of image pixel intensities. ~~At high frame rates, the distribution is usually skewed heavily toward zero (i.e., no signal).~~ Take note of the mean and standard deviation for the unprocessed image.

6.1.2.

NOTE: At high frame rates, it is not unusual for the distribution to be skewed heavily toward zero (i.e., no signal).

6.1.3. From the "ImageJ" ~~ImageJ~~ m~~M~~enu, ~~S~~select "Image" > "Adjust"> "Brightness and Contrast" (or press Shift + Ctrl + H) to ~~A~~apply a brightness/contrast filter.

6.1.4. On the "B~~b~~rightness and C~~c~~ontrast" menu, ~~P~~press the "Set" button to define the image limits. ~~Choose~~Set the minimum value to be ~~such that the intensity limits are set by~~ the mean value plus one standard deviation ~~from the statistics obtained in step 5.1.2~~, and ~~set~~ the maximum value to be the maximum intensity of the image (both based on statistics obtained in Section ~~5.1~~6.1.2).

NOTE: ~~obtained in step 5.1.2.~~ This typically eliminates all but the top 10% of pixel intensities.

The number of standard deviations may be varied depending on the desired distribution of pixel intensities.

A custom macro script for performing the intensity capping operation is provided in the Supplemental Material.

From the "ImageJ" ~~ImageJ~~ m~~M~~enu, ~~S~~select "Process" > "Noise" > "Despeckle" ~~.~~

~~Optimization of brightness and contrast often increases the number of saturated pixels, which can appear as local maxima, and thus result in spurious vectors during subsequent cross-correlation.~~

~~The Despeckle function in ImageJ can be used~~ to reduce the number of saturated pixels.

6.1.5.

NOTE: This operation is necessitated by the increased potential for pixel saturation that arises during optimization of brightness and contrast, which can produce spurious vectors during subsequent cross-correlation.

From the "ImageJ" ~~ImageJ~~ m~~M~~enu, ~~S~~select "Process" > "Filters" > "~~-~~Gaussian Blur" with a radius of 1.5 to reduce artifacts arising from the ~~. Select the radius to be 1.5. This value is selected because~~

~~D~~despeckling can occa~~s~~sionall~~y~~ removal of~~e~~ illuminated pixels in a 3x3 neighborhood by the prior despeckling operation.

6.1.6.

Click on the "P~~p~~olygon" tool, and then click within the image to outline the ~~The *Gaussian Blur* function in ImageJ can be used to correct this effect.~~

6.1.7. r~~R~~egion of interest (ROI).

From the "ImageJ" ~~ImageJ~~ m~~M~~enu, select "Edit" > "Clear Outside" ~~definition~~to remove

6.1.8. ~~S~~sensor noise in locations where no signal is expected (e.g., areas beyond vessel wall boundary), which can decrease overall SNR.

~~The ImageJ *ROI Definition* function, followed by the *Clear Outside* function, can be used to black out regions outside the ROI, thereby increasing SNR.~~

6.2. ~~Data analysis~~PIV Calculation

NOTE: This portion of the protocol ~~e section below~~ employs a third-party PIV plug-in for ImageJ ~~for conducting PIV analyses, . Ensure the plug-in has been installed before implementing any of the operations below.~~which relies upon Gaussian peak-fitting to enable estimation of displacement with sub-pixel accuracy.

**Formatted:** Indent: Left: 0.75", First line: 0.25", No bullets or numbering
**Formatted:** Highlight
**Formatted:** Indent: Left: 1", No bullets or numbering
**Formatted:** Font: Not Bold, Highlight
**Formatted:** Highlight
**Formatted:** Indent: Left: 0.75", No bullets or numbering
**Formatted** ...
**Formatted:** Outline numbered + Level: 3 + Numbering Style: 1, 2, 3, … + Start at: 1 + Alignment: Left + Aligned at: 0.5" + Indent at: 0.75"
**Formatted:** Outline numbered + Level: 3 + Numbering Style: 1, 2, 3, … + Start at: 1 + Alignment: Left + Aligned at: 0.5" + Indent at: 0.75"
**Formatted:** Font: (Default) +Body (Calibri), Not Italic, Font color: Auto, Highlight
**Formatted** ...
**Formatted:** Highlight
**Formatted:** Indent: Left: 0.75", No bullets or numbering
**Formatted:** Indent: Left: 1"
**Formatted:** Font: (Default) +Body (Calibri), Font color: Auto, Highlight
**Formatted:** Indent: Left: 0.75", No bullets or numbering
**Formatted:** Highlight
**Formatted:** Outline numbered + Level: 3 + Numbering Style: 1, 2, 3, … + Start at: 1 + Alignment: Left + Aligned at: 0.5" + Indent at: 0.75"
**Formatted** ...
**Formatted** ...
**Formatted** ...
**Formatted:** Font: (Default) +Body (Calibri), Font color: Auto, Highlight
**Formatted:** Highlight
**Formatted:** Outline numbered + Level: 3 + Numbering Style: 1, 2, 3, … + Start at: 1 + Alignment: Left + Aligned at: 0.5" + Indent at: 0.75"
**Formatted** ...
**Formatted:** Highlight
**Formatted** ...
**Formatted** ...
**Formatted:** Justified
**Formatted** ...
**Formatted** ...

6.2.1. From the “ImageJ” ~~ImageJ~~ m~~M~~enu, ~~Cross-correlation~~Sselect “Plugins” > “Macros” > “Run…” and navigate to the saved macro “Supplemental Cod~~d~~e 2.ijjm” to ~~perform a batched correlation on~~cross-correlate successive image pairs.

NOTE: The ~~code performs an algorithm~~macro ~~is~~proceeds as follows:

1)

Cross-correlation of the intensity field within consecutive images is first performed to determine the local displacement of advected tracer particles, i.e. ~~(i.e.~~ the first image pair ~~is~~consists of the first and second images~~images #1 and #2, and~~ the second image pair ~~pair is~~consists of the second and third images, etc ~~#2 and #3, etc.)~~ ; 2)

a

~~The ImageJ PIV script allows multi-pass evaluation of the PIV fields.~~

~~Here, a~~A two-step multi-pass evaluation ~~was adopted~~is then performed with initial and final interrogation window sizes of 256 x 256 pixels and 128 x 128 pixels, respectively; and finally, 3) ~~. After the correlation is performed for all image pairs,~~ the macro performs a temporal average to further reduce the ~~potential for introduction~~appearance of spurious vectors.

~~NOTE: The peak in the correlation signal is typically not a discrete maximum at a single location, and thus peak fitting is needed to estimate the displacement with sub-pixel accuracy. The ImageJ PIV plug-in employs Gaussian peak-fitting for this purpose.~~

6.3. Normalized median test (NMT)

6.3.1. From the “ImageJ” ~~ImageJ~~ m~~M~~enu, select “Plugins” > “Macros” > “Run…” and navigate to the saved macro “Supplemental Code 3.ijjm” to ~~perform a batched vector validation using~~validate the velocity fields via the normalized median test.

NOTE: The macro ~~algorithm performs~~is proceeds as follows: 1) ~~Perform NMT for vector validation.~~

~~Each vector is compared to its eight nearest neighbors and the median value is determined.~~

e~~E~~ach vector ~~is in each~~in an instantaneous vector field is first compared to its eight nearest neighbors ~~and~~to compute the median value ~~is determined~~; 2) ~~.~~

t~~T~~he array of residual errors is then ~~then~~ calculated as the difference

**Formatted:** Justified, Indent: Left: 0.55", No bullets or numbering

**Formatted:** List Paragraph, Outline numbered + Level: 3 + Numbering Style: 1, 2, 3, … + Start at: 1 + Alignment: Left + Aligned at: 0.5" + Indent at: 0.75"

**Formatted:** Not Highlight

**Formatted:** Font: (Default) +Body (Calibri), Font color: Auto

**Formatted:** List Paragraph, Indent: Left: 0.75"

**Formatted:** List Paragraph, Indent: First line: 0.5"

**Formatted:** Normal, Indent: Left: 0.5", First line: 0.5", No bullets or numbering

**Formatted:** Normal, Indent: Left: 1", No bullets or numbering

**Formatted:** Indent: Left: 1"

**Formatted:** Font: (Default) +Body (Calibri), Font color: Auto

**Formatted:** Font: (Default) +Body (Calibri), Font color: Auto

**Formatted:** Font: (Default) +Body (Calibri), Font color: Auto

**Formatted:** Font: (Default) +Body (Calibri), Font color: Auto

**Formatted:** Font: (Default) +Body (Calibri), Font color: Auto

**Formatted:** Normal, Indent: Left: 1", No bullets or numbering

**Formatted:** Indent: Left: 1"

**Formatted:** Font: (Default) +Body (Calibri), Font color: Auto

**Formatted** ...

**Formatted** ...

**Formatted** ...

**Formatted:** Not Highlight

**Formatted:** Font: Bold

**Formatted:** List Paragraph, Indent: Left: 0.75"

**Formatted** ...

**Formatted:** List Paragraph, Indent: First line: 0.5"

**Formatted:** Indent: Left: 1", No bullets or numbering

**Formatted:** Font color: Black

**Formatted:** Font color: Black

**Formatted:** Font color: Black

**Formatted** ...

**Formatted:** Font: (Default) Calibri, Font color: Black

**Formatted:** Font: (Default) Calibri, Font color: Black

between each neighboring vector and the ~~median vector magnitude~~calculated median; ~~.~~3) t~~T~~he difference between the vector under investigation and the median neighboring vector value is then normalized by the median of the residuals; 4) ~~5.1. T~~this is then compared to a threshold value (typically 0.2 pixels), which can be varied based on *a priori* knowledge of noise during image acquisition; and finally, 5) ~~.~~

~~a~~A temporal average of all ~~A custom macro script for performing the NMT operation is provided in the Supplemental Material.~~

~~This script performs the normalized median test on each~~ validated instantaneous vector fields ~~before averaging them, since~~ is performed to produce a composite field, as this has been shown to increase the vector field quality[24].

~~A custom macro script for performing the cross-correlation operation is provided in the Supplemental Material.~~

~~Averaging~~

~~Temporal averaging provides a means for mitigating the potential for introduction of spurious vectors, due to mismatching of local maxima in the cross-correlation for a given frame-pair.~~

~~Obtain an average of each velocity component at each grid point.~~

~~Normalized median test (NMT)~~

~~Perform NMT for vector validation.~~

~~Each vector is compared to its eight nearest neighbors and the median value is determined.~~

~~The array of residual errors is then calculated as the difference between each neighboring vector and the median vector magnitude.~~

~~The difference between the vector under investigation and the median neighboring vector value is normalized by the median of the residuals.~~

~~This is compared to a threshold value (typically 0.2 pixels), which can be varied based on *a priori* knowledge of noise during image acquisition.~~

~~A custom macro script for performing the NMT operation is provided in the Supplemental Material.~~

~~This script performs the normalized median test on each instantaneous vector field before averaging them, since this has been shown to increase the vector field quality[22].~~

**REPRESENTATIVE RESULTS:**

Figure 2 illustrates the PDMS tissue phantom fabrication process. The phantoms designed herein are intended for the study of flow in idealized wide-necked, saccular, intracranial aneurysms, as well as proximal branching perforator arteries. Important additional design features include: 1) a

**Formatted:** Font: (Default) Calibri, Font color: Black

**Formatted:** Font: (Default) Calibri, Font color: Black

**Formatted:** Font: (Default) Calibri, Font color: Black

**Formatted:** Font: (Default) Calibri, Font color: Black

**Formatted:** Font: (Default) +Body (Calibri), Font color: Auto

**Formatted:** Font: Bold

**Formatted:** Font: (Default) Calibri, Not Bold, Font color: Black

**Formatted:** Font: (Default) +Body (Calibri), Font color: Auto

**Formatted:** Left, Outline numbered + Level: 3 + Numbering Style: 1, 2, 3, … + Start at: 1 + Alignment: Left + Aligned at: 0.5" + Indent at: 0.75"

**Formatted:** Font: (Default) +Body (Calibri), Font color: Auto

**Formatted:** Normal, No bullets or numbering

**Formatted:** Font: (Default) +Body (Calibri), Font color: Auto

**Formatted:** Normal, No bullets or numbering

common reservoir that all vessels drain into, to ensure unencumbered fluid egress from the phantom, otherwise droplet formation may occur at the smaller vessel outlets; 2) a bubble trap, to facilitate bubble removal; 3) an outer cavity wall, to ensure parallelism of the vessel with the horizontal plane, as well as precise definition of the final phantom slab height, length and width; and 4) use of a 21 gauge hypodermic needle shank (820 µm nominal outer diameter) for molding of the perforator artery, due to our printer's inability to define such features with sufficient fidelity. Faithful reproduction of all design features is observed throughout.

Representative results for PIV-based flow characterization performed using the current protocol are presented in Figures 3 and 4. These studies were performed using phantom inlet flow rates of 100 mL/min, data acquisition rates of 2000 fps, and temporal averaging over spans of 0.05 s. Figure 3 shows representative image frames within the perforator artery, before and after intensity capping as well as corresponding surface plots of the 8-bit pixel intensity values. Both demonstrate that intensity capping significantly increases peak definition above the noise floor (i.e., increases SNR), which is critical to ensuring accuracy when performing subsequent cross-correlation. Figure 4 shows the effects of intensity capping and NMT operations on the velocity vector field. Marked improvement in field uniformity is observed, thus further underscoring the importance of maximizing SNR to minimize data dropout.

**FIGURE AND TABLE LEGENDS:**

**Figure 1: Particle image velocimetry setup.** Reliance upon an open-source image analysis and pre/post-processing framework reduces demand upon the instrumentation for measuring meso-scale flows, thus eliminating the need for many of the costly components of typical PIV systems (e.g., pulsed laser, synchronizer, cylindrical optics, &/or proprietary software).

**Figure 2: PDMS-based tissue phantom fabrication process:** a) CAD model of neurovascular phantom mold; b) Printed ABS mold, after removal of support material; c) Casting and curing of PDMS within the ABS mold; d) Partial dissolution of ABS mold material; and e) Completed PDMS phantom, with inset showing final dimensions of ~~key~~ critical features, as well as the region of interest (ROI) in the perforator artery where the PIV measurements were made. ~~.~~

**Figure 3: Effect of intensity capping operation on image SNR.** Representative image frame and corresponding pixel intensity surface plots within the perforator artery, before (a, b) and after applying the intensity capping operation (c, d).

**Figure 4: Effects of intensity capping and NMT operations on velocity vector fields:** Representative instantaneous velocity vector field within the perforator artery derived from: ~~(~~a) unprocessed image data; ~~(~~b) intensity capped data; and ~~(~~c) intensity capped data + NMT post-processing.

**Figure 5: Effect of interrogation window sizing on correlation quality.** Optimal window sizing occurs when the value of the zero-normalized correlation coefficient is maximized, and the

**Formatted:** Font: Not Bold

**Formatted:** Font: Not Bold

standard deviation is minimized.

**DISCUSSION:**

The protocol described herein outlines a simplified~~e~~ ~~and relatively low-cost~~ method for performing PIV studies to visualize neurovascular flows at physiologically-relevant dimensions and flow conditions ~~*in vitro*~~*in vitro*. In doing so, it serves to complement protocols reported by others that have also focused on simplifying the quantification of ~~ying~~ vector fields, but within very different contexts that require consideration of far larger length-scales[25]~~[23]~~ or lower flow rates[26, 27](e.g. atmospheric or microcirculatory flows), and thus, reliance upon ~~simplification~~ schemes that are incompatible with the current application.

The most important considerations for successful implementation of PIV lie in the minimization of flow field artifacts and maximization of image quality. Several steps in the tissue phantom fabrication process are critical to both of these criteria. For example, thorough degassing is crucial since air entrained within the PDMS during mixing can lead to bubble formation within the final phantom, which can adversely affect both feature fidelity and optical clarity. Additionally, minimization of surface roughness of the ABS mold is desired, since the PDMS casting process faithfully reproduces even the most minute imperfections (e.g., build lines, surface pores, scratches, etc.), thus resulting in surface roughness in the final phantom that can decrease optical clarity and increase potential for bead accumulation. While the protocol described herein has proven sufficient for the current application~~beyond the scope of the current protocol,~~ , there are numerous reports in the literature of means for reducing such roughness, should there be need (e.g., acetone vapor smoothing[28], or optimization of layer thickness and part orientation with respect to build direction)[29]~~)~~.

Parameter selection for video capture is also critical to ensure a high-fidelity vector field. Optimal SNR is typically achieved at the highest achievable frame rate that still allows sufficient bead exposure (maximum frame rate being limited by minimum exposure time). Gain can be used to amplify the signal, but this also increases sensor noise.

If the maximum velocity can be estimated from other flow parameters (e.g., inlet volumetric flow rate), then a lower bound on the required frame rate can be estimated using the following relation[30]:

$$f_{sampling} > \frac{v_{max} \cdot c_{calibration}}{h_{interrogation\ window}} \qquad \textbf{(1)}$$

where $f_{sampling}$ is the camera acquisition rate (Hz), $v_{max}$ is the maximum expected velocity (mm/s), $c_{calibration}$ is the calibration constant (pixels/mm), and $h_{interrogation\ window}$ is the size of the interrogation window (pixels)~~.~~

~~If the sampling frame rate matches $f_{sampling}$, maximum local velocities are not captured via cross-correlation of image pairs, since the distance traveled by tracer particles in between frames exactly matches the length scale of the interrogation windows. Therefore, the camera should be~~

**Formatted:** Normal, No bullets or numbering

**Formatted:** Font: (Default) +Body (Calibri), Font color: Auto

**Formatted:** Normal, No bullets or numbering

**Formatted:** Not Highlight

**Formatted:** Font: (Default) +Body (Calibri), Font color: Auto, Not Highlight

**Formatted:** Not Highlight

**Formatted:** Font: (Default) +Body (Calibri), Font color: Auto, Not Highlight

**Formatted:** Font color: Auto, Not Highlight

**Formatted:** Normal

**Formatted:** Font: (Default) Cambria Math, Font color: Auto, Not Highlight

**Formatted:** Font: (Default) Cambria Math, Font color: Auto, Not Highlight

**Formatted:** Font: (Default) Cambria Math, Font color: Auto, Not Highlight

**Formatted:** Font: (Default) Cambria Math, Font color: Auto, Not Highlight

**Formatted:** Font: (Default) Cambria Math, Font color: Auto, Not Highlight

**Formatted:** Font: (Default) Cambria Math, Font color: Auto, Not Highlight

**Formatted:** Font: (Default) Cambria Math, Font color: Auto, Not Highlight

**Formatted:** Font: (Default) Cambria Math, Font color: Auto, Not Highlight

**Formatted:** Font: (Default) Cambria Math, Font color: Auto, Not Highlight

**Formatted:** Font: (Default) Cambria Math, Font color: Auto, Not Highlight

**Formatted:** Font color: Auto, Not Highlight

**Formatted:** Not Highlight

**Formatted:** Font: (Default) +Body (Calibri), Font color: Auto, Not Highlight

**Formatted:** Normal, Indent: Left: 0"

**Formatted:** Not Highlight

**Formatted:** Normal, No bullets or numbering

**Formatted:** Font: (Default) +Body (Calibri), Font color: Auto, Not Highlight

~~set to acquire images at a higher frame rate~~.

~~However, For the current application, it was found that cross-correlation is optimized when tracer particles travel ≤ 20% of the interrogation window width per frame-pair (see Discussion section for further details).~~

~~For example, w~~While ~~Equation 1 prescribes a lower limit for the frame rate, better~~ more optimal values can be determined using so-called correlation quality estimation techniques, such as the zero-normalized correlation coefficient[11]. In this technique, the averages of complementary signals from each frame-pair are first subtracted, and then normalized by the standard deviation of their intensities[11]. If a displacement of the original signal exists, such that all peaks and valleys match, the time-shifted value of this signal will be equal to one. Conversely, if there is no displacement that can align these signals, the value will be zero. This information is included in the ImageJ PIV output for each vector, and it can be plotted as its own field to ~~see if~~verify whether there are spatial effects contributing to poor correlation (e.g., uneven lighting). The correlation coefficient can also be averaged over a field as an overall estimate of its quality. Finally, this quantity may also be plotted against varying frame rates or interrogation window sizes to determine an optimum. Figure 5 illustrates the results from such an analysis using a Monte-Carlo synthesized particle field with displacements consistent with our experimentally-measured flows (a typical technique for characterizing correlation quality[11]). The results show that the interrogation window size and frame rate should be chosen such that a particle field is displaced by ≤ 20% of the interrogation window size per frame-pair to maximize the correlation coefficient, while minimizing its variability.

Although the protocol described herein has proven sufficient for meeting the needs of the current application, ~~Finally,~~ it is important to acknowledge its limitations. ~~of the current protocol.~~ For example~~,~~, ~~while the use of a fluorescence microscope with continuous, volumetric illumination allows for simplification of the imaging setup (relative to pulsed lasers and light-sheet illumination), this comes at the cost of additional background fluorescence, thus requiring the implementation of various image processing operations prior to cross-correlation (i.e., intensity capping , Dedespeckle, Gaussian Blur, and ROI operations described in Protocol Section 5). Similarly, while the NMT provides a means for improving the velocity vector field after cross-correlation, it is important to emphasize that this is just one of many vector validation techniques that could be used[22, 30], each with their own unique advantages and disadvantages that may make their use more suitable for applications beyond those described here.~~ while contrast enhancement via intensity capping offers ease of implementation, transformations of the entire distribution of pixel intensities may improve SNR further[31]. Similarly, although correlation-based tracking is well-established and provides sufficient resolution for reliably estimating first-order flow characteristics relevant to hemodynamics (e.g., intra-aneurysmal velocity), other techniques may offer higher spatial resolution (e.g., hybrid PIV/PTV, least squares matching)[32, 33], and thus greater accuracy when considering characteristics that are more sensitive to velocity field resolution (e.g., wall shear stress, in-plane vorticity). Likewise, while the NMT provides a means for improving the velocity vector field after cross-correlation, it is important to emphasize that

**Formatted:** Not Highlight

**Formatted:** Normal, No bullets or numbering

**Formatted:** Font: (Default) +Body (Calibri), Font color: Auto, Not Highlight

this is just one of many vector validation techniques that could be used[24, 34], each with their own unique advantages and disadvantages that may make their use more suitable for applications beyond those described here.

~~SimilarlyIn addition, the outlined approaches for image pre-processingfiltering, PIV calculation, and vector validation methods have all been chosen for their relative ease of implementation,; but each of these techniques are only one of several options and may be suboptimal in terms of accuracy when compared against more sophisticated methods. For instance, while image pre-filteringprocessing in this protocol employs a simple statistical threshold for contrast enhancement, transformations of the entire distribution of pixel intensities may improve the SNR[30]. Additionally, although the flow quantification technique outlined (i.e. correlation-based tracking) is well-established and enables sufficient resolution to estimate first-order flow characteristics relevant to hemodynamics (e.g. intra-aneurysmal velocity), other analysis techniques exist which can potentially achieve higher spatial resolution (e.g. hybrid PIV/PTV, least squares matching)[31, 32]. While out of scope of the current protocol, Tthese techniques may be more relevant for researchers interested in confirming the accuracy of estimates which are functions of higher-order spatial derivatives and are therefore more sensitive to velocity field resolution (e.g. wall shear stress, in-plane vorticity).~~

~~SimilarlyLiekewise, while the NMT provides a means for improving the velocity vector field after cross-correlation, it is important to emphasize that this is just one of many vector validation techniques that could be used[23, 33], each with their own unique advantages and disadvantages that may make their use more suitable for applications beyond those described here.~~

Lastly, while our experimental setup seeks to mimic physiologically-relevant flow rates and length scales for the neurovasculature, it does not currently ~~provide opportunity for~~allow the analysis of ~~imposing~~ pulsatile flows. This has not been a limitation for our current application, since ~~However, since t~~the range of Womersely numbers in much of the neurovasculature tends to be ~~tend to be(~~ ≤ 1 ( ~~(~~i.e., there is minimal additive effect of multiple cardiac cycles)[35], which ~~this suggests~~suggests that ~~the~~ steady-state conditions ~~used herein~~ are sufficient to ~~resemble~~ recapitulate ~~oscillatory behavior during specific~~discrete time points along the cardiac waveform in which the flow rate is comparable. ~~Moreover~~However, for applications ~~with~~ where the ~~larger~~ Womersely number is larger~~s~~ (e.g., vasculature closer to the heart), we envision potential for introducing pulsatility through the use of an ~~we anticipate potential for easily integrating pulsatile flow can be easily readily implemented~~ity within the existing setup. For example, others ~~have shown that an~~ Arduino, which could be used to ~~may be used to~~ send the ~~motor~~ pump a time-varying PWM ~~, pulsewidth modulated (PWM)~~ voltage waveform that enables mimicking of ~~the~~ a ~~pulsatile~~ cardiac flow profile ~~seen *in vivo*~~[36–38].

~~**Conclusions:**~~

~~Within this protocol, we have demonstrated simplified methods for fabricating meso-scale neurovascular phantoms and characterizing the flow fields therein via PIV. For researchers interested in vascular flow, variants of this protocol may be particularly useful for early exploratory studies, where the cost of standard PIV systemsinstrumentation would be otherwise~~

**Formatted:** Highlight

~~prohibitive.~~

**ACKNOWLEDGMENTS:**
The authors acknowledge partial support for this project provided by a Collaborative Seed Grant from the Office of Research and Economic Development at UC Riverside.

**DISCLOSURES:**
The authors declare no competing financial interests.

**REFERENCES**

1. Grant, I. Particle image velocimetry: A review. *Proceedings of the Institution of Mechanical Engineers, Part C: Journal of Mechanical Engineering Science*. **211** (1), 55–76, doi: 10.1243/0954406971521665 (1997).
2. Lindken, R., Rossi, M., Große, S., Westerweel, J. Micro-Particle Image Velocimetry (µPIV): Recent developments, applications, and guidelines. *Lab on a Chip*. **9** (17), 2551, doi: 10.1039/b906558j (2009).
3. Hove, J.R., Köster, R.W., Forouhar, A.S., Acevedo-Bolton, G., Fraser, S.E., Gharib, M. Intracardiac fluid forces are an essential epigenetic factor for embryonic cardiogenesis. *Nature*. **421**, 172, at <http://dx.doi.org/10.1038/nature01282> (2003).
4. Ando, J., Yamamoto, K. Vascular Mechanobiology. *Circulation Journal*. **73** (11), 1983–1992, doi: 10.1253/circj.CJ-09-0583 (2009).
5. Conway, D.E., Breckenridge, M.T., Hinde, E., Gratton, E., Chen, C.S., Schwartz, M.A. *Fluid Shear Stress on Endothelial Cells Modulates Mechanical Tension across VE-Cadherin and PECAM-1*. *Current Biology*. **23** (11), at <http://www.sciencedirect.com/science/article/pii/S0960982213004909>. (2013).
6. Kuhlencordt, P.J. *et al.* Accelerated Atherosclerosis, Aortic Aneurysm Formation, and Ischemic Heart Disease in Apolipoprotein E/Endothelial Nitric Oxide Synthase Double-Knockout Mice. *Circulation*. **104** (4), 448–454, doi: 10.1161/hc2901.091399 (2001).
7. Lieber, B.B., Stancampiano, A.P., Wakhloo, A.K. Alteration of hemodynamics in aneurysm models by stenting: Influence of stent porosity. *Annals of Biomedical Engineering*. **25** (3), 460–469, doi: 10.1007/BF02684187 (1997).
8. Bulusu, K. V., Plesniak, M.W. Experimental Investigation of Secondary Flow Structures Downstream of a Model Type IV Stent Failure in a 180˚ Curved Artery Test Section. *Journal of Visualized Experiments*. (113), e51288–e51288, doi: 10.3791/51288 (2016).
9. Tseng, Q. *et al.* Spatial organization of the extracellular matrix regulates cell-cell junction positioning. *Proceedings of the National Academy of Sciences of the United States of America*. **109** (5), 1506–11, doi: 10.1073/pnas.1106377109 (2012).
10. Shavit, U., Lowe, R.J., Steinbuck, J. V Intensity Capping: a simple method to improve cross-correlation PIV results. *Experiments in Fluids*. **42** (2), 225–240, doi: 10.1007/s00348-006-0233-7 (2007).
11. M. Raffel, C. Willert, S. Werely, J.K. *Particle Image Velocimetry: a Practical Guide*. Springer. New York. (2007).
12. Kerl, H.U. *et al.* Implantation of Pipeline Flow-Diverting Stents Reduces Aneurysm Inflow

Without Relevantly Affecting Static Intra-aneurysmal Pressure. *Neurosurgery*. **74** (3), 321–334, at <http://dx.doi.org/10.1227/NEU.0000000000000253> (2014).

13. Lieber, B.B., Livescu, V., Hopkins, L.N., Wakhloo, A.K. Particle Image Velocimetry Assessment of Stent Design Influence on Intra-Aneurysmal Flow. *Annals of Biomedical Engineering*. **30** (6), 768–777, doi: 10.1114/1.1495867 (2002).
14. Charonko, J., Karri, S., Schmieg, J., Prabhu, S., Vlachos, P. *In vitro*, time-resolved PIV comparison of the effect of stent design on wall shear stress. *Annals of biomedical engineering*. **37** (7), 1310–21, doi: 10.1007/s10439-009-9697-y (2009).
15. Rand, P.W., Lacombe, E., Hunt, H.E., Austin, W.H. Viscosity of normal human blood under normothermic and hypothermic conditions. *Journal of Applied Physiology*. **19** (1), 117–122, doi: 10.1152/jappl.1964.19.1.117 (1964).
16. Kenner, T., Leopold, H., Hinghofer-Szalkay, H. The continuous high-precision measurement of the density of flowing blood. *Pflügers Archiv European Journal of Physiology*. **370** (1), 25–29, doi: 10.1007/BF00707941 (1977).
17. Hoyt, L.F. New Table of the Refractive Index of Pure Glycerol at 20°C. *Industrial & Engineering Chemistry*. **26** (3), 329–332, doi: 10.1021/ie50291a023 (1934).
18. Cai, Z., Qiu, W., Shao, G., Wang, W. A new fabrication method for all-PDMS waveguides. *Sensors and Actuators A: Physical*. **204**, 44–47, doi: https://doi.org/10.1016/j.sna.2013.09.019 (2013).
19. Bouillot, P., Brina, O., Ouared, R., Lovblad, K.-O., Farhat, M., Pereira, V.M. Particle imaging velocimetry evaluation of intracranial stents in sidewall aneurysm: hemodynamic transition related to the stent design. *PloS one*. **9** (12), e113762, doi: 10.1371/journal.pone.0113762 (2014).
20. Trager, A.L., Sadasivan, C., Lieber, B.B. Comparison of the *in vitro* hemodynamic performance of new flow diverters for bypass of brain aneurysms. *Journal of biomechanical engineering*. **134** (8), 084505, doi: 10.1115/1.4006454 (2012).
21. Clauser, J. *et al.* A Novel Plasma-Based Fluid for Particle Image Velocimetry (PIV): *In-Vitro* Feasibility Study of Flow Diverter Effects in Aneurysm Model. *Annals of Biomedical Engineering*. **46** (6), 841–848, doi: 10.1007/s10439-018-2002-1 (2018).
22. Johnston, I.D., McCluskey, D.K., Tan, C.K.L., Tracey, M.C. Mechanical characterization of bulk Sylgard 184 for microfluidics and microengineering. *Journal of Micromechanics and Microengineering*. **24** (3), 035017, doi: 10.1088/0960-1317/24/3/035017 (2014).
23. Lee, J.N., Park, C., Whitesides, G.M. Solvent Compatibility of Poly(dimethylsiloxane)-Based Microfluidic Devices. *Analytical Chemistry*. **75** (23), 6544–6554, doi: 10.1021/ac0346712 (2003).
24. Meinhart, C.D., Wereley, S.T., Santiago, J.G. A PIV Algorithm for Estimating Time-Averaged Velocity Fields. *Journal of Fluids Engineering*. **122** (2), 285, doi: 10.1115/1.483256 (2000).
25. Bosbach, J., Kühn, M., Wagner, C., Raffel, M., Resagk, C. Large-Scale Particle Image Velocimetry of Natural and Mixed Convection. *13th Int Symp on Applications of Laser Techniques to Fluid Mechanics* (2006).
26. Meinhart, C.D., Wereley, S.T., Santiago, J.G. PIV measurements of a microchannel flow. *Experiments in Fluids*. **27** (5), 414–419, doi: 10.1007/s003480050366 (1999).
27. Lima, R. *et al.* *In vitro* blood flow in a rectangular PDMS microchannel: experimental observations using a confocal micro-PIV system. *Biomedical Microdevices*. **10** (2), 153–167,

**Formatted:** Font: Italic

**Formatted:** Font: Italic

**Formatted:** Font: Italic

**Formatted:** Font: Italic

doi: 10.1007/s10544-007-9121-z (2008).

28. Kuo, C.-C., Mao, R.-C. Development of a Precision Surface Polishing System for Parts Fabricated by Fused Deposition Modeling. *Materials and Manufacturing Processes*. **31** (8), 1113–1118, doi: 10.1080/10426914.2015.1090594 (2016).
29. Kang, K., Oh, S., Yi, H., Han, S., Hwang, Y. Fabrication of truly 3D microfluidic channel using 3D-printed soluble mold. *Biomicrofluidics*. **12** (1), 014105, doi: 10.1063/1.5012548 (2018).
30. Prasad, A.K. Particle Image Velocimetry. *Current Science*. **79** (1), 51–60 (2000).
31. Dellenback, P.A., Macharivilakathu, J., Pierce, S.R. Contrast-enhancement techniques for particle-image velocimetry. *Applied Optics*. **39** (32), 5978–5990, doi: 10.1364/AO.39.005978 (2000).
32. Cowen, E.A., Monismith, S.G. A hybrid digital particle tracking velocimetry technique. *Experiments in fluids*. **22** (3), 199–211 (1997).
33. Gruen, A.W. Adaptive least squares correlation: a powerful image matching technique. *South African Journal of Photogrammetry, Remote Sensing and Cartography*. **14** (3), 175–187, at <http://citeseerx.ist.psu.edu/viewdoc/summary;jsessionid=8478C7133B070BA354E5DED2EFF60262?doi=10.1.1.93.6891\nhttp://www.idb.arch.ethz.ch/files/alsm_awgruen.pdf> (1985).
34. Nogueira, J., Lecuona, A., Rodríguez, P.A. Data validation, false vectors correction and derived magnitudes calculation on PIV data. *Measurement Science and Technology*. **8** (12), 1493–1501, doi: 10.1088/0957-0233/8/12/012 (1997).
35. Loudon, C., Tordesillas, A. The Use of the Dimensionless Womersley Number to Characterize the Unsteady Nature of Internal Flow. *Journal of Theoretical Biology*. **191** (1), 63–78, doi: https://doi.org/10.1006/jtbi.1997.0564 (1998).
36. Drost, S., De Kruif, B.J., Newport, D. Arduino control of a pulsatile flow rig. *Medical Engineering and Physics*. **51**, 67–71, doi: 10.1016/j.medengphy.2017.10.006 (2017).
37. Tsai, W., Savaş, Ö. Flow pumping system for physiological waveforms. *Medical & Biological Engineering & Computing*. **48** (2), 197–201, doi: 10.1007/s11517-009-0573-6 (2010).
38. Kato, T., Indo, T., Yoshida, E., Iwasaki, Y., Sone, M., Sobue, G. Contrast-enhanced 2D cine phase MR angiography for measurement of basilar artery blood flow in posterior circulation ischemia. *AJNR. American journal of neuroradiology*. **23** (8), 1346–51, at <http://www.ncbi.nlm.nih.gov/pubmed/12223376> (2002).

**Formatted:** Indent: Left: 0", Hanging: 0.19"

Normalized Median Test ImageJ Macro